THE PETROLOGY, GEOCHRONOLOGY AND GEOCHEMISTRY OF THE WHITE BEAR ARM COMPLEX AND ASSOCIATED UNITS

THE PETROLOGY, GEOCHRONOLOGY AND GEOCHEMISTRY OF THE WHITE BEAR ARM COMPLEX AND ASSOCIATED UNITS, GRENVILLE PROVINCE, EASTERN LABRADOR

By

STEPHEN ANTHONY PREVEC, B.Sc.

A Thesis

Submitted to the School of Graduate Studies

in Partial Fulfilment of the Requirements

for the Degree

Master of Science

McMaster University

December 1987

MASTER OF SCIENCE (1987) McMASTER UNIVERSITY

(Geology) Hamilton, Ontario

TITLE: Petrology, Geochronology and Geochemistry of the White Bear Arm Complex and Associated Units, Grenville Province, Eastern Labrador

AUTHOR: Stephen Anthony Prevec, B.Sc. (McMaster University)

SUPERVISOR: Dr. R.H. McNutt

NUMBER OF PAGES: xv, 155

Abstract

The Hawke River Terrane of the Grenville Province in eastern Labrador is dominated by a coronitic gabbronorite to anorthosite body plus associated amphibolitic to granodioritic bodies known as the White Bear Arm Complex (WBAC). Petrographic and geochemical evidence supports a constant volume sub-solidus diffusion origin for double coronas of orthopyroxene and amphibole around olivine. Geochemical evidence suggests that corona formation was not completely isochemical, requiring an influx of potassium, iron and magnesium, but on a whole-rock scale was probably closed to the latter two elements. Nd and Sr isotopic evidence indicates that the coronas did not form as a response to a much later (eg. Grenville aged) metamorphic event, and probably developed during post-crystallisational cooling or during a metamorphism shortly thereafter.

The WBAC is cut by a monzonitic to granodioritic body mineralogically and chemically similar to the WBAC 'monzonite', known as the Paradise Arm Pluton (PAP). Petrographic, geochemical, and field relationship evidence indicates an igneous origin for the PAP and the WBAC monzonite. Both of these units have been subjected to low grade (greenschist facies) metamorphism. The WBAC and the PAP are hosted by the Paradise Metasedimentary Gneiss Belt, an

aluminous paragneiss which has been raised to middle to upper amphibolite grade metamorphism, except immediately adjacent to the contact with the WBAC, where granulite grade has been obtained, forming high-temperature aluminosilicates such as osumilite and sapphirine. The contact zone has also been contaminated by fluids from the gabbronorites, reflected by petrography, elemental and isotopic geochemistry.

Field relationships and geochemistry are ambiguous regarding whether the monzonitic units were derived by fractional crystallisation of the gabbronorite or partial melting of the paragneisses, but trace element variation favours the latter model. The PAP is a product of physical, geochemical and Sr isotopic mixing between a granodioritic end-member and a paragneissic one.

Sm-Nd isotope systematics on whole-rocks do not provide a precise emplacement age for the WBAC gabbronorite, but indicate a Labradorian age (*ca.* 1.65 Ga old). Rb-Sr whole-rock systematics show a Labradorian-aged trend and a steeply sloping trend interpreted as a mixing line with an unspecified crustal component, possibly corresponding to the potassium metasomatism indicated earlier. Rb-Sr on minerals from two rocks produces a precise age of 1675 ± 15 Ma and a similar, imprecise age.

The WBAC monzonite and the Paradise Arm Pluton give Rb-Sr ages of 1621 ± 11 Ma (MSWD=24) and 1573 ± 18 Ma (MSWD=9) respectively, with low initial $^{87}Sr/^{86}Sr$ ratios around 0.7040. These are interpreted as a minimum emplacement age and a mixing line, respectively. The PMGB paragneisses give a Rb-Sr age of 1630 ± 16 Ma (MSWD=35), with an initial $^{87}Sr/^{86}Sr$ composition around 0.704. All ages are equal within expanded 2σ error of each other (ie. MSWD=1), and give Labradorian ages. There is no evidence of Grenville-aged (*ca.* 1.0 Ga old) metamorphism.

Rb-Sr isotopic and ϵ_{Nd}-ϵ_{Sr} variations suggest crustal contamination of the gabbronorites, although the contaminant cannot be identified. Two separate mechanisms are required to generate the observed trends: a fluid metasomatism and a bulk-rock crustal contamination, or else contamination by currently unidentified low Sr crustal material. The WBAC gabbronorites provide evidence for 'extra'-LREE-depleted mantle beneath eastern Labrador at 1.65 Ga, with ϵ_{Nd} of at least +7.6.

Acknowledgements

Acknowledgements are due first and foremost to Dr. Robert McNutt for his guidance, patience and support over the past five years, as well as for instigating and supporting this project. Acknowledgements are also due to Dr. Charles Gower for his inspiration and interest throughout, and in suggesting this project and supporting the field aspects.

Technical acknowledgements are due the following people: to Dave Jones for his assistance with solid source mass spectrometry and humour; to Ota Mudroch for assistance with XRF analyses plus incidental SEM and XRD; to Len Zwicker for thin section work and Jack Whorwood for photographic work and assistance; to Dr. Henry Longerich, Dr. John Greenough and Jeff Vinot at MUN for permission and assistance using the electron microprobe; to Dr. Choudari Khamineni and Barry Machin for permission and assistance using the mineral separation lab at the GSC in Ottawa, and to Jim McAndrew for his assistance in operating the ICP-MS.

Invaluable advice and comment was forwarded by Dr. Alan Dickin regarding mass spectrometry and geochemistry, and without whose assistance REE-isotope geochemistry would almost certainly not have been possible. Dr.s Dickin and McNutt are

also acknowledged for responding to unexpected phone calls from the mass spec. lab on Sunday afternoons during the waning months of this thesis.

Valuable assistance was also volunteered by Dr.s Denis Shaw, Brian Burley and Larry Heaman.

Unflagging moral support was supplied by Kathy Teeter, especially during times of frustrating reanalyses of REE isotopes. Competition was again supplied by Mike, and thanks also to the rest of the fourth-floor crowd and RGW's boys.

Table of Contents

List of Figures

List of Tables

List of Appendices

CHAPTER 1: INTRODUCTION

The Grenville Province in southeastern Labrador is dominated by a group of high grade metamorphic terranes characterised by a metamorphic age of *circa* 1650 Ma, of which probably the least well studied is the newly designated Hawke River Terrane (Gower, 1987). This terrane includes an elongate gabbronorite plus minor granodiorite complex known as the White Bear Arm Complex (Gower *et al.*, 1985), hosted by high grade metasedimentary gneisses of the Paradise Metasedimentary Gneiss Belt (PMGB) and cut by the Paradise Arm Pluton. No geochronology has been done on these units, except for a zircon age on a microgranitoid dyke in the White Bear Arm Complex, defining a minimum emplacement age of 1543 Ma for the gabbronorite.

1.1 Purpose of Study

The goals of this study are principally to determine the age and origin of the White Bear Arm Complex using the radioactive decay schemes of ^{87}Rb to ^{87}Sr ($t_{½}$ = 4.89x10^{10} a) and ^{147}Sm to ^{144}Nd ($t_{½}$ = 1.06x10^{11} a), major and trace elements, and petrology. Based on the same criteria, the age and origin and the genetic relationships of the associated felsic units, consisting of the WBAC "monzonites", the Paradise Arm Pluton, and the PMGB gneisses can be investigated. The same data can

also be used to suggest the degree of crustal contamination of the WBAC mafics, and any implications thereof, and also may indicate to what degree this terrane was affected by Grenville-aged metamorphic overprinting.

Corona structures in the White Bear Arm Complex gabbros between olivine and plagioclase have implications for the cooling history of the rock and its postcrystallisational history.

1.2 Location and Accessibility

The field area is located in eastern Labrador (re. Figure 1.1), with the sampled locations lying within an area comprising five NTS 1:50,000 scale map sheets (13 H/1, 2, 3 and 13 A/15 and 16), spread within an area about 80 km long and 25 km wide.

Field work was done through the support of the Newfoundland Department of Mines and Energy, Mineral Development Division, with C.F. Gower, from base-camps in Paradise River, Spotted Island and Port Hope-Simpson. Access to the sampling areas was completely helicopter supported, focussing on outcrops identified by prior walking traverses done during the reconnaissance mapping presented in Gower *et al.* (1985, 1986, and 1987).

Exposure and accessibility were excellent for the gabbro-norites, which are massive and outcrop in strong positive relief, so that relatively fresh samples were easily obtained. The metasediments, monzonites, and the Paradise Arm Pluton granitoids were all recessive-weathering, so that suitably large and accessible outcrops were almost invariably located in river courses, and consequently secondary alteration in the form of sericitisation of feldspar had occured to some extent in all of the samples from these units.

FIGURE 1.1

The Grenville Province in eastern Labrador
Adapted from Gower (1987)

LMT = Lake Melville Terrane
MMT = Mealy Mountains Terrane

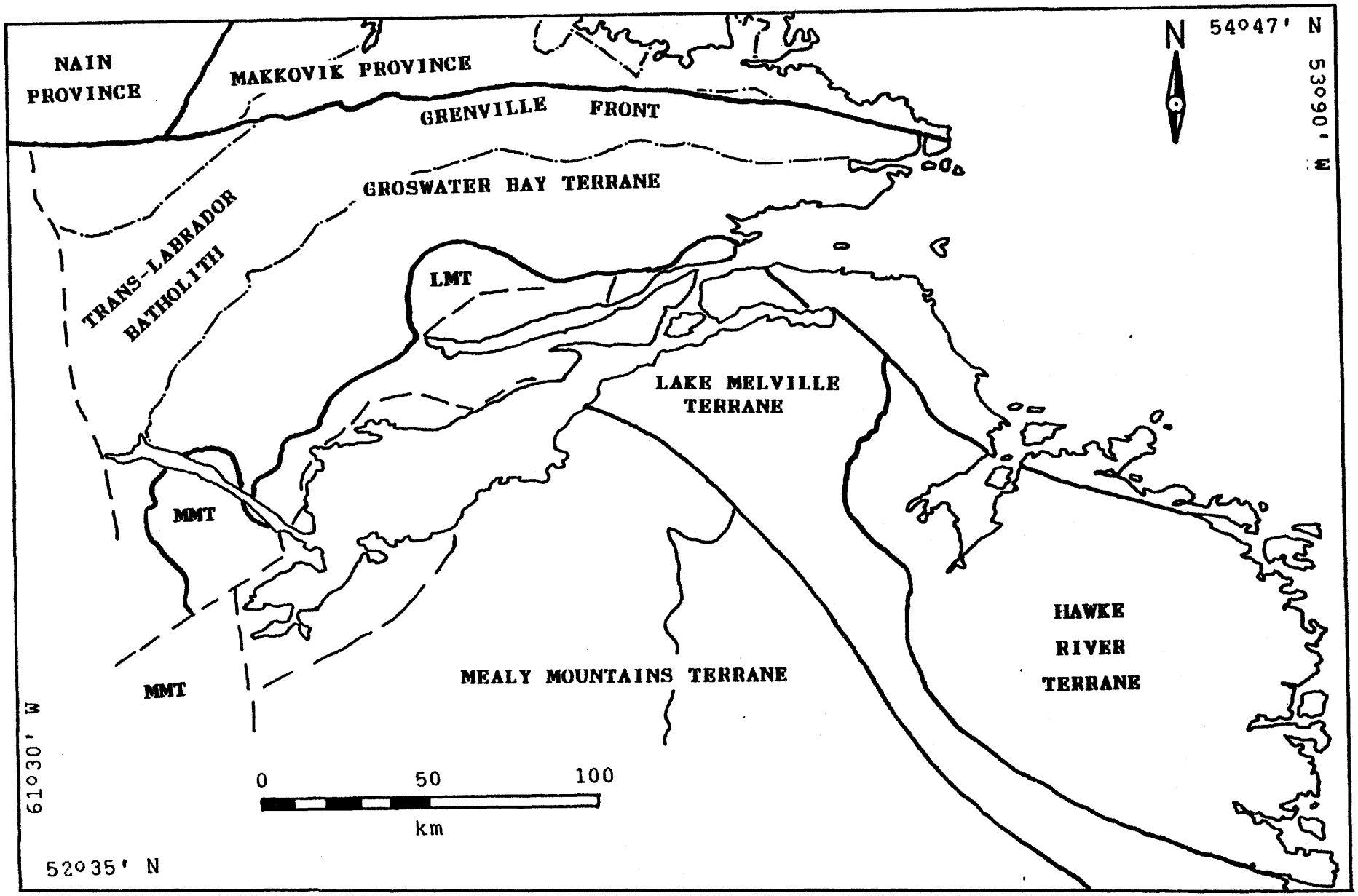
NAIN PROVINCE
MAKKOVIK PROVINCE
GRENVILLE FRONT
GROSWATER BAY TERRANE
TRANS-LABRADOR BATHOLITH
LMT
LAKE MELVILLE TERRANE
MMT
MMT
MEALY MOUNTAINS TERRANE
HAWKE RIVER TERRANE
N
54°47' N
53°00' W
61°30' W
52°35' N
0
50
100
km

CHAPTER 2: INTRODUCTION TO THE GRENVILLE PROVINCE

The Grenville Province is an elongate terrane crossing Ontario, Québec, Labrador, and the northwestern United States, with related outliers in Newfoundland, the Appalachians, the southwestern United States, Scandinavia and the United Kingdom (eg. Sanders *et al.*, 1984). The Grenville Province in Canada alone encompasses nearly a million square kilometres (Moore, 1986), and is composed principally of high grade metamorphic and plutonic rocks. Originally defined by correlation with the "type" locale near Grenville, Québec, the Grenville Province was defined as a lithological entity based on reconnaissance K-Ar dating characterised by an isotopic age of 950 ± 150 Ma (Stockwell, 1961). Due to inconsistencies invited by this definition, whereby much of the plutonism within the boundaries of the Grenville Province gives pre-Grenville ages (eg. Thomas *et al.*, 1986; Easton, 1986), structural criteria are now favoured.

More extensive isotopic dating using U-Pb in zircon and ilmenite, Rb-Sr and Sm-Nd whole rock as well as the K-Ar and $^{40}Ar/^{39}Ar$ methods suggests that the Grenville Orogeny peaked at about 1.1 Ga. This event occurred throughout Ontario (Easton, 1986).

The Grenville Province in Labrador is bounded to the north by an east-west trending plutonic body roughly colinear

with the Grenville Front known as the Trans-Labrador Batholith, which separates the Grenville Province to the south from the Churchill and Makkovik Provinces to the north, as shown in Figure 1.1. The Churchill Province is of late Archean to early Proterozoic age, having suffered its most recent pervasive metamorphic event between 1850 and 1800 Ma ago, and consists principally of granitoid gneisses and the Labrador Trough supracrustals. The Makkovik Province, as defined by Gower and Ryan (1986), consists of supracrustals and felsic volcanics dated at between 1767 and 1676 Ma old (Wardle *et al.*, 1986), and is underlain by reworked Archean Nain Province crust.

The Trans-Labrador Batholith (TLB) is a relatively heterogeneous body lying just south of the Grenville Front, as defined by Gower *et al.* (1980), except at it's eastern end where it is crossed by the Front and lies partially within the Makkovik Province. The TLB is dominantly composed of quartz monzonite, granodiorite, and granite (Wardle *et al.*, 1986), and has been reliably dated at 1650 ± 5 Ma by zircon U-Pb systematics (Wardle *et al.*, 1986). Both older and younger ages have been obtained from within the batholith, by U-Pb on zircon as well as U-Pb from other minerals (titanite and monazite) and by other decay schemes on whole rocks. The older ages are from along the northern boundary, suggesting contamination from or inheritance of older material, and the

younger ages from scattered intrusions thought to be associated with later (*circa* 1500 to 1375 Ma old) volcanism (Wardle *et al.*, 1986).

South of the TLB lie a number of high grade metamorphic terranes of upper amphibolite to granulite facies (Gower and Owen, 1984) typefied by a 1650 Ma metamorphic age and concordant plutonism. These include high grade plutonic and metasedimentary terranes, massif anorthosite and gabbroic bodies of various sizes, and several terranes recognised as allochthons.

East of the Mealy Mountains Intrusive Suite, consisting of an anorthosite massif plus associated monzonite and gabbro (Emslie, 1976), lie at least two distinct lithotectonic terranes, trending subparallel to the TLB at their north-western ends and trending northwest to southeast to the east of the Mealy Mountains. The two recognised terranes are the Groswater Bay Terrane, bounded to the north by the TLB and to the south by the Lake Melville Terrane, which in turn is bounded to the south and west by the Mealy Mountains Terrane.

The Groswater Bay Terrane (Gower and Owen, 1984) consists of both ortho- and paragneisses and granitoid to mafic intrusions. East of the Mealy Mountains, it can be subdivided into two lithotectonic entities; the Domino Domain, dominated

by granitoid plutonic rocks, often K-feldspar megacrystic and locally gneissose or migmatised, and mafic rocks including layered gabbroic rocks as well as amphibolite dikes, and the Earl Island Domain, which borders the units of this study, lithologically and texturally similar to rocks to the west and south as described in Gower *et al.* (1985) and dominated by biotite-hornblende to quartz diorite and hornblende-bearing granodiorite. The latter rock is dominant in the southeast of this domain, interpreted as representing a higher level rock than the diorite further north (Gower *et al.*, 1986). Granitic and megacrystic granitoid rocks are also present in the Earl Island Domain, as well as mafic intrusives. Both domains contain minor enclaves of muscovite and sillimanite-bearing metasedimentary gneiss, thought to represent enclaves not cogenetic with their current granitoid hosts (Gower *et al.*, 1986).

South of the Earl Island Domain lies the Paradise Metasedimentary Gneiss Belt (PMGB), consisting of pelitic to semipelitic gneiss plus lesser quantities of metasedimentary rocks of various origins, including quartzite, metapsammitic gneiss, banded iron formation, and calc-silicate rocks, as well as amphibolites (Gower *et al.*, 1986). The PMGB is bounded to the south by the Paradise Arm Pluton, a K-feldspar megacrystic granitoid rock, and the White Bear Arm Complex, a gabbro-norite complex with pods of monzonite, anorthosite, and

troctolite. Figure 2.1 shows agmatitic contacts between K-feldspar megacrystic rock and metagabbronorite from within the WBAC.

2.1 The Hawke River Terrane

Previous workers (eg. Gower and Owen, 1984; Gower *et al.*, 1985; Gower *et al.*, 1986) have defined the boundary between the Groswater Bay and the Lake Melville Terranes along the contact between the Earl Island Domain granodiorites and the PMGB paragneisses. Recently, however, a new terrane has been proposed based on structural, geophysical and geochronological evidence, identified as the Hawke River Terrane (Gower, 1987), shown in Figures 1.1 and 2.2. This terrane is structurally defined by thrust and strike-slip faults along its southern and western boundaries, and less well defined by a variably faulted or intrusive northern limit. The terrane also displays a high positive Bouger gravity anomaly, and linear aeromagnetic and structural trends (Gower, 1987).

The Earl Island Domain, the PMGB, the Paradise Arm Pluton and the White Bear Arm Complex comprise the Hawke River Terrane. Whether or not the Domino Domain belongs to this package or to the Groswater Bay Terrane has yet to be determined. The PMGB and the Paradise Arm Pluton both trend subparallel to the WBAC mafic complex, although a gabbronorite

body referred to as the Sand Hill Big Pond Gabbronorite (Gower *et al.*, 1986) is isolated from the WBAC by the Paradise Arm Pluton.

The PMGB was sampled within and to the northeast of a zone averaging about five kilometres in width from the border of the WBAC gabbronorite, defined as a contact metamorphic zone (Gower *et al.*, 1986; Gower, 1987).

To the southwest of the WBAC lies the Gilbert River Shear Belt (Gower *et al.*, 1987), which consists of varying proportions of paragneiss, K-feldspar megacrystic granitoid, and orthogneiss, as well as an anorthositic unit, the Alexis River anorthosite (Gower *et al.*, 1985; 1987). The gneissic and granitoid units are mineralogically similar to rocks on the northeast side of the WBAC, but the genetic relationship has not yet been established.

The Groswater Bay Terrane, the Lake Melville Terrane, the Hawke River Terrane and the Mealy Mountains Terrane give zircon ages ranging from 1735 to 1566 Ma, with the majority around 1660 Ma (Schärer *et al.*, 1986). Geochronological evidence (Schärer *et al.*, 1986; Schärer and Gower, in press) suggests that the Lake Melville Terrane was affected by circa 1000 Ma "Grenville aged" metamorphism much more than were the neighbouring terranes.

Figure 2.1

Sharp, agmatitic contact between K-feldspar megacrystic monzonite and melanocratic amphibolitised gabbronorite (from sample location CG-84-365)

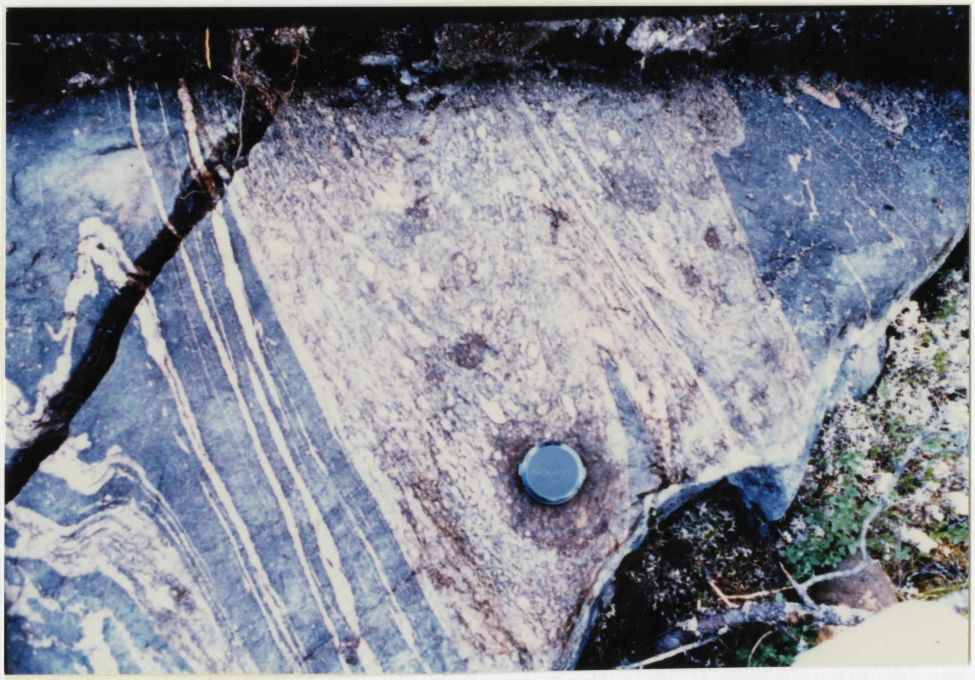

FIGURE 2.2

The Hawke River Terrane, with locations of sample sites for this study
Adapted from Gower et al (1987)

SHBP = Sand Hill Big Pond gabbronorite
PMGB = Paradise Metasedimentary Gneiss Belt
PAP = Paradise Arm Pluton
WBAC = White Bear Arm Complex

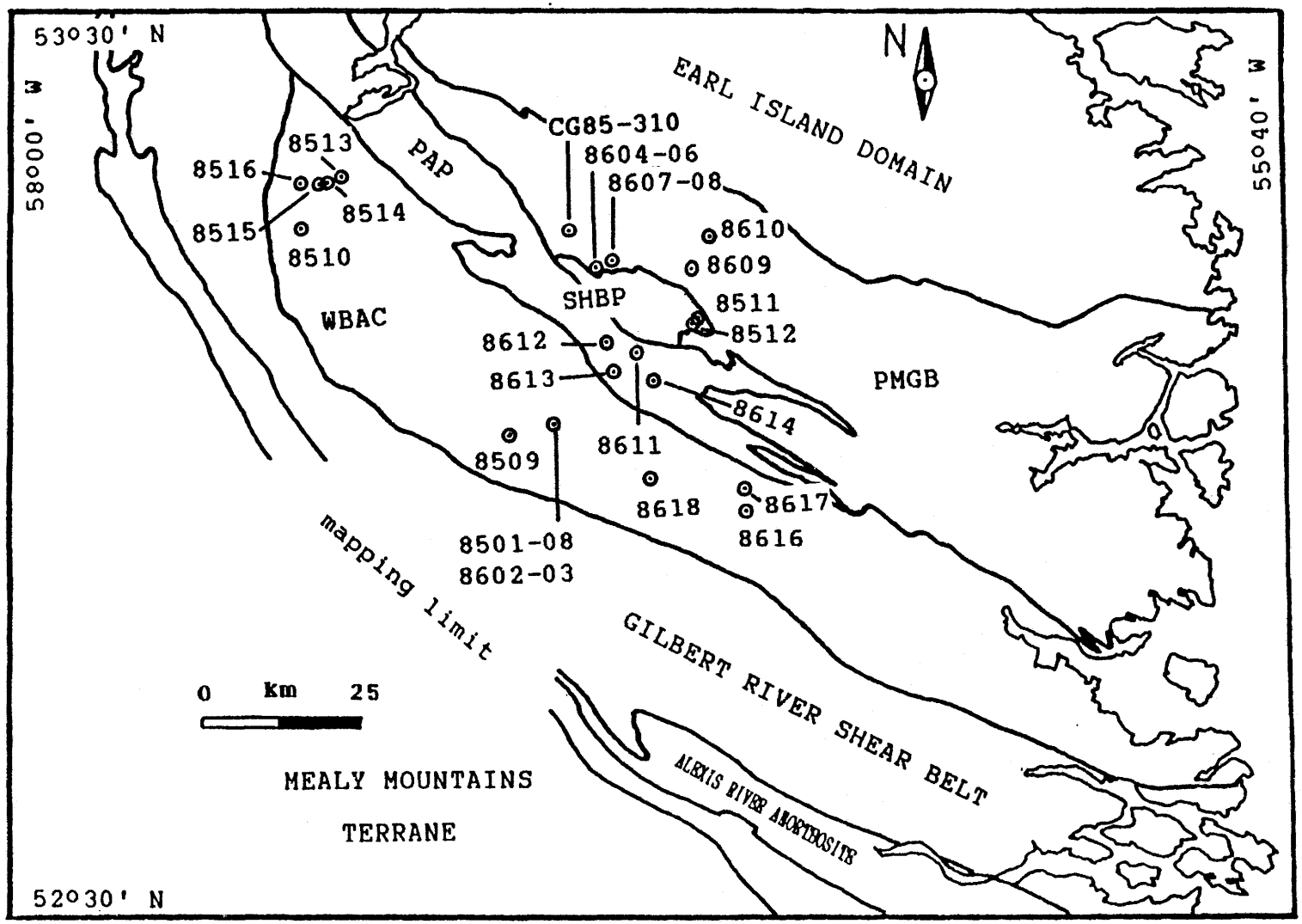
53°30' N
58°00' W
55°40' W
52°30' N
N
EARL ISLAND DOMAIN
PAP
WBAC
SHBP
PMGB
CG85-310
8604-06
8607-08
8513
8516
8514
8515
8510
8610
8609
8511
8512
8612
8613
8614
8611
8509
8618
8617
8616
8501-08
8602-03
mapping limit
GILBERT RIVER SHEAR BELT
ALEXIS RIVER AMPHIBOLITE
0 km 25
MEALY MOUNTAINS
TERRANE

2.2 Previous Work

Although some geological investigation has been done along the Labrador coast in the Hawke River Terrane (listed in Gower *et al.*, 1986), the first geological map was produced by Eade (1962), at 1:50,000 scale. Some mineral exploration reconnaisance was undergone for British Newfoundland Corporation (BRINCO) Ltd., mostly along the coast as well. The only reasonably intensive geological study was that recently undergone and currently in progress by Gower for the Newfoundland Department of Mines and Energy (Gower *et al.*, 1985; 1986), at 1:100,000 scale.

2.2.1 Geochronology

While no geochronology has been done directly on the dominant lithologies of the White Bear Arm Complex, Schärer *et al.* (1986) have reported a combined zircon and monazite age from a microgranitic dike intruding a mylonite located within the White Bear Arm Complex giving an upper intercept at 1566 ± 13 Ma, and a lower (monazite) intercept of 1029 ± 2 Ma. The upper intercept provides a minimum age for the complex of 1553 Ma. However, without using the monazite to constrain the zircon discordia line, the upper intercept is very poorly constrained. Uranium-lead mineral work on zircons from a quartz diorite, a granite and an orthogneiss from the southern

Domino Domain, well within the Hawke River Terrane give upper intercept ages of 1668 +6/-4 Ma, 1663 ± 3 Ma and 1671 +6/-4 Ma respectively (Schärer and Gower, in press). Sphene ages are all around 1645 Ma, and are concordant. Zircons from the Sandwich Bay area suggest original ages up to 1683 Ma (Scharer and Gower, in press).

The Michael Gabbros in the Groswater Bay Terrane were dated at 1426 ± 6 Ma (Schärer *et al.*, 1986), which agrees with less precise Rb-Sr ages of 1461 ± 96 Ma and 1383 ± 56 (Fahrig and Loveridge, 1981; Brooks, 1982, respectively). A layered gabbroic to monzonitic complex at Grady Island in the Groswater Bay Terrane gives a Rb-Sr age of 1630 ± 30 Ma (Brooks, 1983). Layered mafics and anorthosites from the Mealy Mountains suggest an age of about 1.6 Ga, based on Rb-Sr, Sm-Nd, and Pb isotopes (Ashwal *et al.*, 1986), and the Mealy Dikes which postdate the massif have been dated at 1380 ± 54 Ma (Emslie *et al.*, 1984).

CHAPTER 3: PETROGRAPHY

3.1 White Bear Arm Complex

3.1.1 Mafic Units - Gabbronorite (Coronites)

The White Bear Arm Complex (WBAC) is composed of fine to coarse-grained, dark grey homogeneous rocks varying in composition from anorthosite to gabbronorite to lherzolite. The mineralogy includes calcic plagioclase, olivine, clino- and orthopyroxene, with the average grain size varying from about 2.0 cm to 1.0 mm. Locally primary layering is present (Fig. 3.1), producing layers enriched in olivine, plagioclase or pyroxene. Where olivine is present, double coronas are ubiquitous, in the form of an inner corona of radial hypersthene and an outer corona of amphibole-spinel symplectite.

Plagioclase is coarse-grained and fresh, displaying albite and carlsbad twins. Michel-Levy tests on the albite twins indicate a plagioclase composition averaging An_{80}. In the coronites the plagioclase is clouded with minute (15 - 50 μm long) acicular crystals of opaques and spinel, seen in Figure 3.2, which are preferentially aligned within a plagioclase grain, but not aligned consistently relative to the twinning in the host grain nor relative to the inclusions in adjacent plagioclases. The degree of plagioclase clouding

correlates positively with the degree of olivine replacement (corona formation) to a point, such that in completely replaced coronites the degree of clouding is less than at intermediate stages. This suggests that the plagioclases in the completely replaced coronites has begun to recrystallise. In olivine-absent or olivine-poor rocks such as anorthosite (8502) or norite (8603) clouding is minimal to absent. Plagioclase is unclouded in thin coronas immediately surrounding primary pyroxenes.

Primary augite and hypersthene are present, and may or may not be associated with the olivine coronas. Schiller exsolution texture is present in both clino- and ortho-pyroxene, and augite nearly always has thick bands of exsolved orthopyroxene and opaques, with the former sometimes replaced by biotite, shown in Figure 3.3. Both pyroxenes are clouded with opaques, increasing with the degree of development of the olivine coronas. The rims of the pyroxenes are relatively clear of inclusions.

Orthopyroxene often displays discontinuous coronas and alteration along internal fractures to biotite, green spinel, and fibrous green amphibole or amphibole-spinel symplectite. Similarly, the red brown biotite may have a corona of green spinel around it, where biotite lies within the coronas around olivine. This suggests replacement of the outer amphibole-

spinel corona by biotite, where spinel has been excluded from the biotite. The coronas around orthopyroxene are slightly better developed where olivine corona development has progressed, but are relatively poorly developed at all stages. Clinopyroxene may show minor alteration at contacts with plagioclase, such that opaques in the augite are associated with spinel and biotite, but this alteration is very poorly developed and irregular. In olivine-free rocks, fibrous green amphibole and spinel may be associated with clinopyroxene, in a similar fashion.

Olivine, where present, is ubiquitously surrounded by a thin inner corona of colourless orthopyroxene, most commonly as radially oriented blades, less commonly as elongate massive grains, which may display shiller exsolution textures. Alternatively, the opx corona may be a single optically continuous grain, which is *not* associated with an amphibole-spinel outer corona, shown in Figure 3.4. The orthopyroxene inner corona is surrounded by an outer corona of fibrous green amphibole, usually symplectic with fine green pleonaste spinel. The latter mineral is also found as discrete coarser grains inside the inner corona. The outer corona is less sharply defined than the inner corona, and is about the same width (about 0.2 mm, on average) or slightly larger than the inner one. Where primary clinopyroxene abuts the inner corona or the olivine the amphibole corona is not present. There is often a layer

of coarser spinel grains, usually at the interface between the symplectite and hypersthene coronas, but occasionally dividing the symplectite corona into two coronas; an inner corona of spinel-free fibrous amphibole, and an outer coarser one of amphibole-spinel symplectite, shown in Figure 3.5. The double amphibole corona is best developed in the early stages of corona formation. The rare presence of spinel symplectite in the outer margins of clinopyroxene grains in rocks with well developed coronas represents the anhydrous equivalent of the amphibole-spinel corona.

The central olivine is replaced by hypersthene as the radial plates of the inner corona grow inwards until all of the olivine is gone, as shown in Figure 3.6. The replaced olivine core may also be occupied by fine grained randomly oriented hypersthene, or more commonly a core of coarse, sometimes clouded hypersthene plates, occasionally included by clusters of magnetite and hematite vermicules. Remnants of earlier hydrous alteration products and hematite are often diffused between hypersthene grains in the core.

The olivine contains fractures filled with magnetite, hematite, or antigorite. The olivine itself may be altered to bowlingite or pseudomorphed by iddingsite (Fig. 3.3), and occasionally may be largely replaced by single grains of magnetite, within the hypersthene corona.

In well developed coronas, a brown, non-fibrous amphibole, often containing spinel vermicules, forms coronas around biotite. Spinel grains in rocks with poorly developed coronas may have coronas of fibrous green amphibole, which may represent the precursor to later coronas consisting of a very thin corona of orthopyroxene surrounded by brown amphibole, and finally to spinel and associated magnetite surrounded by biotite, shown in Figure 3.7.

3.1.2 Mafic Units - Amphibolite

One sample from the WBAC was an amphibolite, consisting of equigranular hornblende with included blebs of quartz, and almost ubiquitously sericitised plagioclase. Michel-Levy tests on albite twinning, where available, indicate a plagioclase composition of An_{40}. Radioactive haloes around tiny inclusions within the amphibole are also observed, suggesting the presence of zircon.

3.1.3 Monzogabbro

Two samples associated with the monzonite are dominated by plagioclase and hornblende or pyroxene-hornblende. One sample (8616A) displays elongate laths of labradorite (An_{65}) plagioclase, seen in Figure 3.8, with some of the coarser grains exhibiting exsolved blebs of alkali-feldspar and

quartz. The plagioclase is relatively fresh, showing only rare patches of sericitic alteration. The mafic mineralogy is ortho- and clinopyroxene with minor opaques or orthopyroxene-biotite with minor opaques, clino-pyroxene and secondary hornblende, the latter forming along the pyroxene rims. The pyroxenes are granoblastic with an average grain size around 0.5 mm.

Myrmekitic intergrowths of untwinned plagioclase and vermicular quartz are present in 8616B, usually associated with alkali feldspar but occasionally without. Zircon is present often associated with opaques.

3.1.4 K-feldspar Megacrystic Monzonite

This unit is dominated by coarse-grained microcline megacrysts, ranging in length from 0.5 to 4.0 cm ,shown in hand specimen in Figure 3.9, and associated quartz and plagioclase. Other megacrysts are untwinned plagioclase grains, displaying sericitic alteration. The non-megacrystic matrix is dominantly quartz and plagioclase, relatively equigranular at about 0.5 mm. Quartz is also present as fine-grained polygranular elongate veinlets, displaying weakly to non-undulose extinction, surrounding coarser grained plagioclase and alkali-feldspar. The composition of the plagioclase (Michel-Levy) ranges from An_{25} to An_{40} averaging An_{35}.

Albite, pericline, and carlsbad twins are all observed as are inclusions of quartz and alkali-feldspar within the plagioclase megacrysts. Bent twin lamellae are common in the plagioclase megacrysts.

The mafic minerals are biotite and green hornblende in varying proportions, usually equigranular, ranging from 0.3 to 1.0 mm in length. The hornblende shows simple twinning. These minerals define the fabric, although in some cases (eg. 8617A) the biotite is relatively evenly distributed, and while oriented, is non-gneissose. Minor phases include magnetite, at least in part, hematite, anhedral brown sphene (the latter mineral occasionally displaying distinct multiple twinning), and subhedral to anhedral apatite and zircon.

Wine-red garnet is common, ranging from small (2.5 mm) anhedral chunks to coarser (6 - 7 mm) subhedral variably broken up grains. The garnet appears either as small independent anhedral grains included within the foliation, or as coarser grains which are broken up or are in the process of breaking up parallel to the fabric. The larger grains contain quartz, plagioclase, biotite, hornblende and zircon, and are intimately assocoated with opaques. One section (85-09) shows distinct augen textures associated with the garnet grains, shown in Figure 3.10, with poorly defined pressure shadows, where in some cases there is a tendency for biotite or

hornblende to appear exclusively at opposite ends of a garnet grain, suggesting locally variable pressure-temperature microsystems.

Brownish yellow allanite, seen in Fig. 3.11, is associated with the mafic minerals, the former sometimes showing euhedral outlines although normally subhedral, and usually rimmed by a thin corona of a colourless higher birefringent mineral. The allanite is occasionally zoned, and produces pleochroic haloes in biotite. Pennite chlorite is also present in small amounts as rims on biotite grains.

Fracturing of the rocks is common, where the fractures are filled with biotite and opaques.

3.2 Paradise Arm Pluton

The Paradise Arm Pluton (PAP) is white to pink in colour, medium to coarse-grained, with an average grain size of about 3 mm, and varies in texture from massive to foliated. The pluton is consists of coarse-grained microcline megacrysts, ranging in diameter from 1 to 22 mm and varying from 5 to 35 % of the mode (Gower et al, 1986), quartz, plagioclase, non-megacrystic alkali feldspar and biotite. The plagioclase is altered to sericite in patches. As a result of the alteration, the twinning is faint or missing in most cases,

although albite, pericline, and carlsbad twins are all present. Michel-Levy testing on the limited number of albite-twinned grains available indicates an average composition of An_{40} ranging from An_{35} to An_{45}. The plagioclase is strongly deformed, with bent twin lamellae and radial or undulose extinction. There are commonly areas of myrmekitic intergrowths at plagioclase-potash feldspar interfaces, where vermicular quartz is hosted by untwinned plagioclase.

The mafic minerals include reddish brown to pale brown biotite mica, ranging in length from 0.5 to 1.5 mm, averaging about 1 mm long laths. It displays pleochroic haloes, indicative of inclusions of zircon or monazite, too small to be positively identified optically. Oxides such as hematite and magnetite are often intimately associated with biotite, and are elongated parallel to the biotite cleavage. Magnetite is often present in zig-zagging veins infilling fractures in feldspars as well. The brown biotite is altered to anhedral shreds of green biotite and occasionally even further to an aquamarine, pleochroic, anomalously low birefringent biotite, (distinguished from chlorite by its length slow character and uniaxial negative optic sign, but probably in transition from biotite to chlorite) in the presence of magnetite. Coarse grained (0.2 to 0.5 mm long) sphene, zircon and apatite are associated with the mafic bands, particularly with magnetite.

One section (86-11A) shows well developed fibrous sillimanite, as well as sillimanite in small equant grains, crosscutting biotite and associated with muscovite. Sillimanite does not appear in any other thin section from this unit, and may represent an enclave of metasedimentary gneiss, or a remnant thereof. Subhedral garnet is present in one specimen (86-13), shown in Figure 3.12. The fabric defined by the biotite flows weakly around the garnet, which is aligned parallel to the fabric. Inclusions of magnetite and biotite within the garnet, displaying a concentric ringed pattern, suggest helicitic texture.

Also identified in 86-13 is green pennite chlorite, displaying the characteristic 'Berlin blue' interference colours, shown in Fig. 3.13. Pennite occurs as fibrous sheafs associated with the brown biotite and magnetite, where the chlorite is forming at the expnse of the biotite. Minor muscovite is present in section 86-11A, secondary to and cross-cutting the fabric defined by the biotite, with which it is associated.

Calcite in small veinlets is present in one section (86-13), shown in Fig. 3.14, associated with fine grained quartz and biotite rimming a large, altered plagioclase grain.

Yellow brown, very weakly pleochroic to non-pleochroic

Figure 3.1

Primary layering in coronitic gabbronorite shown at large scale in A and finer scale in B. Note the decreasing proportions of olivine to plagioclase from the bottom up, until a new olivine-rich layer begins (from 8502)


A

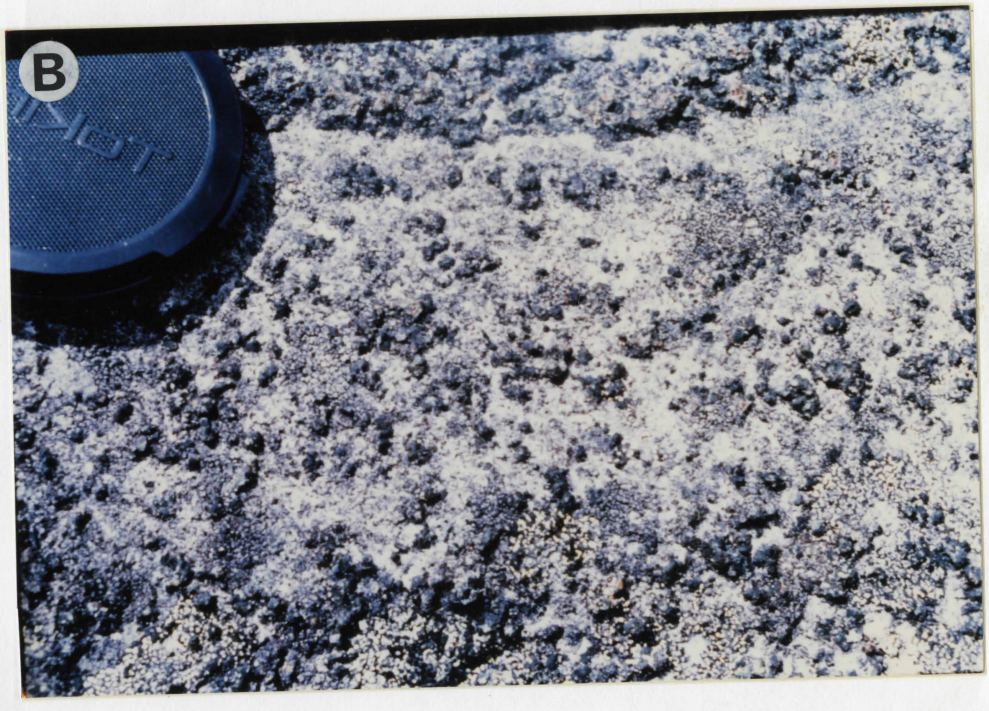
B

Figure 3.2

Clouding of plagioclase by spinel in coronitic sample 8511 in plane-polarised light (ppl)

A: (x160) width of field is 0.6 mm
B: (x400) width of field is 0.25 mm

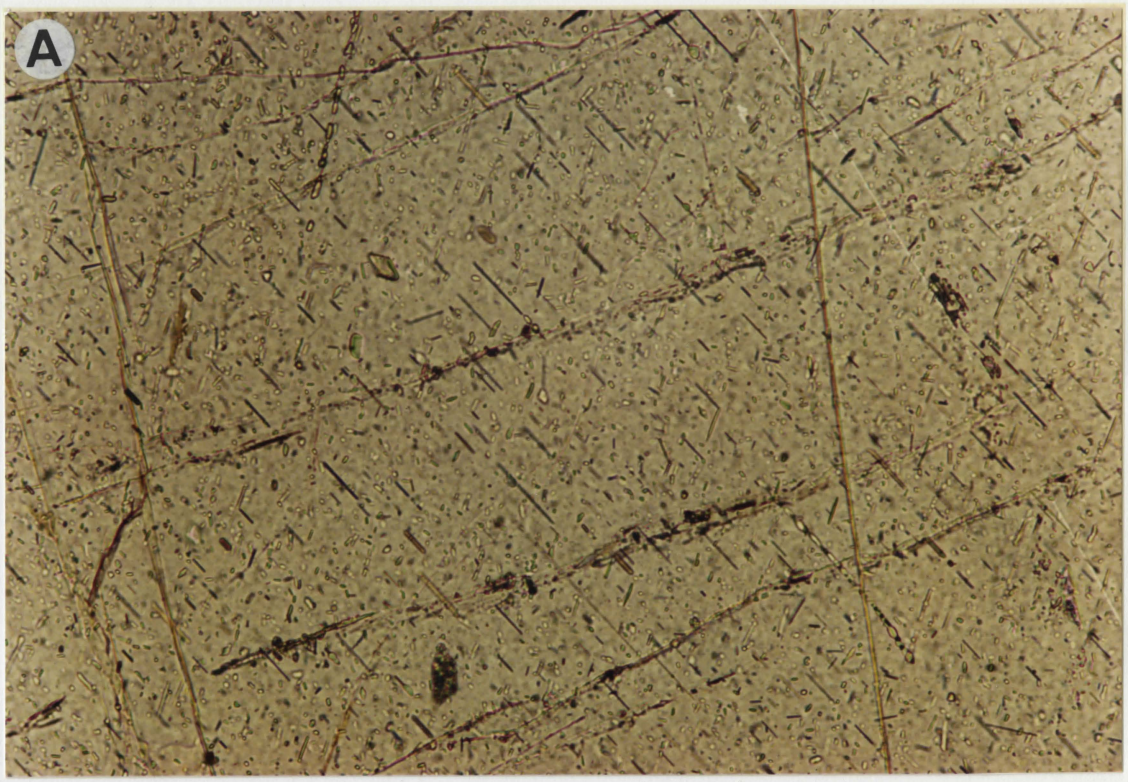
A

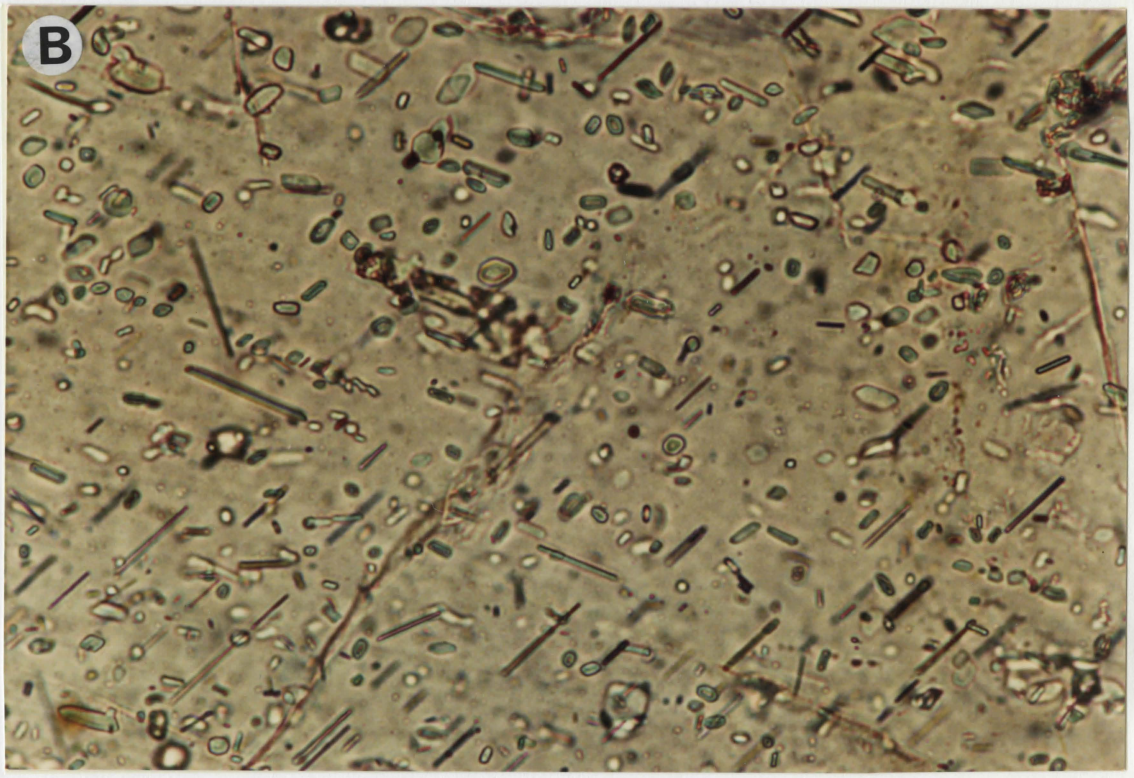
B

Figure 3.3

Dark brown biotite and opaques replacing exsolved lamellae of orthopyroxene in a clinopyroxene grain hosted by olivine, from 8511.

(ppl: x25) width of field is 4 mm

Figure 3.4

Optically continuous orthopyroxene corona around olivines, showing absence of corresponding outer amphibole-spinel symplectite corona, from 8512.

(xp: x25) width of field is 4 mm

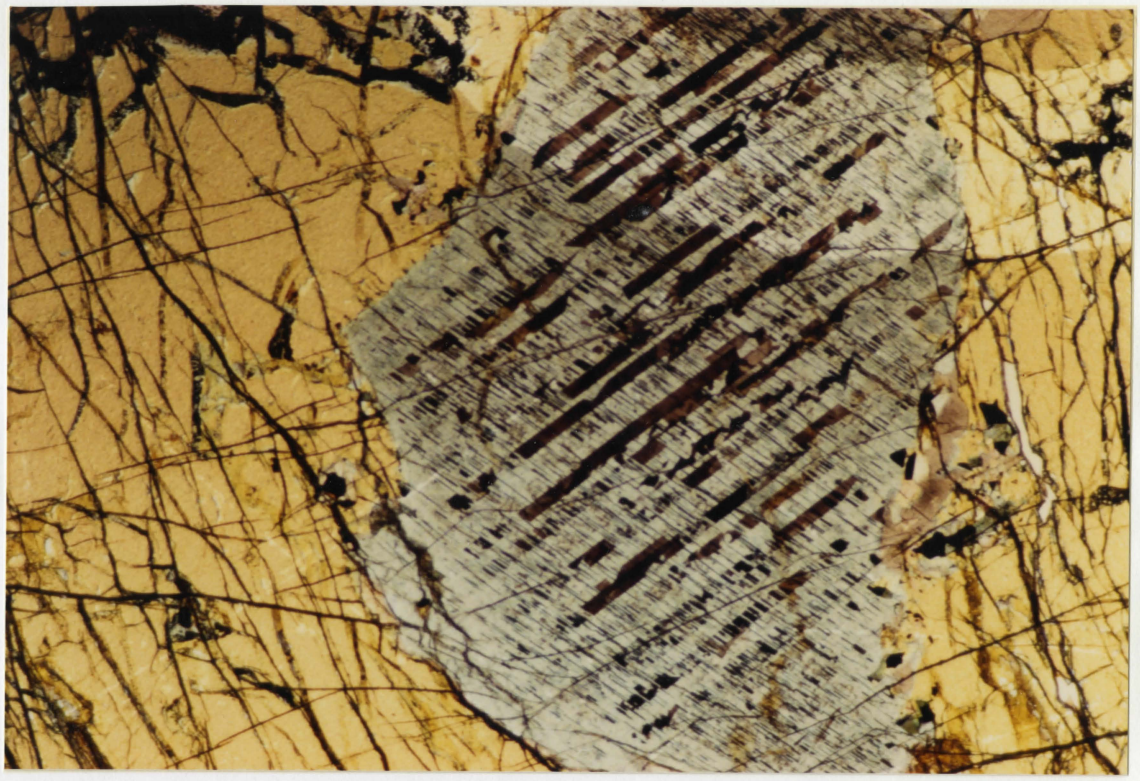

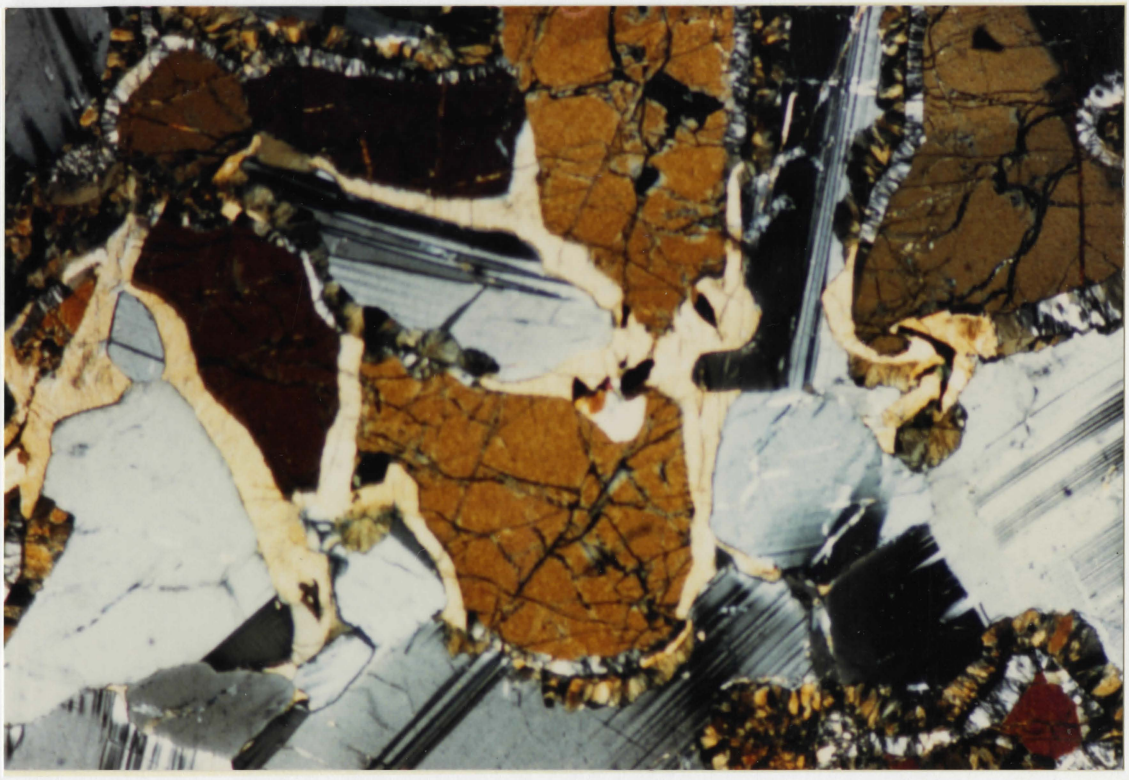

Figure 3.5

Double outer corona around olivine, showing an inner tabular spinel-poor amphibole layer, and an outer plumose, spinel-rich amphibole layer. Centre of picture shows hydrous replacement of olivine in 8511.

(ppl: x63) width of field is 1.5 mm

Figure 3.6

Late stage of corona development showing outer corona of fibrous amphibole with biotite and opaques surrounding a core of coarse-grained orthopyroxene and scattered vermicular biotite, from 8502.

(ppl: x25) width of field is 4 mm

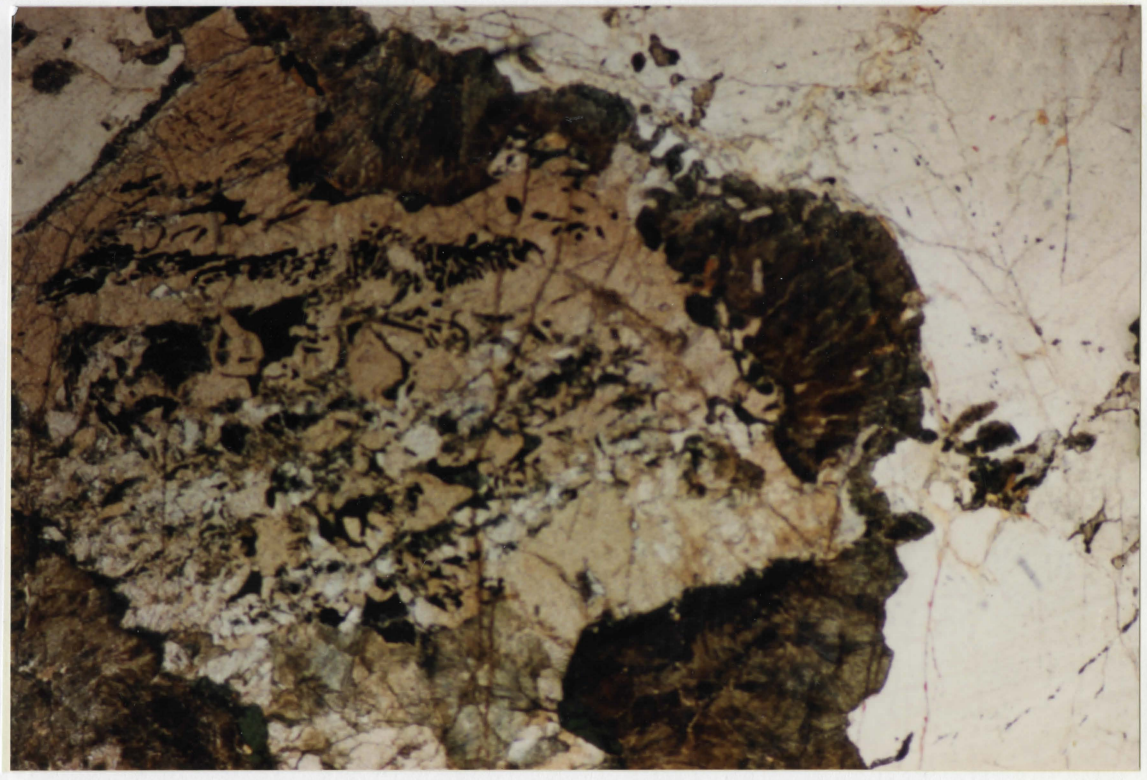

Figure 3.7

Spinel grain surrounded by red-brown biotite, which is in turn rimmed by a poorly-developed corona of hypersthene, from 8507.

(ppl: x63) width of field is 1.5 mm

Figure 3.8

Igneous textured gabbroic rock: subhedral to anhedral grains of ortho and clinopyroxene amongst subhedral laths and anhedral grains of plagioclase, from 8616 A.

(xp: x25) width of field is 4 mm

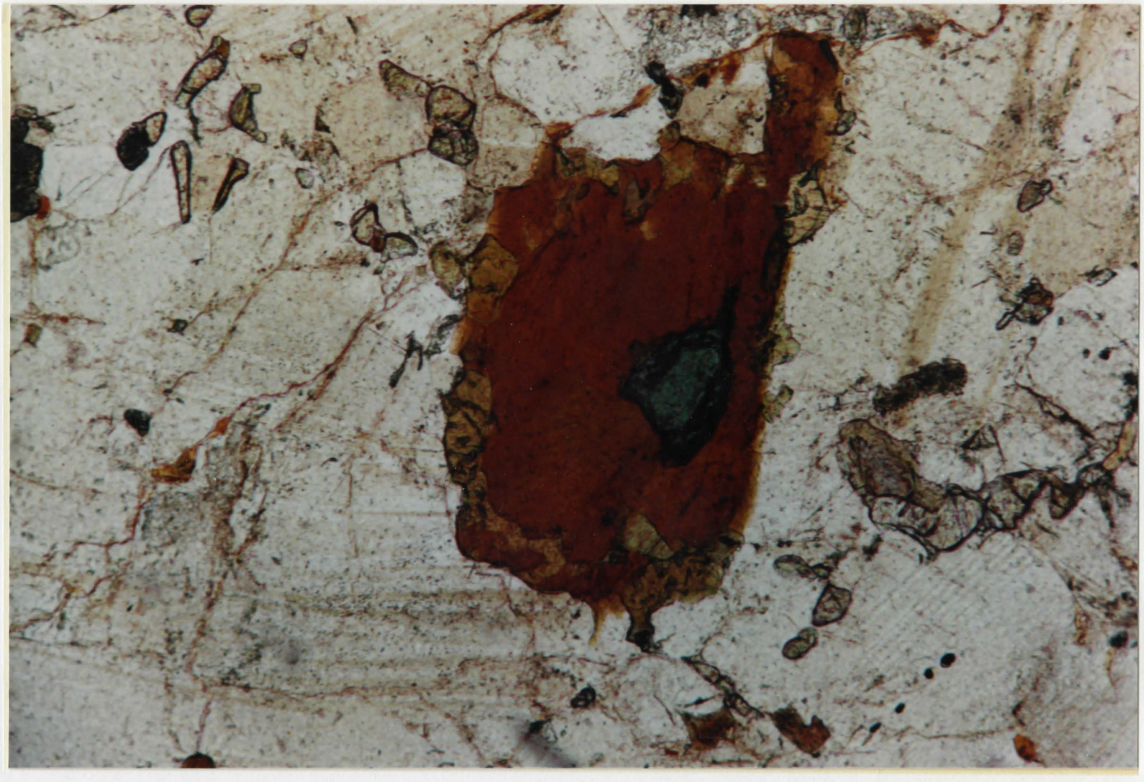

Figure 3.9

Coarse-grained, well-developed K-feldspar megacrysts in a K-feldspar megacrystic monzonite (sample 8617 A).

Width of field is about 6 cm

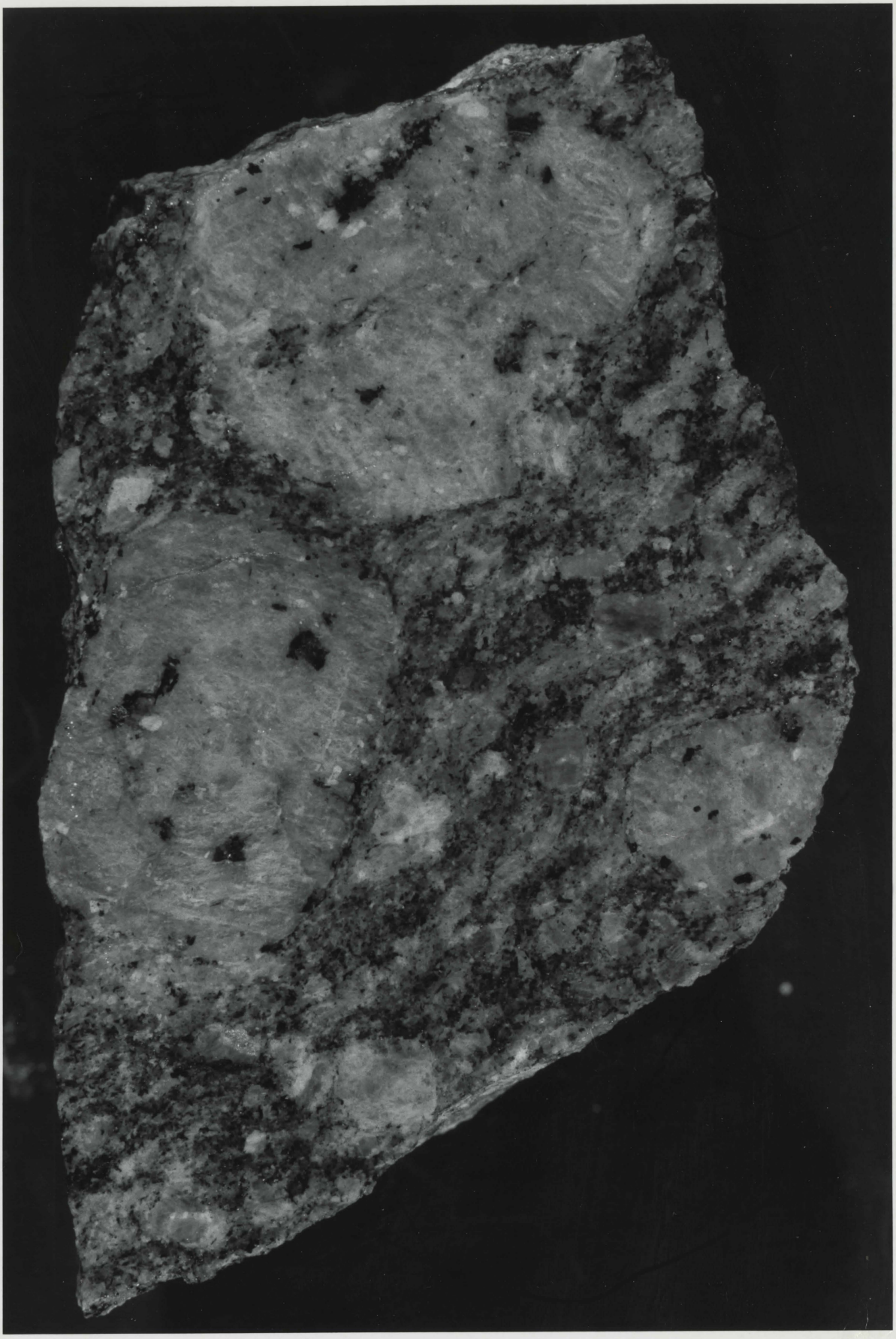

Figure 3.10

Anhedral garnet in augen structure where surrounding biotite, hornblende and quartz all "flow" around the garnet, from 8509.

(xp: x25) width of field is 4 mm

Figure 3.11

Allanite grain associated with biotite and opaques, showing distinct core and rim, with zoning of the outer rim, from 8509.

(xp: x160) width of field is 0.6 mm

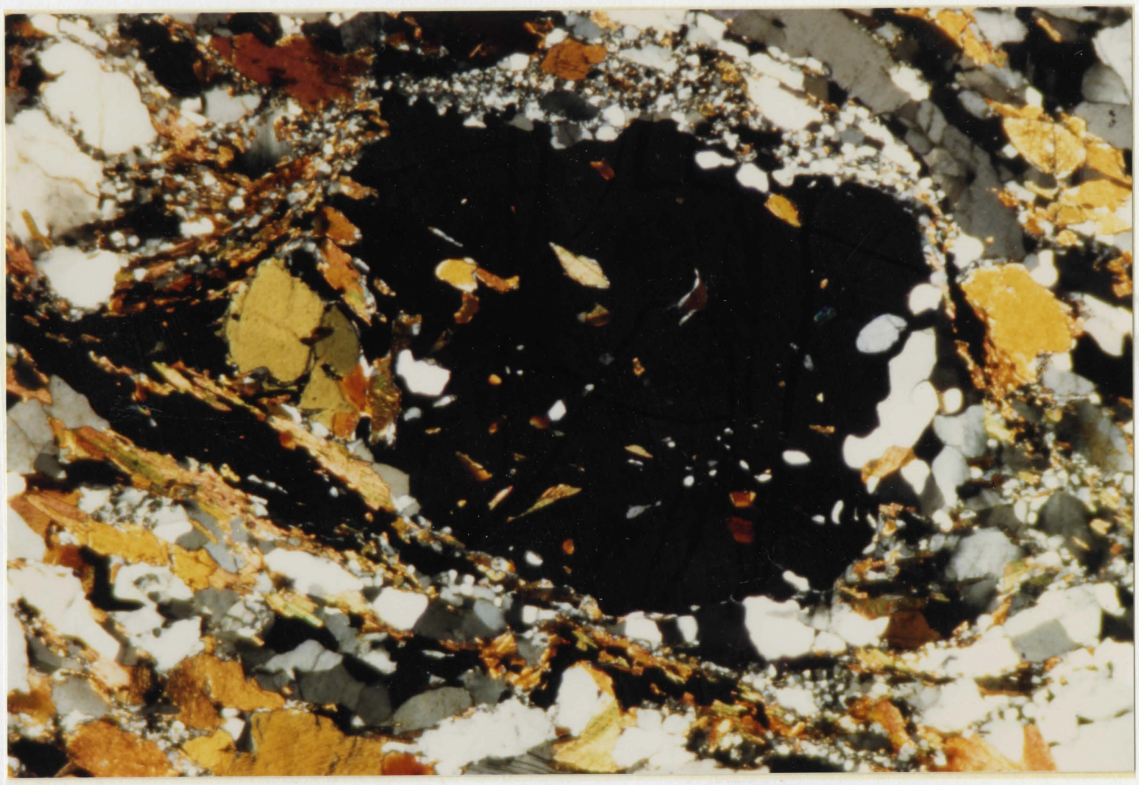

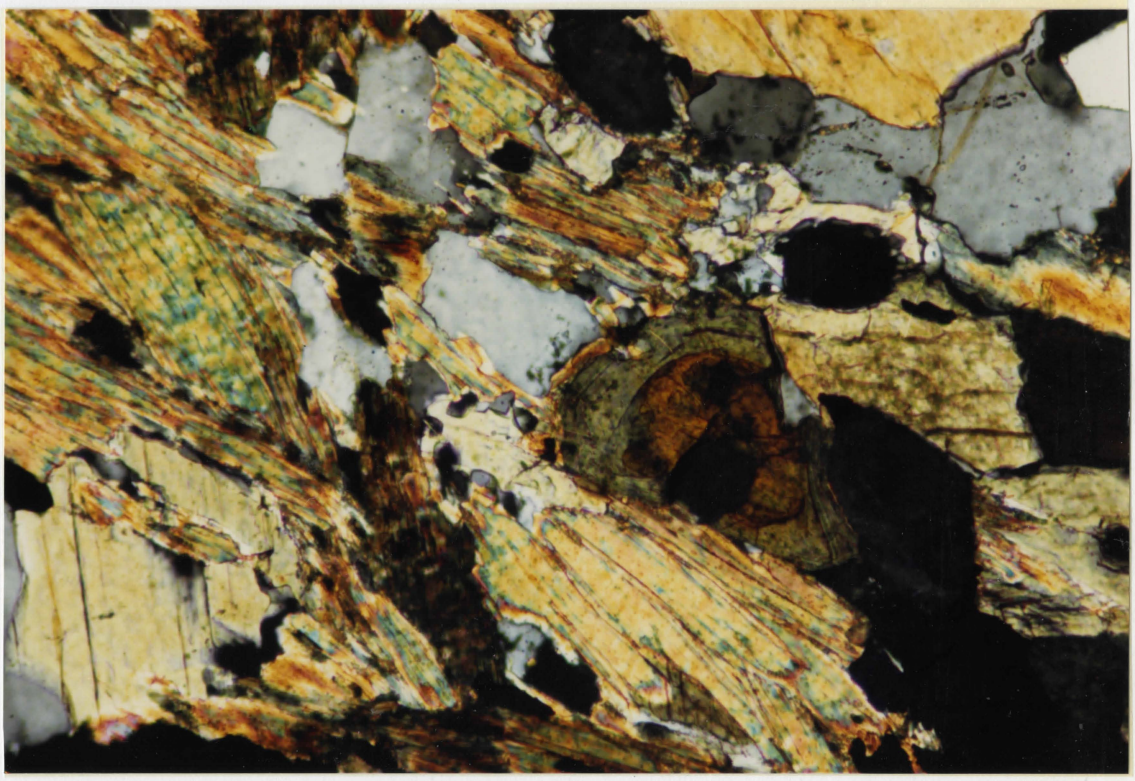

Figure 3.12

Garnet grain showing internal structure defined by opaque inclusions and biotite. The surrounding mica weakly circumvents the garnet but is essentially unaffected, in 8613.

(ppl: x63) width of field is 1.5 mm

Figure 3.13

Pennite chlorite associated with magnetite and biotite, showing a distinctive "saw-tooth" texture on the left, also from 8613.

(ppl: x63) width of field is 1.5 mm

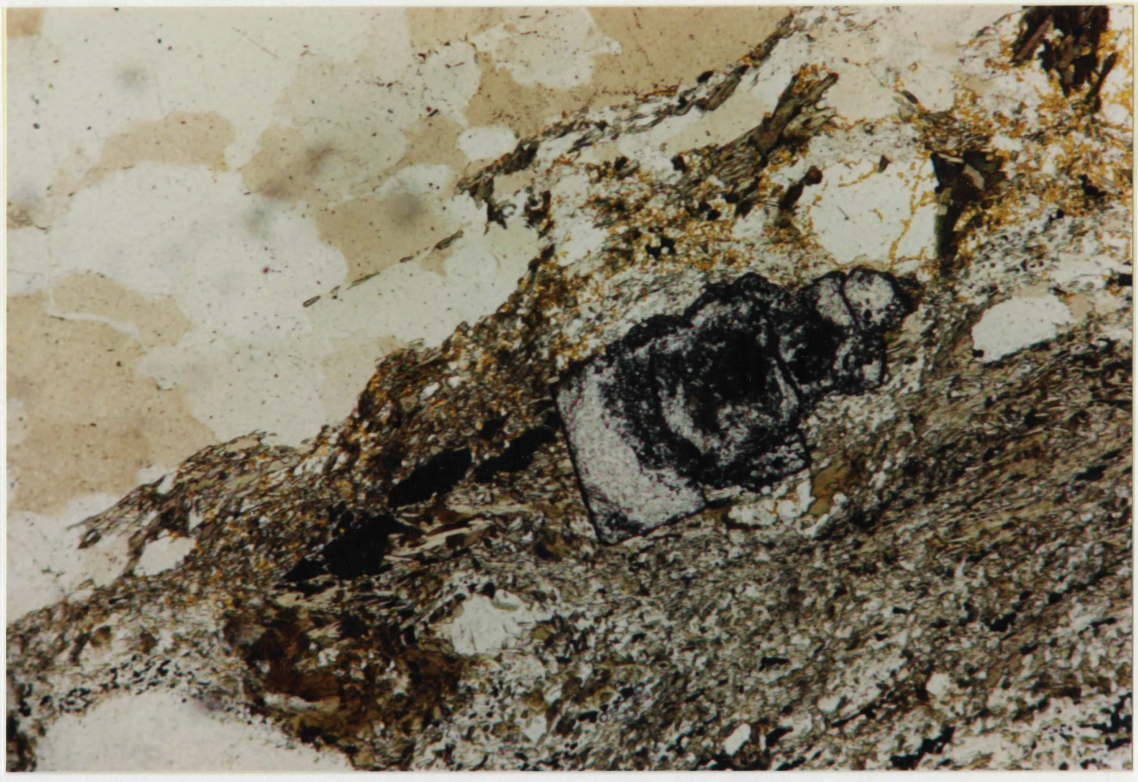

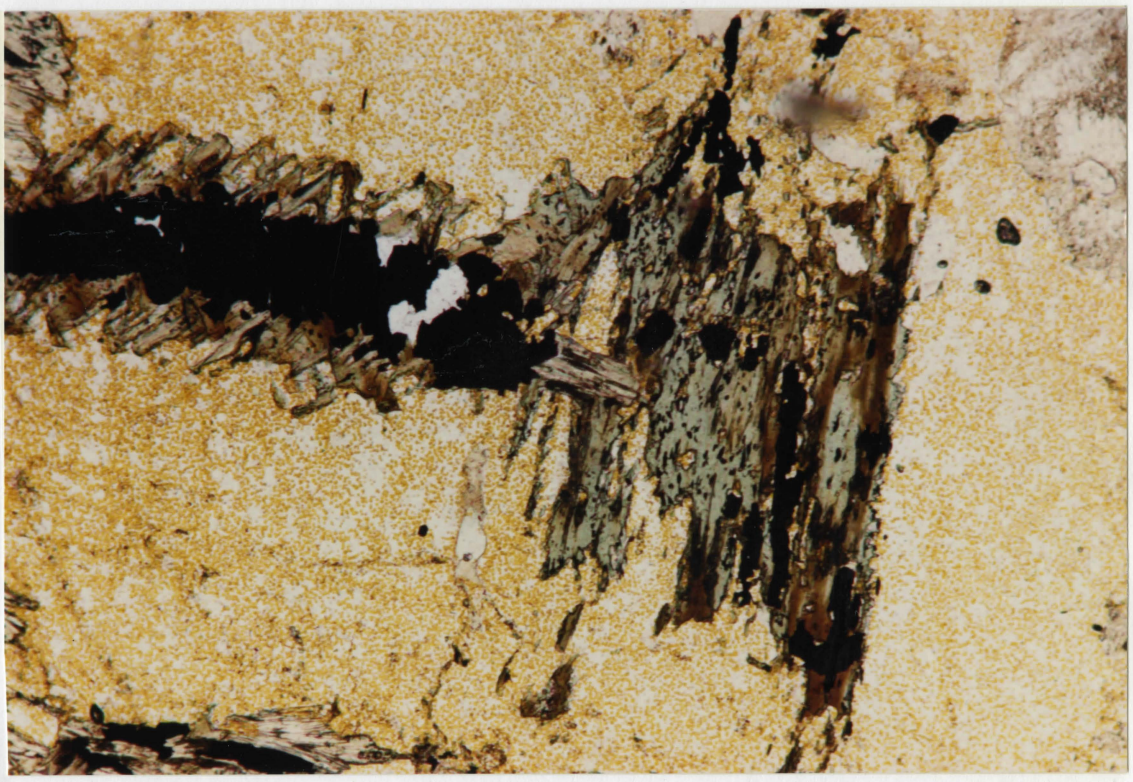

Figure 3.14

Calcite associated with quartz in between a coarse plagioclase grain and a band of strongly gneissose biotite, in 8613.

(xp: x63) width of field is 1.5 mm

Figure 3.15

Bright blue birefringent muscovite at the lower right superposed over biotite, as are sillimanite fibres at the upper left, in 8609 B.

(xp: x25) width of field is 4 mm

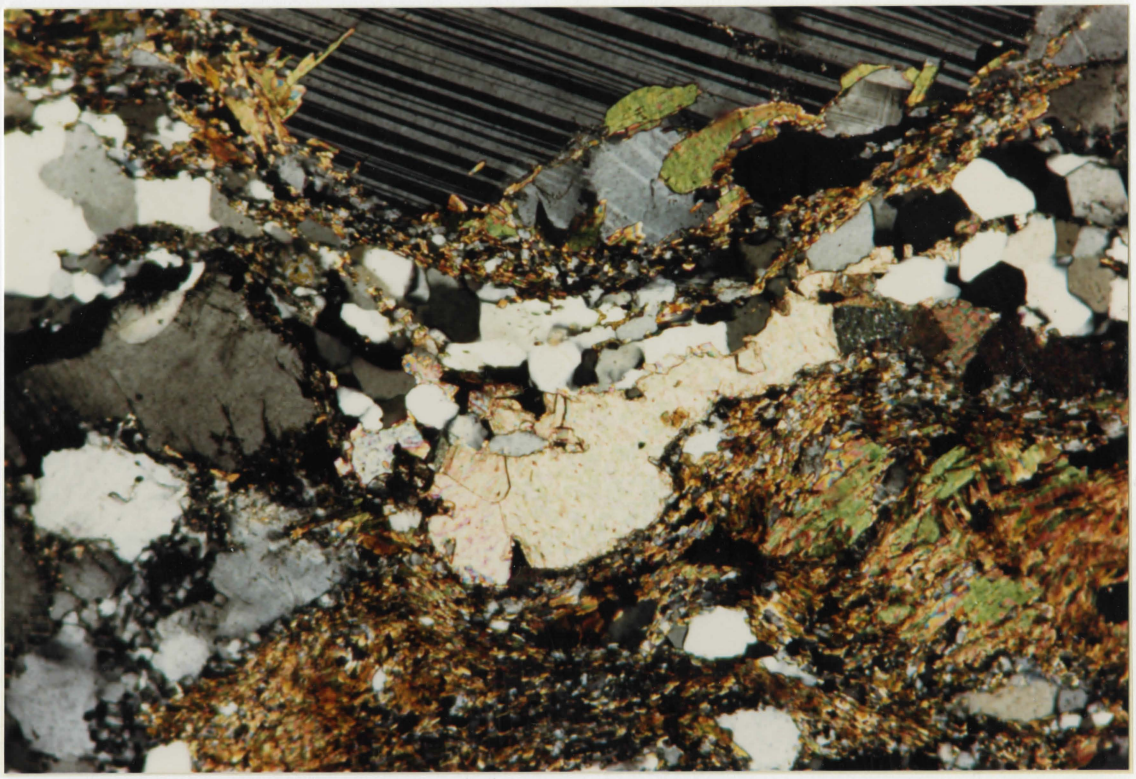

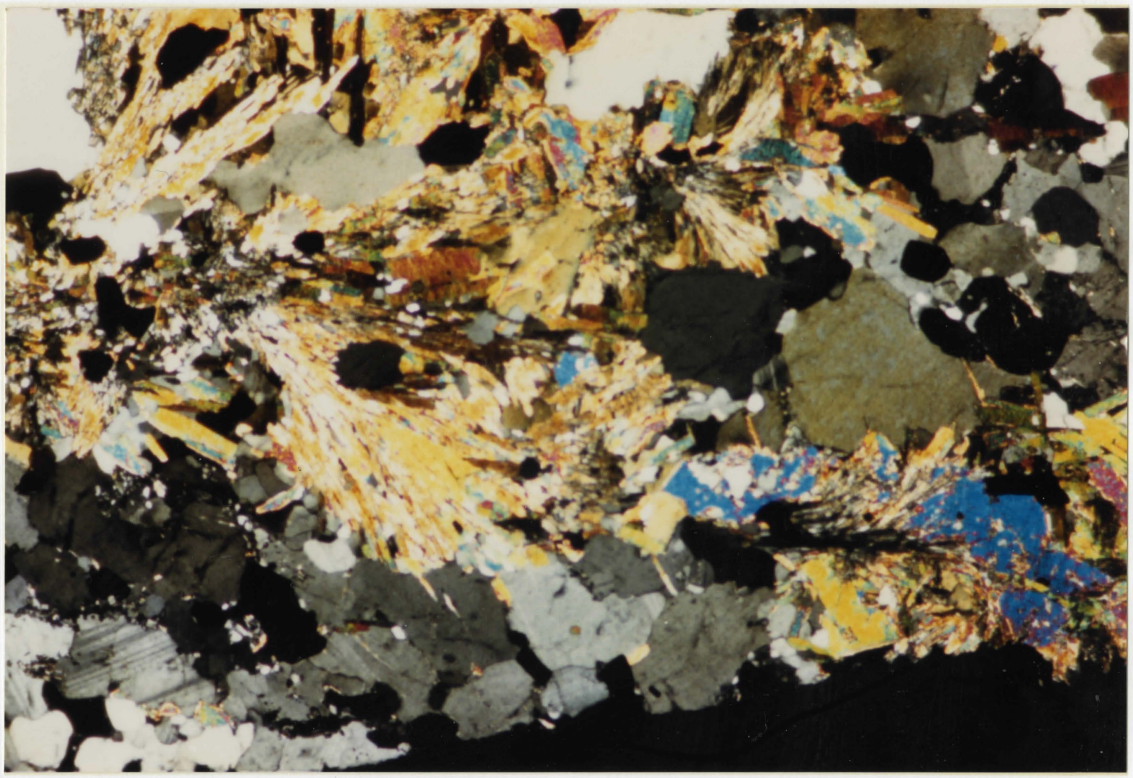

allanite is present in this unit, associated with the mafic mineral assemblage, in general, and in particular with zircon and sphene of similar grain size (0.5 mm), often intimately associated with apatite. The allanite is often rimmed by colourless, moderately birefringent mineral which may be epidote.

3.3 Paradise River Metasedimentary Gneiss Belt

3.3.1 Metasedimentary Gneisses

The rocks from the southwestern PMGB, outside the influence of the WBAC, are buff to black weathering grey gneisses. Rusty weathering restite bands and garnets are common in more heavily metamorphosed equivalents (diatexites) to the northwest (Gower et al, 1986). The rocks in this study are characterised by coarse-grained elongate pods or lenses up to 1.0 cm long consisting of microcline (1 - 2 mm long), quartz and plagioclase grains. Biotite and sillimanite are the common aluminosilicates.

The microcline is restricted to the coarser grained lenses, while quartz and plagioclase occur also as finer grains among the melanosome. Plagioclase is moderately to strongly sericitised, and often contains exsolved alkali feldspar and quartz. Albite and pericline twinning are

common, often bent or warped, but carlsbad twinning is absent. Michel-Levy tests on albite twins indicate a plagioclase composition averaging An_{35}. Quartz occurs as coarse grains within the leucosomic pods, showing moderately undulose extinction, as fine grains within the melanosome, and as sub-vermicular grains in plagioclase at plagioclase-alkali feldspar interfaces.

The melanocratic layers are composed of brown biotite and fibrous to columnar sillimanite, both minerals exhibiting a common, strong orientation. Sillimanite occurs as radial sheafs of fine acicular crystals, evenly distributed fine acicular crystals, clots of oriented columnar fibres, individual coarse grains, and very commonly as small equant grains, scattered throughout the melanosome. Opaques are present as elongate strings or shreds of magnetite and bright red-orange hematite. Biotite shows pleochroic haloes from 500-50 μm diameter inclusions of zircon grains.

Muscovite is common both as small shreds and as coarse flakes, associated with the sillimanite and biotite as shown in Figure 3.15, but oriented obliquely to the gneissosity, occasionally traversing leucosomic pods between two melanocratic layers. Radial biotite and sillimanite are often associated with leucosomic pods, where the sheafs of the radial minerals are oriented normal to the gneissosity.

Garnet, kyanite, and cordierite were not identified, although these minerals are reported elsewhere in this unit (Gower et al, 1986).

3.3.2 Anhydrous Pelitic Gneiss

Most of the rocks in the belt of "charnockitic gneisses" (Gower et al, 1986) adjacent to the gabbronorite are similar in texture and appearance to the PMGB gneisses discussed above, but near the contact the gneissosity disappears, grain size decreases, and orthopyroxene appears. These latter rocks are dark grey to black in colour, grey weathering, fine to medium grained and locally non-gneissose. Adjacent to the contact, the rocks are dominantly plagioclase, orthopyroxene and opaques, with biotite, quartz and minor alkali feldspar. The rocks are massive and the grain size is relatively coarse and much more equigranular than that further from the contact.

Plagioclase occurs as coarse grains, averaging about 2.0 mm, displaying albite and pericline twinning, exsolved blebs of alkali feldspar, and occasionally altered to patches of sericite. Michel-Levy tests indicate a bimodal plagioclase composition distribution, where the majority are around An_{40}, but some grains are labradorite, though varying widely from An_{53} to An_{69}. Quartz and alkali feldspar also occur as coarse grains, the former showing strongly undulose extinction.

Strongly pleochroic hypersthene is abundant, occuring as discrete subhedral to anhedral grains and as thin coronas around opaque grains, shown in Figure 3.16. Sillimanite is present as elongate laths within or rimming opaque grains, converting at the terminations to sheafs or clusters of fine fibrous sillimanite. Sillimanite also occurs as fine acicular needles lining the boundary between plagioclase grains, aligned normal to the grain contact.

The opaque grains are occasionally inset with green pleonaste spinel and/or zircon grains, and may also be inset with small rectangular grains of orthopyroxene, which shows weak pink colour or pink-brown to colourless dichroism. These hypersthene grains are usually terminated in radial biotite and sillimanite. Coarse grains of cordierite, showing characterisic twinning and pleochroic haloes around minute inclusions, are almost always in close association with this assemblage.

Biotite grains vary from coarse fresh red-brown flakes to fine laths intergrown with sillimanite. The coarse grained biotite is always associated with opaques, and is occasionally rimmed by hypersthene, as shown in Figure 3.17.

The other characteristic texture of these contact zone rocks, apart from the magnetite-hematite-sillimanite-biotite-

orthopyroxene assemblage, is a fine grained complex symplectite involving parallel branches of dendritic hypersthene associated with intergrowths of potash feldspar, quartz and cordierite, associated with relict osumilite, as shown in Figure 3.18. Stoichiometric osumilite is $(K,Na)(Mg,Fe)_2(Mg,Al)_3(Si,Al)_{12}O_{30}$ (simplified from Berg and Wheeler, 1976). The osumilite is never fresh in these rocks, as it is invariably being replaced by the above assemblage. However, the replacement assemblage often pseudomorphs subhedral outlines of the preexisting osumilite grain, and remnant osumilite is colourless with very low birefringence and uniaxial to biaxial with a small 2V. It may also display pleochroic haloes around small inclusions, although not to the same extent as in cordierite. Scattered throughout these symplectites are randomly oriented acicular sillimanite crystals, and occasionally biotite as well. Related textures include inclusions of vermicular quartz in cordierite (Fig. 3.19) and blebs of K-feldspar in plagioclase adjacent to the osumilite-symplectite. Quartz-plagioclase myrmekite is also present, hosted by K-feldspar. Less commonly, vermicular opaques associated with hypersthene are present (Fig. 3.20), although not obviously related to the osumilite-breakdown textures.

Serpentinous veins observed in sample 8604 crosscut all other minerals and structures.

Moving away from the contact (ie. from 8606 to 8608 to 8607), the finer grained hypersthene disappears. The feldspar becomes potassic and is characterised by a dusty brown colour and microperthitic texture. The acicular sillimanite rimming the feldspar grains becomes a much thicker layer, and a fine grained "groundmass" of sillimanite, alkali feldspar and minor biotite dominates the rock, presumably the precursor to the symplectite described above. Aggregates of polygranular re-crystallised quartz and feldspar (alkali and plagioclase) are present, also surrounded by sillimanite rims. Coarse microcline grains with microperthitic exsolution, fine vermicular intergrowths, and aligned inclusions of opaques and sillimanite are present in 8607. Intergrown with this are grains of quartz, clouded with opaques at the cores but with clear rims. The texture of 8607 is shown in Figure 3.21.

Coarser grained patches are dominated by plagioclase (showing albite and pericline twins), cordierite, hypersthene and sillimanite. Opaques are coarse grained and have variably embayed rims, still associated with hypersthene and sillimanite.

Fine grained sapphirine ($Mg_7Al_{18}Si_3O_{40}$; Newton et al, 1974) has been reported from these locations (Gower et al, 1986) and confirmed by microprobe analyses (Gower, pers. comm. 1987), but was not identified in these thin sections.

Further from the WBAC contact, but stll within the belt of charnockitic gneisses, from locale CG-85-310, hypersthene and osumilite by-products are no longer present, but the overall texture varies from strongly gneissose to sub-mylonitic. In the latter case the quartz grains are strongly elongated, with aspect ratios up to ten, often showing a feathered texture, shown in Figure 3.22. The elongation is principally defined by quartz, sillimanite, opaques (possibly graphite) and biotite. Megacrysts of plagioclase are present around which the fabric defined by the aforementioned minerals "flows". Whether or not these rocks can be more justifiably associated with the charnockitic pelitic gneisses or the "unaffected" paragneisses further away is debatable.

Figure 3.16

A zircon grain set in a partially hypidiomorphic opaque grain, which is in turn rimmed by a corona of strongly pleochroic hypersthene, from 8606.

(ppl: x63) width of field is 1.5 mm

Figure 3.17

Well-developed biotite and associated opaques surrounded by thin, discontinuous rims of hypersthene, from 8606.

(ppl: x25) width of field is 4 mm

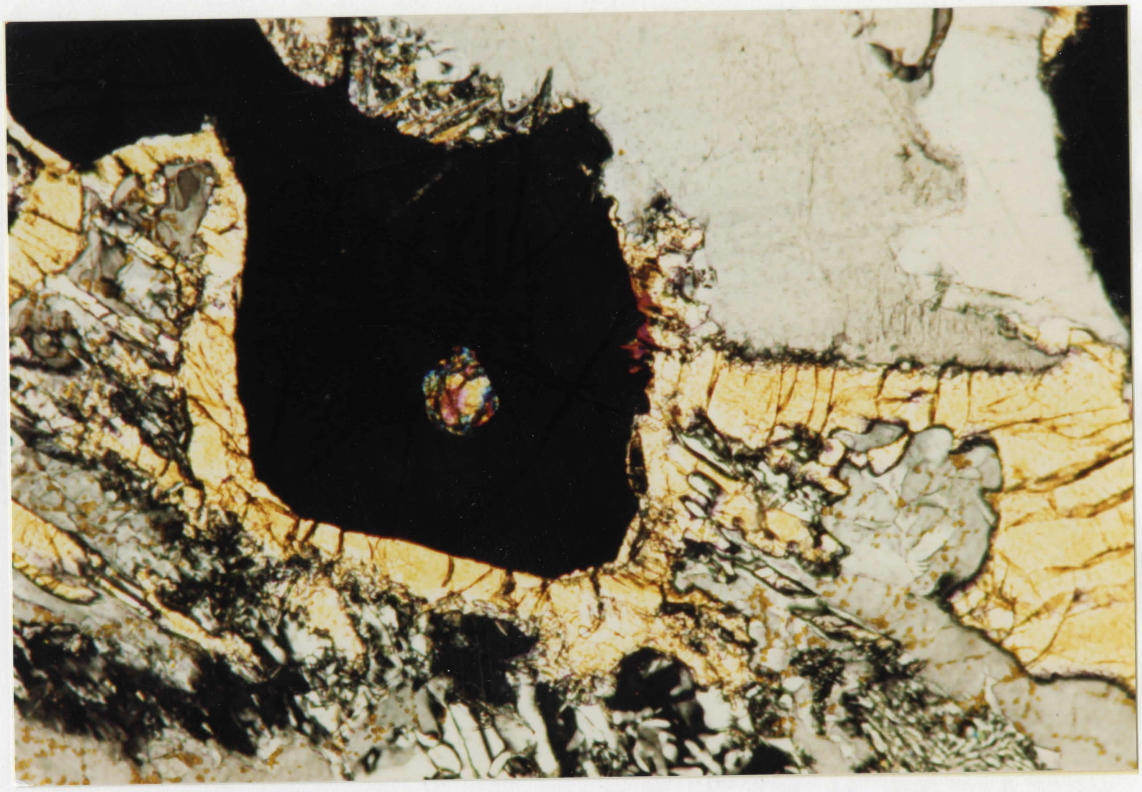

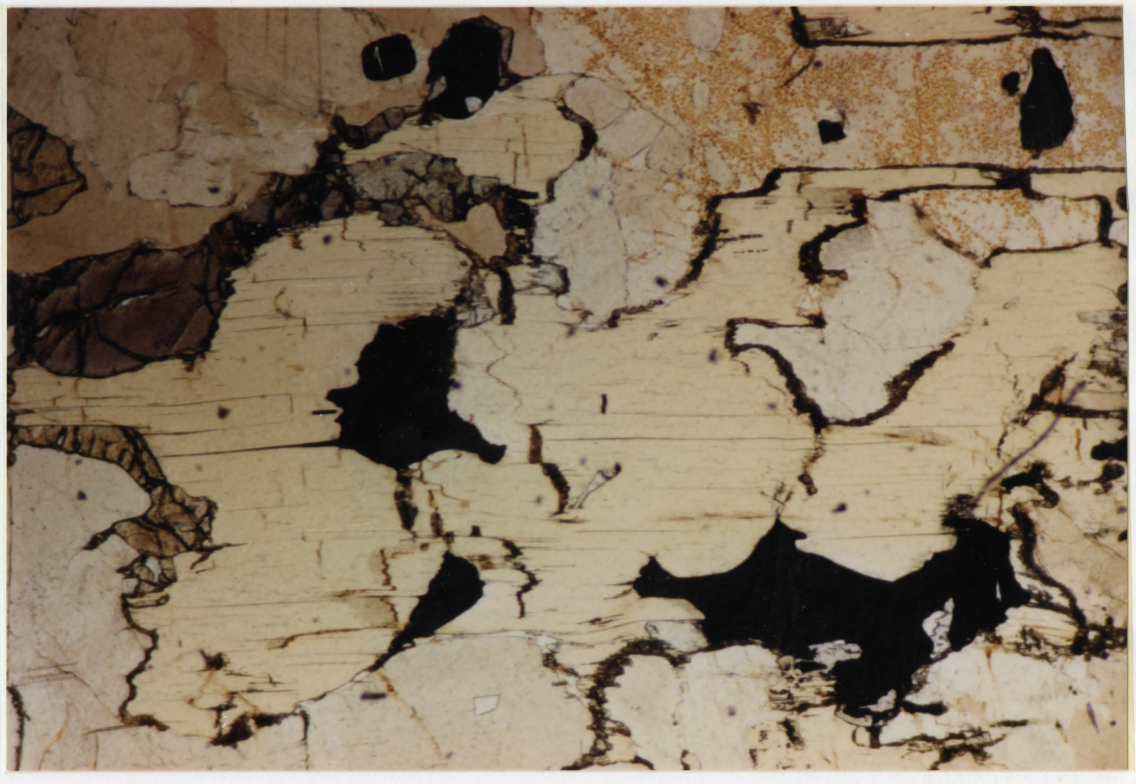

Figure 3.18

Complex intergrowth of quartz, K-feldspar and cordierite with dendritic hypersthene, produced by the breakdown of osumilite, in sample 8604.

A: Crossed polars show fine-grained myrmekitic intergrowths of low refractive index minerals

(xp: x25) width of field is 4 mm

B: Dendritic hypersthene grains, with fine sillimanite laths distributed interstitially. At the upper right the edge of the pre-existing osumilite grain is visible

(ppl: x25) width of field is 4 mm


A

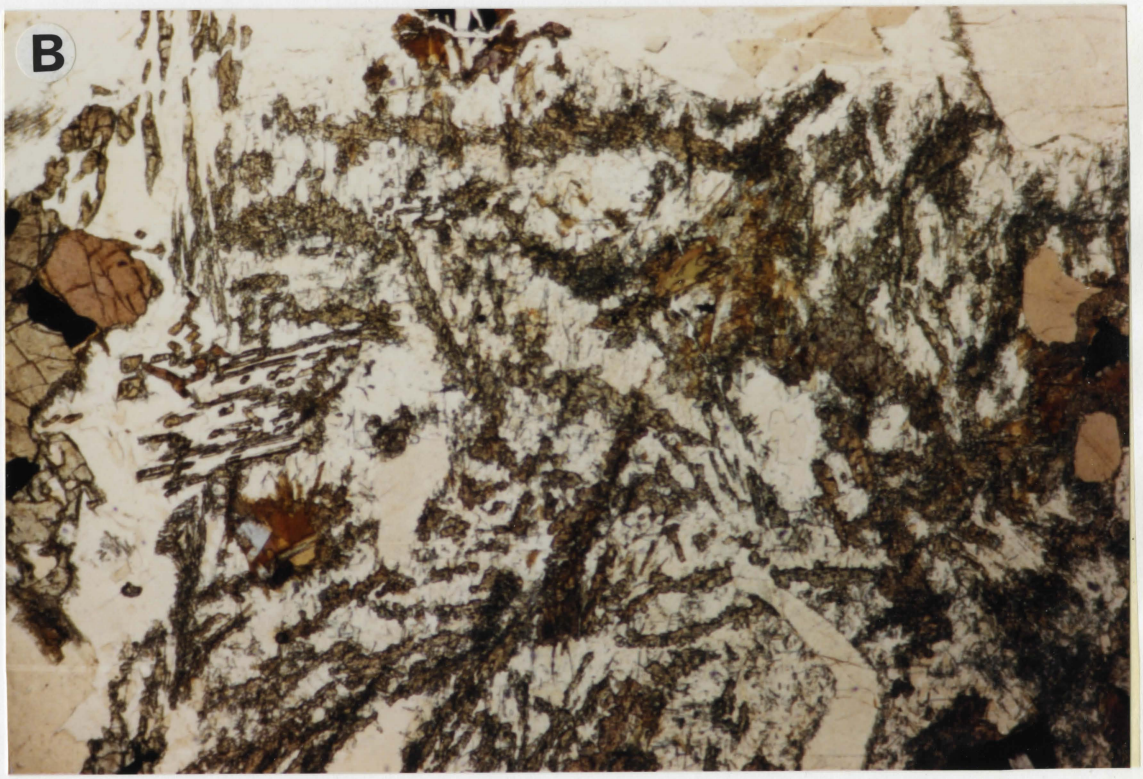
B

Figure 3.19

Coarse-grained intergrowth of cordierite and quartz, associated with osumilite breakdown products (not shown), from 8606.

(xp: x25) width of field is 4 mm

Figure 3.20

Vermicular opaque intergrown with orthopyroxene, hosted by plagioclase in 8604.

(ppl: x63) width of field is 1.5 mm

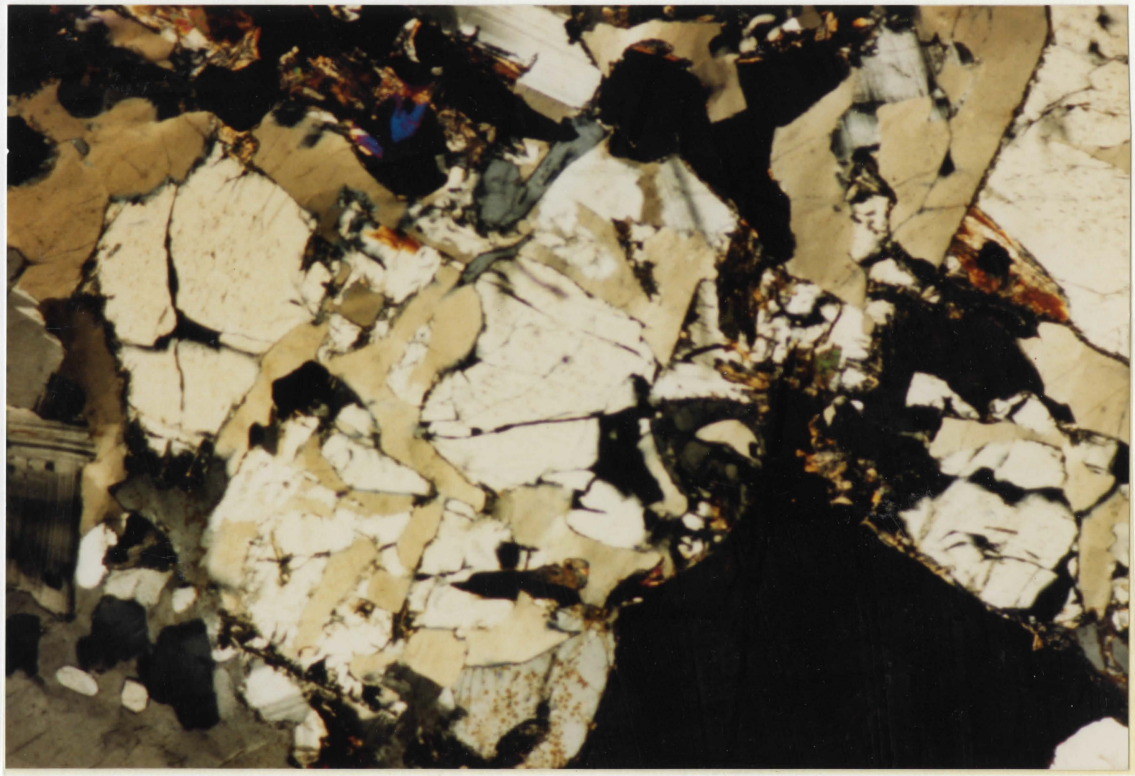

Figure 3.21

Grains of quartz (clear grey to white colour) and fine grained, chert textured feldspathic grains (dark grains with light flecks) surrounded by thick intergranular rims of sillimanite fibres, from 8607.

(xp: x25) width of field is 2.5 mm

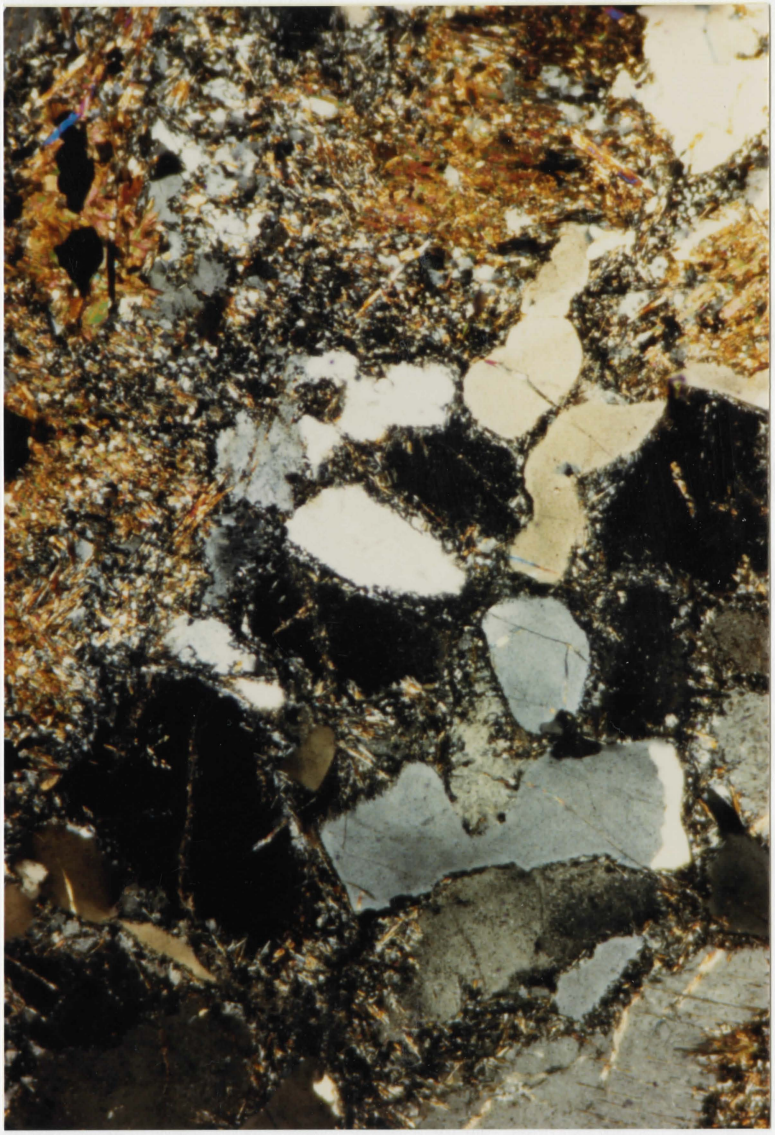

Figure 3.22

Mylonitic to sub-mylonitic paragneiss shown in outcrop in A, from (CG-85) 310, and in thin section in B, showing feathered texture of deformed quartz grains.

B: (xp: x25) width of field is 4 mm

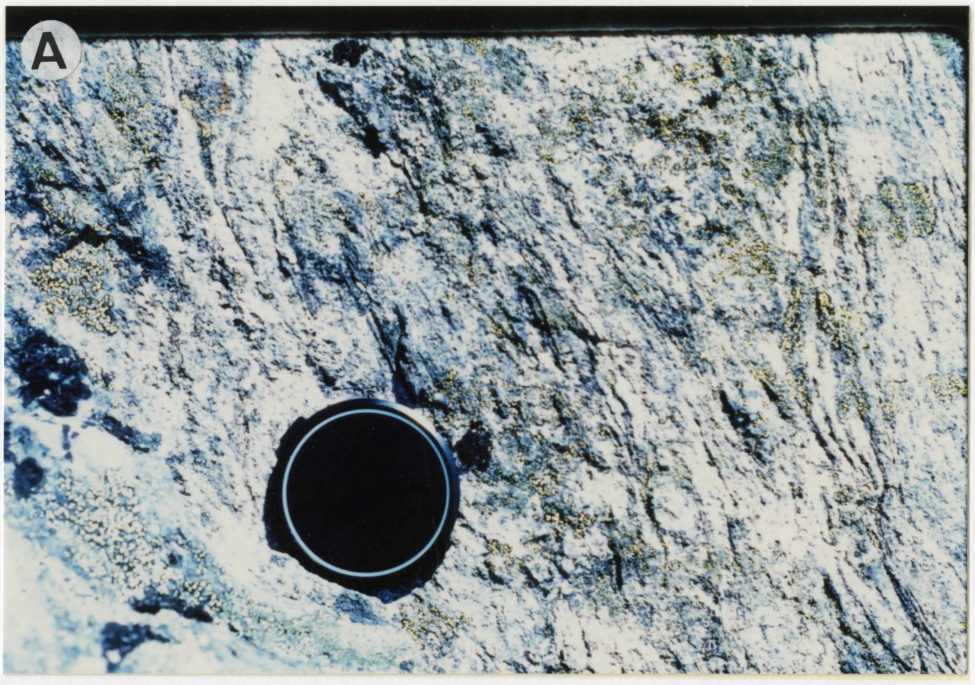
A

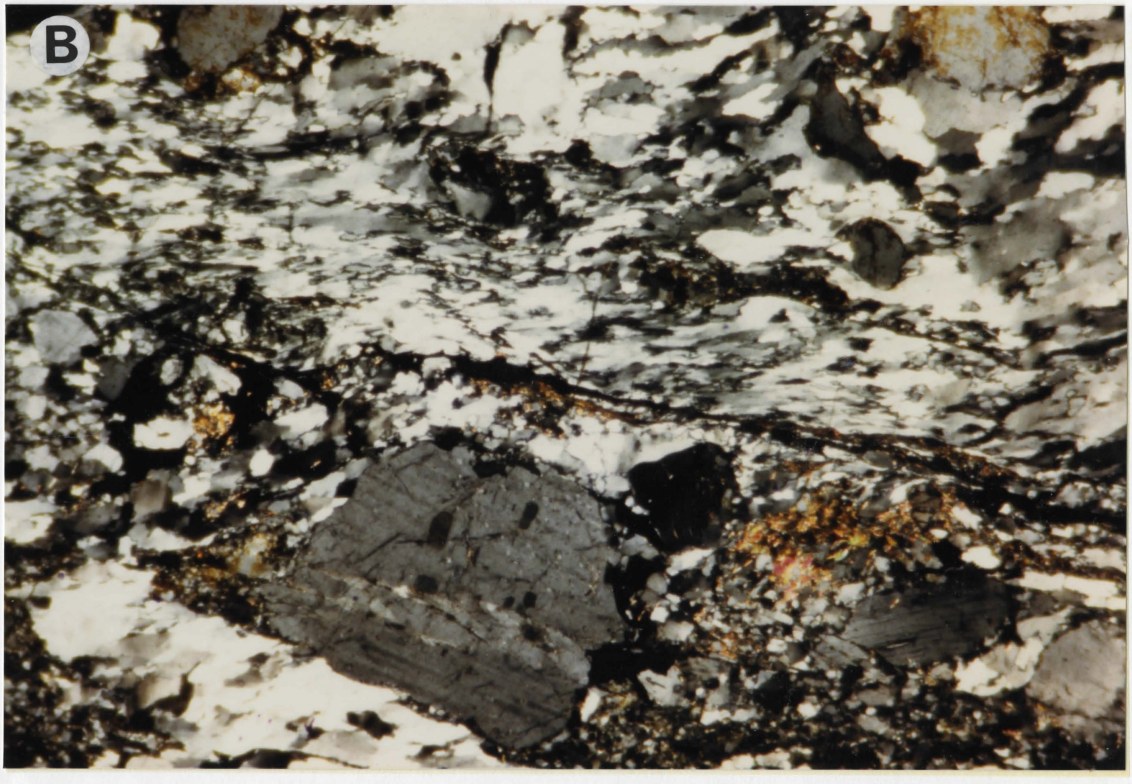
B

CHAPTER 4: DISCUSSION OF PETROGRAPHY

4.1 WBAC Gabbronorites

Based on the modal analyses presented in Appendix 1, the mafic members of the WBAC, including the SHBP gabbronorite, can be classified using the gabbroic rock triangles of Streckeisen (1976), as shown in Figures 4.1 and 4.2. Based on this classification scheme the mafic suite can be classified as anorthosite to leucogabbronorite.

The earliest crystallising phases are calcic plagioclase and magnesian olivine, where plagioclase laths are overgrown and pseudomorphs of well developed olivine faces are present. Primary intercumulus ilmenite, common in similar coronites (eg. Starmer, 1969), is not common in these samples, and all primary intercumulus opaques are invariably associated with green spinel. Coarse grains of magnetite and/or green spinel associated with relict olivine cores appear to be secondary products of olivine breakdown, and are not themselves rimmed, although magnetite may be associated with biotite in more evolved coronites. Augitic clinopyroxene crystallised in the intercumulus spaces between plagioclase crystals, as did orthopyroxene, in the olivine-free or olivine- poor rocks. As total "pore material" (ie. pyroxenes and oxides) comprise > 5 vol. % of the rock, this is an ortho-cumulate (Wager *et al.*,

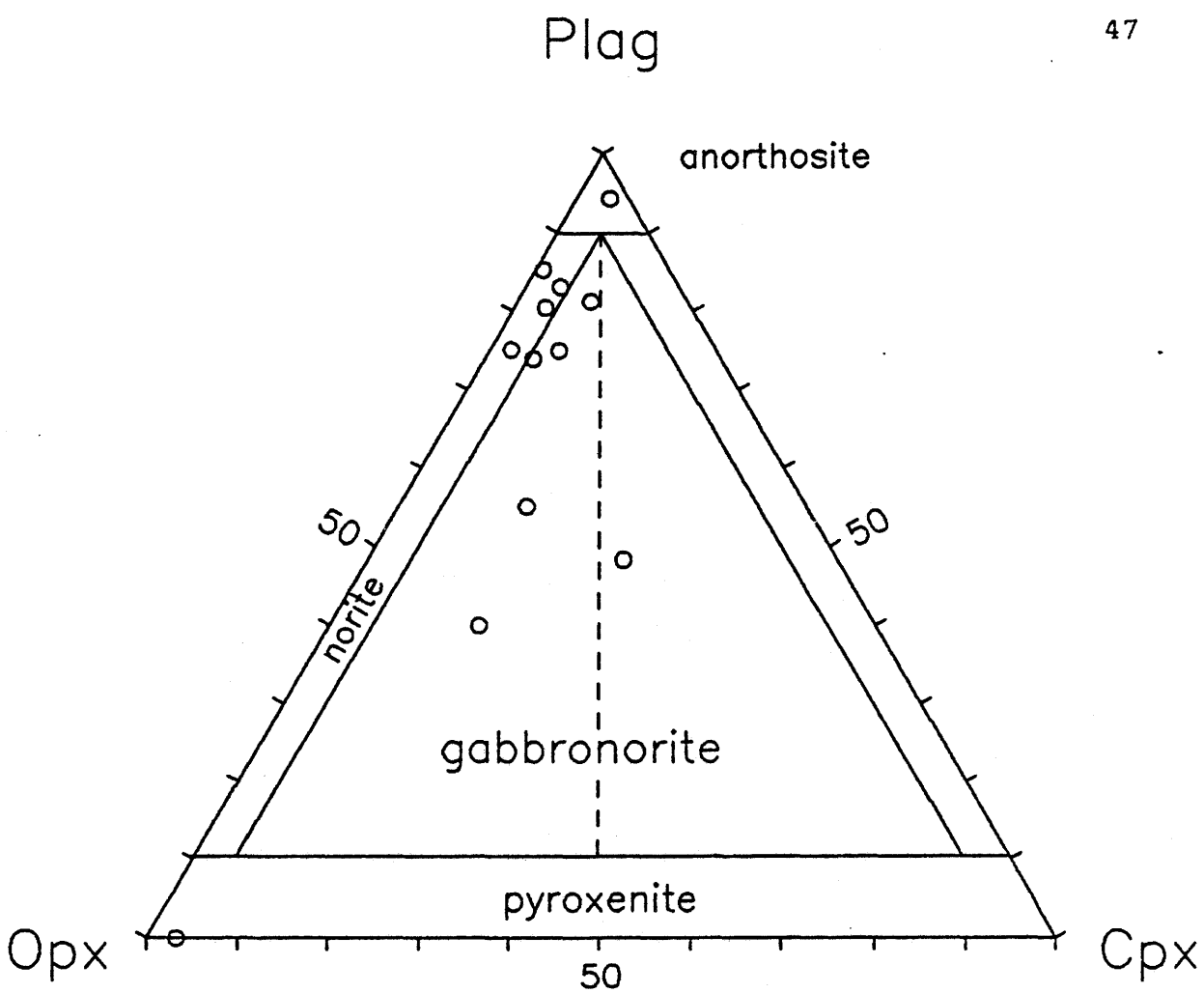

FIGURE 4.1

Modal plagioclase-orthopyroxene-clinopyroxene ternary diagram (Streckeisen, 1976) for WBAC mafic rocks

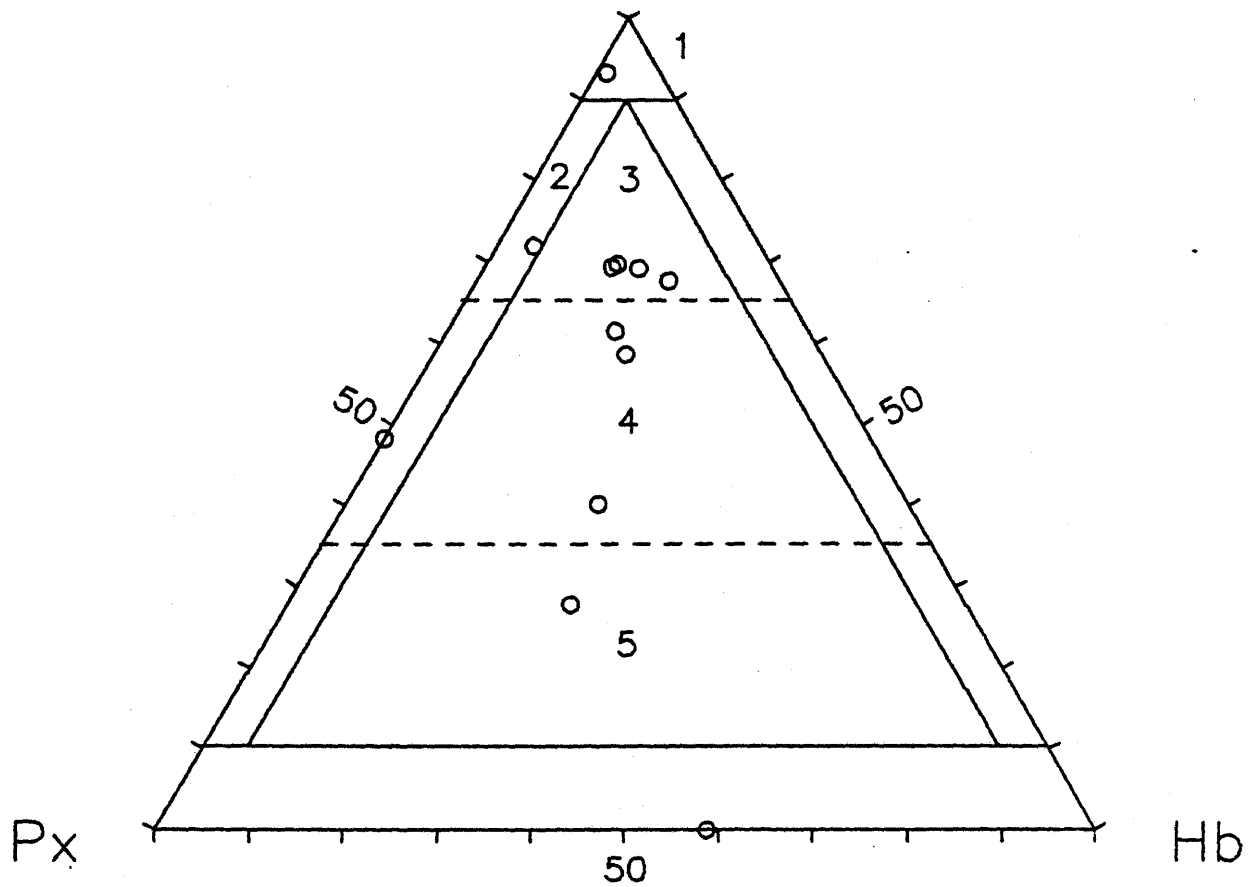

FIGURE 4.2

Modal plagioclase-pyroxene-amphibole ternary diagram (Streckeisen, 1976) for WBAC mafic rocks

Field: 1 = anorthosite
2 = leucogabbronorite
3 = leucopyroxene-hornblende gabbronorite
4 = pyroxene-hornblende gabbronorite
5 = melapyroxene-hornblende gabbronorite

1960).

Clouding of the plagioclase by fine particles of iron oxides and spinel is a phenomenon common to coronites (eg. Murthy, 1958; Reynolds and Frederickson, 1962), and is thought to predate corona formation (Murthy, 1958) but appears to continue on as corona development progresses, such that the more evolved coronites have the more densely clouded plagioclase (Starmer, 1969; Emmett, 1982; this study) until late-stage resorption of the spinel as hydrous metamorphism and recrystallisation of the plagioclase occur. The mechanism for generating these fine inclusions in plagioclase involves the diffusion of Fe and perhaps Mg rich fluids into the plagioclase along discontinuities generated by submicroscopic-scale unmixing of plagioclase, facilitated by prolonged elevated temperatures and water vapour activity (Starmer, 1969; Emmett, 1982). Clear plagioclase rims adjacent to the outer corona around olivine develop after slight clouding has already occurred and synchronously with the formation of the outer corona, according to Starmer (1969). This rim represents a corona of recrystallised plagioclase, where the spinel and Fe oxides have been resorbed and either redistributed in the plagioclase further from the corona or reprecipitated as small magnetite grains in the plagioclase or amphibole. Starmer (1969) suggests that the recrystallised rims lack the dislocations generated by unmixing seen in the (plag.) cores

and hence do not provide sites for fine inclusions to reappear.

According to Starmer (1969), and supported by this study, the hydrous secondary alteration of olivine to serpentine, bowlingite and iddingsite occurs before corona formation because these hydrous minerals, as well as magnetite and hematite, pseudomorph after olivine in rocks with relatively poorly developed coronas and can also be observed in the core of coronas where olivine has been completely replaced by orthopyroxene. This suggests that the olivine was altered along rims and fractures at an early stage.

The main stage of corona development, involving the formation of orthopyroxene and amphibole-spinel symplectite coronas around olivine, is thought to represent synchronous and mutually dependent replacement of olivine and plagioclase respectively by the above minerals (eg. Murthy, 1958; Reynolds and Frederickson, 1962; Frodesen, 1968; Starmer, 1969; Mason, 1969; Griffin and Heier, 1973; England, 1974; van Lamoen, 1979; Emmett, 1982; Emslie, 1983; Mørk, 1985; Mørk, 1986; Gower, 1986). The coronas are formed by reaction between solid plagioclase and solid olivine or pyroxene, although the complete absence of a melt phase in the rock is not necessarily required (Ashworth, 1986b). In contrast, Joesten (1986a, b) favours a primary magmatic origin for this type of

corona based on petrographic, geochemical, and thermodynamic arguments.

Murthy (1958) lists criteria for distinguishing between magmatic reaction rims (ie. between early crystals and later melt) and metamorphic coronas, summarised in Table 4.1. Joesten (1986a) notes that the grain boundaries between orthopyroxene coronas and plagioclase are convex towards orthopyroxene and consequently towards olivine as well, and thus olivine-orthopyroxene displays cuspate terminations. He argues that these features support a magmatic-dissolution related origin rather than a diffusion-controlled origin for the orthopyroxene layer. While the curvature of the olivine and inner corona and the presence of cuspate terminations may be shown to be of magmatic origin, the relevance of this point to the origin of the orthopyroxene is not evident. A diffusion-controlled origin for the orthopyroxene whereby it grows inwards from a primary magmatic olivine, complete with cusps and concavities, is certainly not excluded by this argument.

Joesten (1986a) comments that at the cusps the inner corona should thicken and the outer coronas thin in a diffusion-controlled model. In the WBAC coronites the amphibole-spinel outer corona does indeed thin at the corners of the cusps, but the orthopyroxene does not show thickening.

TABLE 4.1

MAGMATIC REACTION RIMS VS. METAMORPHIC CORONAS

CRITERION	REACTION RIMS	CORONAS
Olivine Composition	Fe-poor olivine	no restrictions
Rim Width	Dependent upon ol. grain-size	Independent of grain size; dependent on water concentration
First corona mineral	Opx or pigeonite	Invariably opx
Opx morphology	Long prisms	Short prisms
Mineral orientation	Tangential to contact	Radial
Mineralogy of outer rim	ol-plag rxn.: produces NO amph-spinel rims	plag replacement: produces amph/sp, garnet, amph rims
Secondary effects	No clouding or recrystallisation	Clouding of plag, cpx, ol; recryst. of px possible
Garnet	Garnet absent	Garnet present

from Murthy (1958)

However, in the cusps the orthopyroxene layer as a whole is indeed thicker, in most cases, as a result of the proximity of the sides of the cusp creating a folding over or intersection of the opx coronas. This is also the case in the Risör coronas discussed by Joesten, but why this is inconsistent with diffusion-controlled growth is unclear. It does not appear that a diffusion-controlled mechanism can be ruled out based solely on petrographic textural evidence.

The orthopyroxene corona represents an inward-moving replacement of olivine and the amphibole-spinel symplectite represents an outward-moving replacement of plagioclase. Hence, the observed boundary between the inner and outer coronas represents the original olivine-plagioclase contact (eg. Griffin and Heier, 1973), except by Joesten (1986a), who maintains that the olivine and the plagioclase were never in direct contact at any time. Occasional transgressions of fibrous amphibole into the orthopyroxene layer may represent local micro-environments where higher water or ionic concentrations have allowed amphibole, nucleating from the inner edge of the outer corona, to grow inwards for short distances as radial sheafs. In general the original boundary is preserved intact.

Joesten (1986a) notes the elongate triangular shape of the orthopyroxene grains, with the apex at the symplectite-opx

contact. He refers to this as "columnar impingement microstructure", consistent with nucleation of orthopyroxene at the original olivine-plagioclase contact and subsequent inward growth into the olivine. He states that grains with their fast growth directions aligned perpendicular to the growth surface (the grain contact) are favoured, and will grow across the full width of the corona layer, pinching out less favourably oriented grains.

Occasionally, in relatively weakly developed coronites of this study (eg. Sample 85-11), the fibrous amphibole outer corona can be differentiated into a distinct inner and outer corona itself; an outer plumose textured amphibole-spinel-symplectite corona, and an inner spinel-free amphibole corona, with parallel grain boundaries normal to the contact. These may be analagous to the columnar and tabular microstructures respectively discussed by Ashworth (1986b), although his tabular amphiboles are single grains in optical continuity over large distances, which are not observed in the sampled WBAC coronas to the same degree as in the Risör rocks (Joesten, 1986a; Ashworth, 1986b). Ashworth (1986b) suggests that the tabular microstructures represent amphibole which has nucleated onto primary magmatic (non-fibrous) amphibole, and hence grew in optical continuity with it, but no non-fibrous amphibole is observed in the WBAC gabbronorites.

Griffin and Heier (1973) have applied the theory of spherulite crystallisation (Keith and Padden, 1963) to corona formation, as both processes involve the crystallisation of phases in a cooling environment. While Griffin and Heier (1973) do not suggest a primary magmatic origin for coronas similar to those in the WBAC, the spherulite analogy requires that the centre of the radial system is the maximum latent heat source. This is valid for both primary magmatic crystallisation or sub-solidus "deuteric" diffusion-related crystallisation, but is difficult to reconcile with secondary metamorphic origin. Keith and Padden (1963) noted that impurities dissolved in the melt create disproportionate increases in melt viscosity and hence a corresponding decrease in the growth rate of the solid. Therefore, the growth rate is dependent on the impurity content in the melt, or matrix, as well as on the outward diffusion of latent heat. As impurities are preferentially excluded from the growing solid phase, a concentration gradient of the impurity is generated in the adjacent matrix, with a maximum at the interface, and a minimum further away where the concentration equals that in the matrix. The width of this impurity layer is defined by Keith and Padden (1963) as $\delta = D/G$, where D is the diffusion coefficient for the impurity in the matrix and G is the growth rate of the crystal in one dimension, ie. along the fibre axis. The nucleation and growth of new crystal occurs within this layer, dependent upon the size relationship between δ and

the average cell diameter "d", equivalent to the diameter of the nuclei from which crystal growth occurs. They found that for cellular growth, of which spherulitic crystallisation is a variation, $d \approx \delta$.

As pure crystal attaches to the nucleation site, excluded impurities collect in the interfibrillar spaces, causing localised depression of the equilibrium melting temperature. If crystal growth is sufficiently slow, relative to the rate of radial outward diffusion of latent heat, then no significant temperature gradient is created. As a result of this essentially isothermal growth, the impurity enriched material between the growing fibres does not crystallise, and consequently elongate fibrous projections develop. Applying this spherulite analogy to the amphibole-spinel sympectite corona, if the growth rate, dependent on the impurity concentration gradient, decays at a slower rate than the heat diffusion rate, then a critical point would be reached where the impurity-rich interfibrillar material could nucleate, forming "impure" (Fe and Mg enriched amphibole) and spinel from excess bivalent Fe and Mg excluded from the amphibole. This critical point would represent the spinel-rich zone marking the transition between tabular and columnar amphibole. As the ratio of the growth rate to latent heat diffusion rate continues to grow, the nucleation and growth of more impurity-rich material would occur, producing elongate rods of spinel

and impure amphibole. According to Keith and Padden (1963), low angle branching would occur rather than thickening of the amphibole fibre, since fibre width is dependent on δ, which would be decreasing if anything, since temperature is decreasing away from the centre. This branching would generate the sheaf-like plumose microstructures seen in the outer coronas, referred to by Ashworth (1986b) as columnar microstructure.

Single optically continuous orthopyroxene grains without outer amphibole-spinel coronas are difficult to reconcile with a post-magmatic diffusion related origin. Ashworth (1986b) suggests that these orthopyroxenes have either nucleated from primary orthopyroxene or have nucleated epitaxially onto the amphibole corona. The latter explanation is precluded by the absence of the amphibole corona, and the absence of a radial inner layer might preclude the formation of an outer layer by removing the nucleation template for radial growth, although this would be indistinguishable from primary development of the whole orthopyroxene corona.

According to Starmer (1969), the presence of thin, discontinuous coronas of amphibole around primary pyroxenes reflects the fact that the plagioclase and the pyroxene are essentially in chemical equilibrium, based on the observation of later garnet coronas in the Risör rocks, not observed in

the WBAC coronites. Alternatively, the coronas are late-forming and have not had time to develop as fully as their counterparts around olivine. In rocks with poorly developed coronas around olivine, clinopyroxene has no corona, and in rocks with relatively well developed coronas clinopyroxene shows only inclusion-free rims where the adjacent mineral is olivine or orthopyroxene, and where the adjacent mineral is plagioclase there may or may not be a thin discontinuous layer of fibrous amphibole. Therefore, coronas around clinopyroxene are not independent of the composition of the adjacent mineral (contrary to Reynolds and Frederickson, 1962).

Given that the orthopyroxene and the amphibole replaced the olivine and the plagioclase, respectively, Reynolds and Frederickson (1962) plotted the three major primary phases against one another; clinopyroxene against original olivine (represented by modal olivine and coronitic orthopyroxene) against primary plagioclase (represented by modal plagioclase and amphibole-spinel symplectite. They interpreted a best-fit line through their data points as representing, approximately, the fractionation path of an originally olivine-plagioclase rock, with the zero-clinopyroxene intercept representing the original composition. A plot using the WBAC gabbronorites, shown in Fig. 4.3, generates a fairly well-defined trend, suggesting a possible protolith with a composition of about 15 to 20% olivine and the remainder being plagioclase.

The following history for the WBAC gabbronorites can be envisioned:

- crystallisation of olivine and calcic plagioclase from the melt
- crystallisation of orthopyroxene, clinopyroxene and spinel phases in the intercumulus spaces
- hydrous alteration of olivine to iddingsite, bowlingite
- incipient corona formation: clouding of plagioclase by fine-grained spinel and minor opaques, contemporaneous with:
- replacement of olivine by orthopyroxene and of plagioclase by amphibole-spinel symplectite, surrounding olivine grains; formation of fibrous amphibole coronas around pyroxene and spinel, at a much slower rate
- resorption of spinel from plagioclase in thin layer in front of leading edge of amphibole corona formation
- replacement of olivine by orthopyroxene and Fe-oxides; replacement of orthopyroxene by biotite (particularly in lamellae in cpx)
- replacement of amphibole by biotite
-resorption of spinel clouding in plagioclase with recrystallisation
-final product, before amphibolitisation, is

olivine-absent, opx-amphibole rock with accessory opaques, spinel and biotite

Both a primary magmatic crystallisation and "secondary" ("deuteric" or metamorphic) diffusion-related origin are feasible and indistinguishable based on petrographic evidence. There is no evidence for any (secondary) prograde metamorphism.

4.2 WBAC Monzogabbros

Two massive pyroxene-bearing samples from the WBAC monzonites, containing calcic plagioclase, are better classified separately as monzogabbros (Nockolds *et al.*, 1978). On a QAP diagram (Streckeisen, 1976) they are classified as quartz-gabbros, shown in Field 4 of Figure 4.4.

Quartz-plagioclase myrmekite in 8616B is hosted by plagioclase without associated K-feldspar, shown in Figure 4.5 A. This can be generated by prograde metamorphism (Ashworth, 1986a), although usually associated with more sodic plagioclase than is observed here. As other myrmekites in the same rock are clearly replacing K-feldspar, as shown in Figure 4.5 B, a more likely explanation is that the myrmekite has completely replaced the pre-existing K-feldspar. Biotite is ubiquitously associated with the myrmekites, often as rosettes

of biotite laths at the corners of the symplectite. This biotite provides a potassium sink. Myrmekite formed by K-feldspar replacement occurs under retrograde metamorphic conditions (Ashworth, 1986a). The breakdown of orthopyroxene to hornblende, biotite and magnetite along grain margins, fractures and embayments is consistent with the same retrograde process. A retrograde metamorphic origin is therefore favoured for the monzogabbros, of post-emplacement cooling ("deuteric") origin rather than a secondary metamorphic event, since no prograde effects are observed and primary igneous textures are preserved.

The monzogabbros have characteristics in common with both the host gabbronorites and the monzonites. In common with the former the monzogabbros possess primary pyroxenes, labradorite plagioclase, and a massive texture. They share with the monzonites the presence of quartz, zircon, minor hornblende, and trace alkali feldspar, albeit present almost exclusively as exsolution from plagioclase. Hence, the monzogabbros may represent gabbronorites which have obtained silica, water, some alkalis, and zircon from the adjacent monzonite. Alternatively, the monzogabbro may represent a higher temperature version of the monzonite which has suffered contamination, in some form, from the gabbronorites.

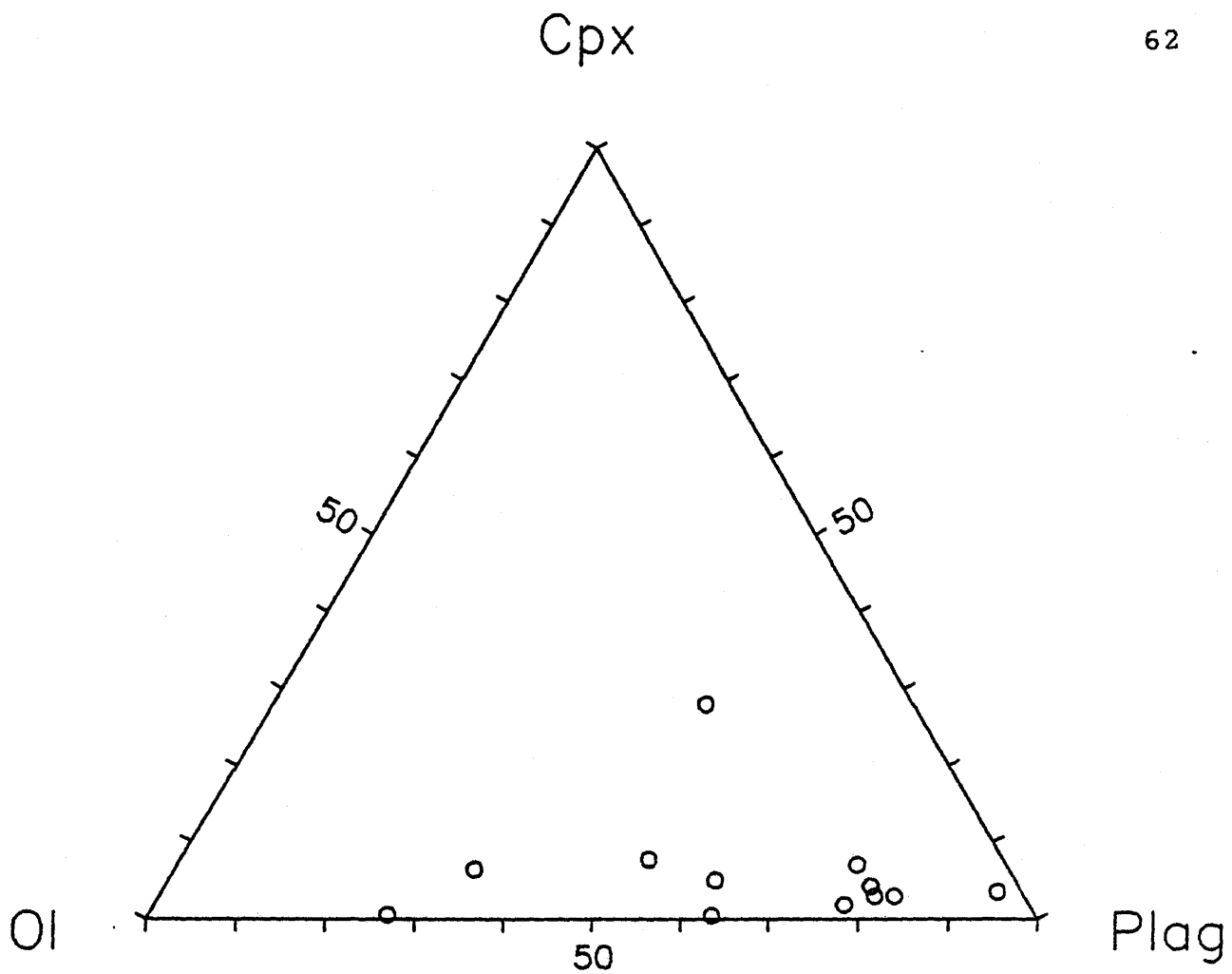

FIGURE 4.3

Variation of projected modes of primary phases (Reynolds and Frederickson, 1962) in WBAC gabbronorites, with best-fit line based on all plotted samples.

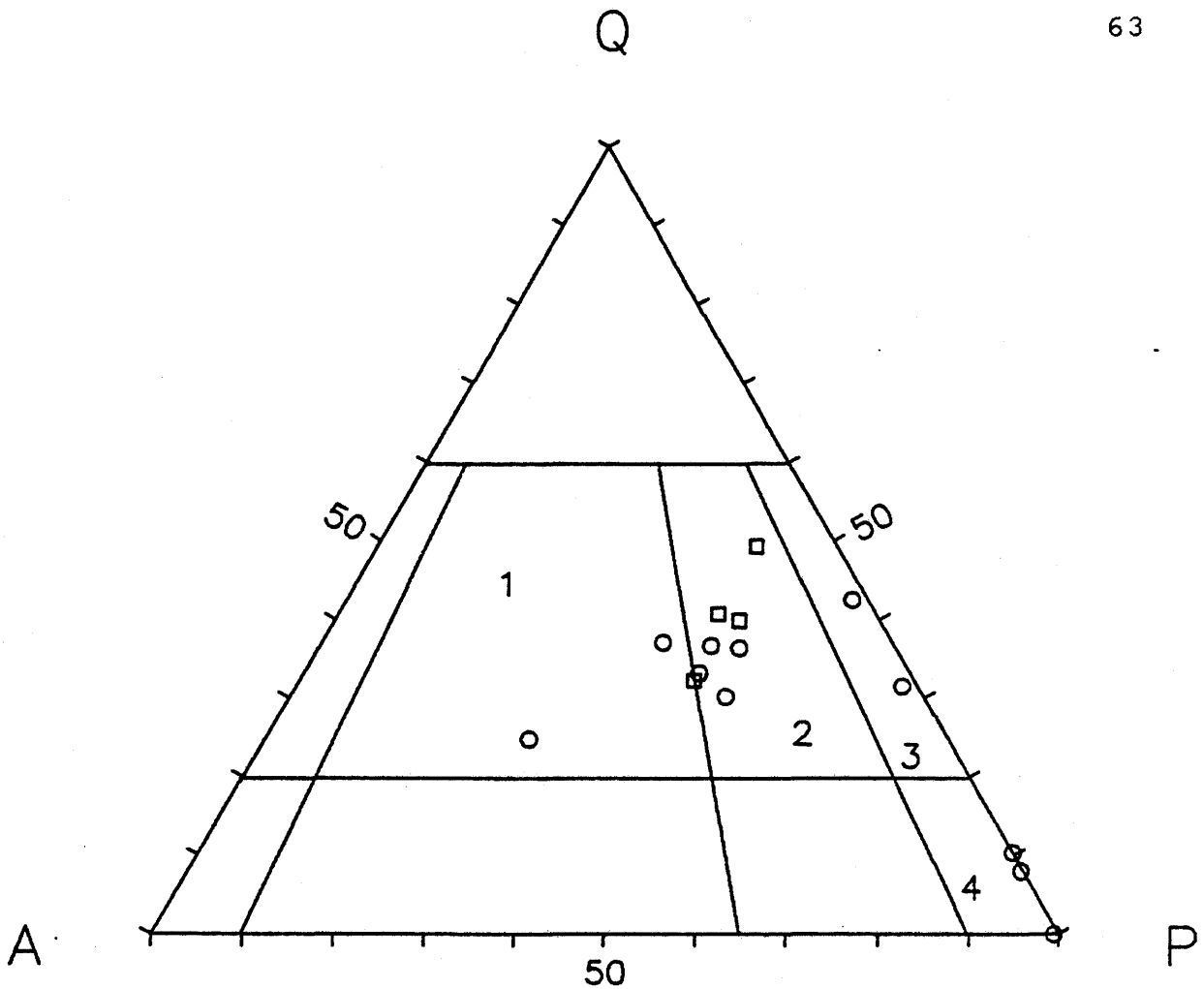

FIGURE 4.4

Modal quartz-alkali feldspar-plagioclase ternary diagram (Streckeisen, 1976)

Symbol: o = WBAC monzonite and monzogabbro
□ = Paradise Arm Pluton

Field: 1 = granite
2 = granodiorite
3 = tonalite
4 = quartz diorite/gabbro/anorthosite

Figure 4.5

A: Quartz-plagioclase myrmekite hosted by plagioclase at the top of the picture, without associated K-feldspar, from 8616 B.

(xp: x63) width of field is 1.5 mm

B: Quartz-plagioclase myrmekite replacing the K-feldspar grain to the upper left. The bright grain in the lower right is plagioclase, also from 8616 B.

(xp: x63) width of field is 1.5 mm


A


B

4.3 WBAC "Monzonites"

These rocks consist of plagioclase, quartz, and alkali-feldspar, with lesser amounts of biotite and hornblende, plus garnet and accessory zircon, sphene and apatite, characteristic of a monzonite (Nockolds *et al.*, 1978). Streckeisen (1976) QAP plots classify these rocks as granitic to tonalitic, but mostly as granodiorites, shown in Figure 4.4.

In outcrop they vary from massive to weakly gneissose. In general, K-feldspar content, whether in megacrysts or in the groundmass, correlates inversely with the degree of fabric definition, or degree of deformation, and with the proportions of mafic minerals. There is a gradation, therefore, between K-feldspar megacrystic and K-feldspar rich, weakly foliated to gneissose rocks to quartz and K-feldspar poor massive rocks, or even further to the pyroxene-bearing monzogabbros.

The megacrysts are probably of igneous origin since the common alignment of inclusions of quartz and plagioclase within a megacryst (eg. in 8509) differs from the alignment of the rock fabric which flows around the megacryst. This suggests that the megacryst predates the fabric and has resisted subsequent deformation and recrystallisation, as is commonly the case (Vernon, 1986). Furthermore, the presence of large euhedral K-feldspar megacrysts (eg. 8617A hand

specimen) and simple twins is believed to be an igneous phenomenon (Vernon, 1986). The weak positive correlation between megacryst size and groundmass grain size also favours an igneous origin, as does the inverse correlation between K-feldspar content and deformation. However, a larger database and more detailed study is required to preclude or confirm an igneous as opposed to a metamorphic origin.

The K-feldspar is very commonly rimmed by fine-grained quartz and the K-feldspar is being replaced by myrmekite where plagioclase is adjacent. The myrmekite begins at what appears to represent the original plagioclase-K-feldspar grain boundary, and the symplectite "front" is curved towards the K-feldspar. This style of myrmekite formation is associated with retrograde metamorphic replacement of K-feldspar (Ashworth, 1986a). This phenomenon is also observed in plagioclase inclusions within K-feldspar megacrysts.

The presence of garnet either in augen structures or as broken-up pieces entrained within the foliation suggests that the garnet predates the most recent deformation, to which it has responded by resisting in the former case, and brittle deformation in the latter case. This may depend on local pressure-temperature conditions or orientation of the garnet grains with respect to local stresses.

The presence of epidote minerals (allanite) and pennite chlorite indicate that this unit can be classified in the upper greenschist facies, with the peak metamorphism being at least in the almandine subfacies of the greenschist facies (Winkler, 1979) or alternatively in the epidote-amphibolite facies (Ehlers and Blatt, 1982), based on the presence of relict garnet. This facies assemblage is stable from approximately one to ten kilobars pressure and 400 to 600°C (Ehlers and Blatt, 1982).

In summary, the petrographic evidence suggests an igneous origin for the monzonites, with subsequent low to middle grade metamorphism. As in the monzogabbros, retrograde metamorphic effects are dominant.

4.4 Paradise Arm Pluton

Mineralogically the PAP is very similar to the WBAC monzonites, both in terms of mineralogy and modal abundance. It is classified as a granodiorite (Streckeisen, 1976), shown in Figure 4.4. The PAP shows fewer textural effects of metamorphism than does the monzonite, in that the former is more massive, though grain sizes are comparable.

The mineral relationships in thin section are also comparable to the monzonite. The foliation, where present,

flows around well-developed K-feldspar megacrysts. Myrmekites, with or without associated sericite, are common at alkali-plagioclase feldspar interfaces, showing the same convex-towards-K-feldspar morphology seen in the monzonites.

Pennite and allanite are both present in trace amounts in the PAP, again suggestive of upper greenschist facies metamorphism. Bent twinning lamellae indicate deformation of plagioclase feldspars and the presence of fine-grained intergranular polycrystalline quartz surrounding large plagioclase and K-feldspar grains also suggests some brittle deformation.

Garnet in sample 8613 shows concentrically ringed inclusions of biotite and opaques, indicating a previous metamorphic history, such that two idiomorphic faces of the garnet are preserved while the rest of the grain has been partially resorbed. A weakly-defined circumventing-flow texture in the adjacent biotite supports a predeformational origin hypothesis for the garnet.

The most significant difference between the PAP and the monzonite is the presence of a muscovite-sillimanite bearing rock in the PAP. Both of these minerals are late phases in this rock, as they are superposed over the other phases, (as is also the case in the PMGB metasediments), and this may represent an influx of alumina from absorption of an enclave

of metasedimentary gneiss, or alternatively the sample represents an enclave itself. However, the absence of gneissosity and the modal composition of 8613 suggests more affinity with the other PAP samples than with the PMGB gneisses.

Petrologic evidence supports a comagmatic and cogenetic origin for the WBAC "monzonites" and the PAP granodiorites, and also suggests a similar metamorphic history.

4.5 Paradise Metasedimentary Gneiss Belt Gneisses

While four samples is too few to accurately characterise the variation of a unit as heterogeneous as this one (Gower et el, 1986), those studied are relatively consistent modally and should provide a basis for comparison with the more anhydrous rocks nearer the WBAC gabbronorite.

The dominant assemblage in this unit is plagioclase, quartz, biotite and K-feldspar. One sample pair is enriched in sillimanite, the other in biotite. The former assemblage plus the gneissosity suggests amphibolite grade metamorphism, in a P-T space of between 500 and 650°C and about 2 to 11 kb (Ehlers and Blatt, 1982). The presence of sillimanite provides a lower temperature limit corresponding to the triple point of the Al_2SiO_5 polymorphs in P-T space. The possible

temperatures for this triple point include 460°C (Brown and Fyfe, 1971), 501°C (Holdaway, 1971), 595 ± 10°C (Althaus, 1967), and 622°C (Richardson *et al.*, 1969). The pressure values corresponding to the minimum temperature for sillimanite stability range from 2 kb (Brown and Fyfe, 1971) to 6.5 kb (Althaus, 1967), but sillimanite stability is not constrained to minimum (or maximum) pressures due to the relatively steep slopes of the univariant lines for kyanite-sillimanite and andalusite-sillimanite in P-T space.

The assemblage sillimanite-muscovite-K-feldspar-quartz represents the "second sillimanite isograd", (the first involving staurolite breakdown), which can be expressed in simplified form as the following reaction (from Turner, 1980):

$$KAl_2(AlSi_3O_{10})(OH)_2 + SiO_2 \rightleftharpoons KAlSi_3O_8 + Al_2SiO_5 + H_2O$$

muscovite quartz K-spar sill

This isograd is well-defined in P-T space (Turner, 1980), providing a slightly higher minimum temperature for sillimanite stability, from about 600°C at 2 kb pressure (where $P_{tot} = P_{H_2O}$) up to 700°C at 5 kb. The muscovite truncates biotite laths and is oriented obliquely to the fabric defined by biotite, and often pseudomorphs preexisting biotite laths. The muscovite in turn is replaced by sillimanite fibres

generally aligned sub-parallel to the biotite. Rosettes or sheafs of biotite and sillimanite respectively are aligned at a high angle to the gneissosity in association with coarser grained leucosomic pods, suggesting post-deformational growth of sillimanite and biotite. However, Vernon (1987) suggests that sillimanite grows in these two habits is a response to local variations in strain. In zones of high strain, sillimanite grows as fibres oriented parallel to the gneissosity, concentrated by leaching of Si and Al from adjacent minerals, but in the leucosomic pods, representing zones of low strain, sillimanite can grow as non-oriented sheafs, contemporaneous with adjacent high-strain growth (Vernon, 1987). This interpretation can be applied to biotite as well, as it also occurs as oriented laths or as rosettes in the leucosomic pods. Vernon (1987) suggests several models for sillimanite formation, the most appropriate in this case being the "Carmichael-type" reactions whereby sillimanite develops from other Al_2SiO_5 polymorphs catalysed by the simultaneous destruction and regrowth of muscovite, with associated growth of sillimanite in biotite. Alternatively, the breakdown of biotite or muscovite and quartz could produce sillimanite (Vernon, 1987).

The coarse-grained laths of sillimanite could be formed either by recrystallisation of preexisting fibrous sillimanite or coarsening of single fine grains of sillimanite. Vernon

(1987) supports the latter explanation, explained by a change from a high-strain into a low-strain zone, as a function of heterogeneous deformation, varying through time. He cites the sharpness of the grain boundaries as evidence for growth as opposed to recrystallisation, which would generate irregularities in the grain margins.

The superposition of sillimanite over muscovite and/or biotite indicates that the first sillimanite isograd has been crossed in a prograde metamorphic reaction. The presence of myrmekite replacing K-feldspar indicates some retrograde metamorphic activity, as observed in the WBAC monzonite and the PAP.

4.6 PMGB "Anhydrous" Gneisses

This subunit, a variation on the PMGB gneisses, is loosely defined on the macro and microscopic evidence of high temperature (ie. contact metamorphism) and locally high pressure (suggested by the presence of mylonites) effects on the PMGB immediately adjacent to the WBAC mafic intrusives. While the term "charnockitic" pelitic gneisses (Gower *et al.*, 1986) is applicable to the rocks near the contact with the gabbronorite, samples taken from further away show evidence of deformation at relatively high pressures, but lack ortho-pyroxene, and are in fact richer in iron and magnesium than

the contact zone rocks. Anhydrous pelitic gneiss is a more appropriate name, as biotite is present only in small amounts, except in one sample (29 Vol. % in 8607). Near the contact the term gneiss is also a misnomer, as the rocks have a massive, non-oriented texture due to recrystallisation at the high temperatures of contact metamorphism.

Arima and Gower (1987) have identified both an osumilite and a hypersthene isograd within the contact zone, a phenomenon found at other osumilite-bearing locations with mafic intrusions into medium grade paragneisses (eg. Berg, 1976; Maijer *et al.*, 1981). Osumilite in high grade terrains such as these and in regionally metamorphosed granulite terrains such as Enderby Land, Antarctica (eg. Ellis *et al.*, 1980), is invariably associated with its breakdown product, a symplectite of quartz, K-feldspar and cordierite, plus dendritic hypersthene (Berg and Wheeler, 1976; Ellis *et al.*, 1980; Grew, 1982). The presence of diffuse sillimanite and biotite associated with these symplectites, as well as the coarsening of the symplectite into vermicular quartz in cordierite is also observed elsewhere (Ellis *et al.*, 1980; Grew, 1982). Experimental data from Hensen (1977) suggests that the reaction Os $\rightleftharpoons$ Cord + Hyp + Or + Qz proceeds to the right with increasing pressure, since $\Delta V_{rxn} < 0$, although the volume change is probably very small (Hensen, 1977).

The presence of cordierite not associated with the breakdown of osumilite is interpreted by Ellis *et al.* (1980) and Grew (1982) as representing a recrystallised symplectite, the cordierite a retrograde phase not stable with quartz under the peak metamorphic conditions (ie. where osumilite is stable).

The absence of garnet in these rocks can be explained by the relative stability of cordierite-hypersthene as opposed to garnet-osumilite. Berg and Wheeler (1976) suggest that garnet-osumilite could become stable at high pressures, but that due to the structural incompatibilities of osumilite and garnet (tetrahedral Mg versus 8-coordinated Mg, respectively), the cordierite-hypersthene field will probably always intervene. This conclusion is supported by the data of Hensen (1977), who notes that the cordierite-hypersthene join is stable up to 10 kb and 1000°C.

Other textural features observed in the PMGB rocks have been described from Antarctic rocks by Grew (1982), including sillimanite overgrowths on spinel, which he interprets as a retrograde feature. He notes the presence of sillimanite and hypersthene intergrowths which he suggests may have developed at the peak of metamorphism. While this feature is not observed in these rocks to any great extent, a similar texture involving intergrown biotite and sillimanite may represent a

retrograde, hydrated version of the opx-sillimanite texture. Hypersthene is altered to biotite along grain boundaries and embayments. Less commonly there are rims of hypersthene around very well developed red-brown biotite. This could conceivably represent lower temperature, hydrous breakdown of osumilite, which involves either biotite (Ellis *et al.*, 1980) or phlogopite (Hensen, 1977), rather than early (ie. pre-granulite facies) biotite rimmed by orthopyroxene. Textural evidence supports the latter alternative, despite the instability of hydrous minerals under the apparently anhydrous conditions required for osumilite stability.

Sapphirine was observed in samples from osumilite-bearing outcrops (Gower, pers. comm.), although it was not found in thin section in this study. However, the P-T stability fields of sapphirine and osumilite can be used to suggest the approximate P-T conditions of metamorphism. A lower temperature limit is provided by the presence of sillimanite in all samples from this unit.

Studies of osumilite in volcanic rocks, a low pressure contact aureole, and an experimental study (listd in Berg and Wheeler, 1976) indicate that osumilite forms only at low pressures of $P_{tot} = P_{H_2O}$, with a maximum less than 1 kb for stoichiometric osumilite (Schreyer and Siefert, 1967). However, in environments where $P_{H_2O} << P_{tot}$ and with low

values of f_{O_2} (Berg and Wheeler, 1976), osumilite is stable under a wide range of temperatures and pressures (Hensen, 1977). He conducted experiments with $P_{H_2O} << P_{tot}$, where osumilite was synthesized from a model pelitic composition between 3.6 and 6.3 kb pressure at 1000°C and between 4.5 and 7.2 kb at 1100°C. He suggests minimum temperatures for osumilite formation of 750 to 800°C from the assemblage cordierite-hypersthene-K-feldspar-quartz, and geothermometry in natural systems suggests temperatures of 900 to 1000°C. Table 4.2 A lists some occurences of osumilite and the pressures and temperatures of formation based on Mg/Fe ratios in associated minerals.

The Enderby Land granulites are both osumilite and sapphirine bearing and hence the regional temperatures and pressures determined by Ellis (1980) and Grew (1982) apply to sapphirine as well as osumilite as presented in Table 4.2 A. Other sapphirine-bearing assemblage P-T estimates are presented in Table 4.2 B. Gittins and Currie (1979) suggest pressures around 6 kb for the assemblage later studied by Arima et al (1986), representing the minimum pressure (and temperature, of 710°C) of the sapphirine stability field (Gittins and Currie (1979) based on Newton et al (1974) and corrected for a non pure-Mg system). Sapphirine-bearing assemblages in Norway (Johansson and Möller, 1986) and in central Labrador (Arima et al, 1986) are interpreted as

TABLE 4.2 A

P-T CONDITIONS OF NATURAL OSUMILITE

OCCURENCE	P(kb)	T(°C)	ASSEMBLAGE	REFERENCE
Granulite facies aureole of anorthosite	3.7-5.0	715-900	Ol-Hy-Aug	Berg (1976)
	3.8-6.6	645-915	Gt-Cd-Hy	"
Gran. facies regional met.	8.0-12.2	900-980	Cpx-bearing	Ellis (1980)
"	7.0-9.0	750-1000	-	Grew (1982)

TABLE 4.2 B

P-T CONDITIONS FOR SAPPHIRINE OCCURENCE

OCCURENCE	P(kb)	T(°C)	ASSEMBLAGE	REFERENCE
Gran. facies regional met.	6	710	-	Gittins and Currie (1979)
"	14.5 ± 2	870 ± 50	Cpx-Ky-Gt	Johansson and Möller (1986)
"	6.5-7.5	937-993 531-675	Sp-Cd Gt-Cd	Harley (1986)
"	9	900	Gt-Opx	Arima et al (1986)

representing very high pressures, between 9 and 14 kb, and temperatures comparable to those estimated for osumilite stability. The 9 kb pressure is a minimum for the Norwegian gneiss since the sapphirine is interpreted as a relict phase from higher grade metamorphic conditions (Johansson and Möller, 1986). The pressure of 14.5 ± 2 kb is interpreted as a maximum since sapphirine is part of a retrograde assemblage (Arima et al, 1986).

Schreinemakers analysis by Hensen (1977) and Ellis *et al.* (1980) indicate a steep positive slope in P-T space for the reaction Os ⇌ Cord + Or + Hyp + Qz where as P increases the reaction moves slowly to the right, and as T increases the reaction moves sharply to the left. Schreinemakers diagrams in Ellis *et al.* (1980) indicate a moderately steep positive dP/dT value for the reaction Os ⇌ Sapph + En + Ksp + Qz indicating that osumilite is favoured by higher temperatures and lower pressures than sapphirine, where the pressure effect is more pronounced than that of the osumilite breakdown assemblage.

Total pressure estimates range from 3.6 kb (Hensen, 1977) or 3.7 kb (Berg, 1976) up to 8 to 10 kb (Ellis, 1980; Grew, 1982). The lower values agree with pressures of ≤4 kb for PMGB osumilites (Arima and Gower, 1987).

In summary, moderately high pressures of 4 to 6 kb, low water pressure (P_{H_2O} < 0.5 to 1 kb) and increasing temperatures will generate osumilite-bearing assemblages from cordierite-hypersthene-K-feldspar-quartz assemblages at around 750 to 800°C, and the former assemblage can remain stable at 900 to 1000°C. Sapphirine would likely be produced at the peak metamorphic conditions at locally higher pressures. After the peak metamorphism, a decrease in temperature or an increase in water pressure would produce degeneration of osumilite to the Cord-Hyp-Ksp-Qz assemblage in the former case or to a biotite or phlogopite-bearing assemblage in the latter case. The presence of biotite indicates that the transformation of osumilite to the above breakdown products is a retrograde reaction rather than a response to increased pressure at high temperatures. The sillimanite-biotite-K-spar assemblage observed in samples further from the contact may represent a hydrous, Fe-bearing variation on the osumilite breakdown reaction Os → Sill + En + Ksp + Qz (Ellis et al, 1980), which proceeds to the right with decreasing temperature.

CHAPTER 5: GEOCHEMISTRY

Major and trace element geochemistry is presented in Appendix 3. Analytical methods are presented in Appendix 2. The major element geochemistry of the WBAC gabbronorites is similar to that of other layered mafic/ultramafic (eg. Muskox, Stillwater intrusions, in Carmichael *et al.*, 1974) and/or coronitic bodies (eg. Mason, 1969; Starmer, 1969). Reduced iron for the WBAC gabbronorite samples was determined using the correction % Fe_2O_3 = % TiO_2 + 1.5, designed by Irvine and Baragar (1971) for unaltered volcanic series rocks. This correction has also been applied to the WBAC "monzonite" and the PAP. Comparison with the Apsley biotite gneiss geochemistry (Shaw, 1972) suggests that this correction is probably not drastically in error (ie. ± 0.5 wt. %). However, there is no justification for applying this correction to the metasedimentary rocks of the PMGB. Nockolds et al. (1978) suggests that the presence of graphite in metamorphic rocks precludes the presence of oxidised iron, so the possibly graphite-bearing sillimanite-biotite PMGB gneisses (see Section 3.3.2) have total iron calculated as FeO. The anhydrous and/or charnockitic PMGB rocks adjacent to the WBAC contact are hematite bearing, so oxidised iron is definitely present. As the composition of the magnetite-spinel series members is unknown, an accurate correction for FeO/Fe_2O_3 based on Ti content is not possible and so the Irvine and Baragar

(1971) correction has been applied arbitrarily.

5.1 Classification of Gabbronorites

The WBAC gabbronorites can be classified using major and trace element diagrams designed for basaltic rocks, distinguishing between tholeiitic, calc-alkaline and alkali basalts, assuming that significant crustal contamination has not occurred. The very low alkali content of the WBAC gabbronorites, shown in Figure 5.1, rules out an alkali basaltic affinity.

Trace elements are unable to differentiate between calc-alkaline and low-potassium tholeiitic basalts, although most of the WBAC samples plot within calc-alkali basalt fields. Ternary diagrams involving titanium, zirconium, yttrium and strontium, shown in Figure 5.2 A and B are unable to distinguish between these two basalt types, but a plot of TiO_2 against Zr (Figure 5.3) favours low-K tholeiites, and shows a Ti depletion for the WBAC rocks relative to the volcanics plotted by Pearce and Cann (1973). Butler and Woronow (1986) derived two functions of variance, defined as Score 1 = $- 0.3707\ \ln(100TiO_2) - 0.0668\ln(Zr) - 0.3987\ln(3Y) + 0.8362\ln(Sr)$ and Score 2 = $-0.3376\ln(100TiO_2) - 0.5602\ln(Zr) + 0.7379\ln(3Y) + 0.1582\ln(Sr)$, in an attempt to minimise the numeric dependence between variables in commonly used ternary

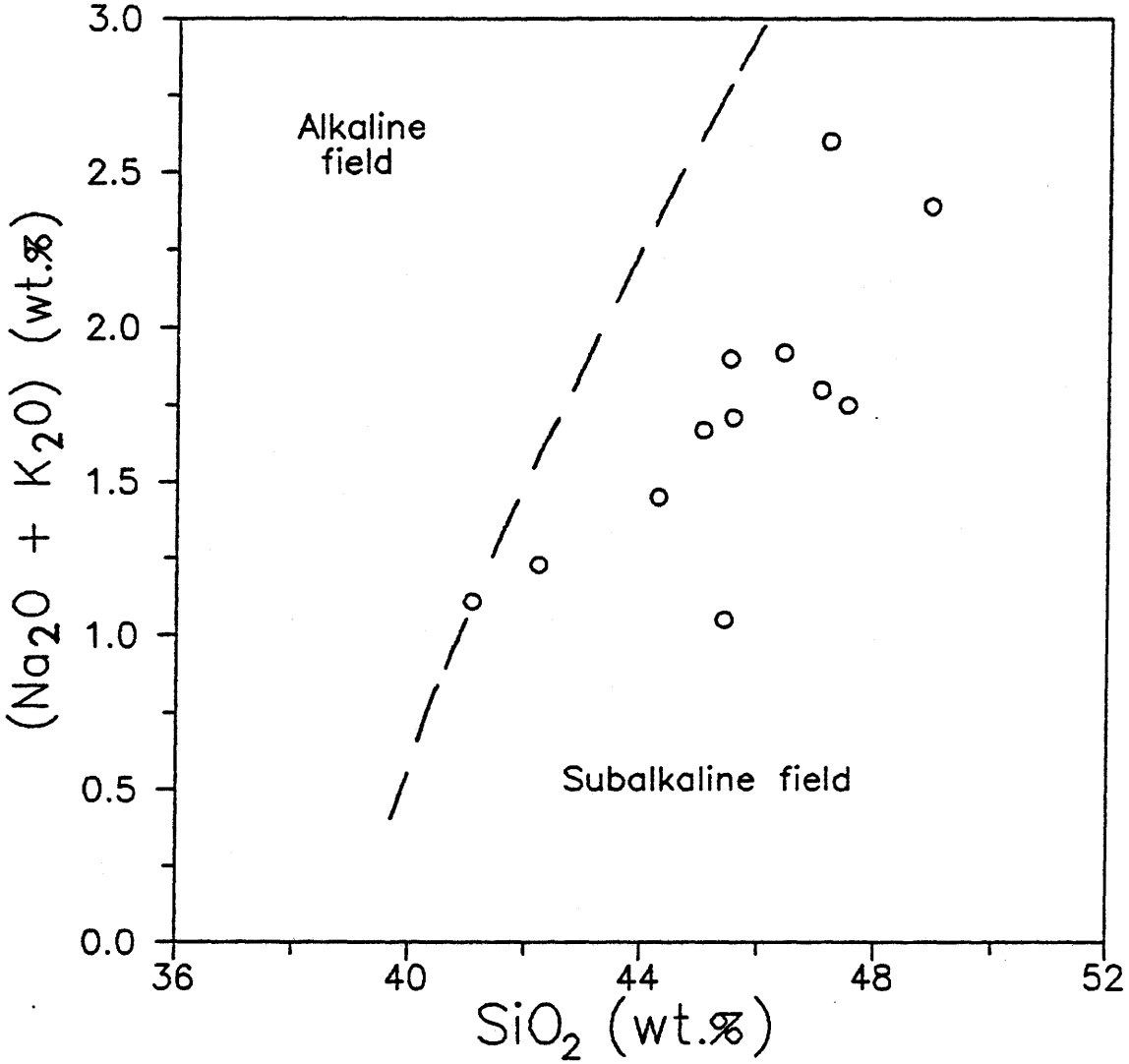

FIGURE 5.1

Total alkalis versus silica
for WBAC gabbronorites

Fields defined by Irvine and Baragar (1971)

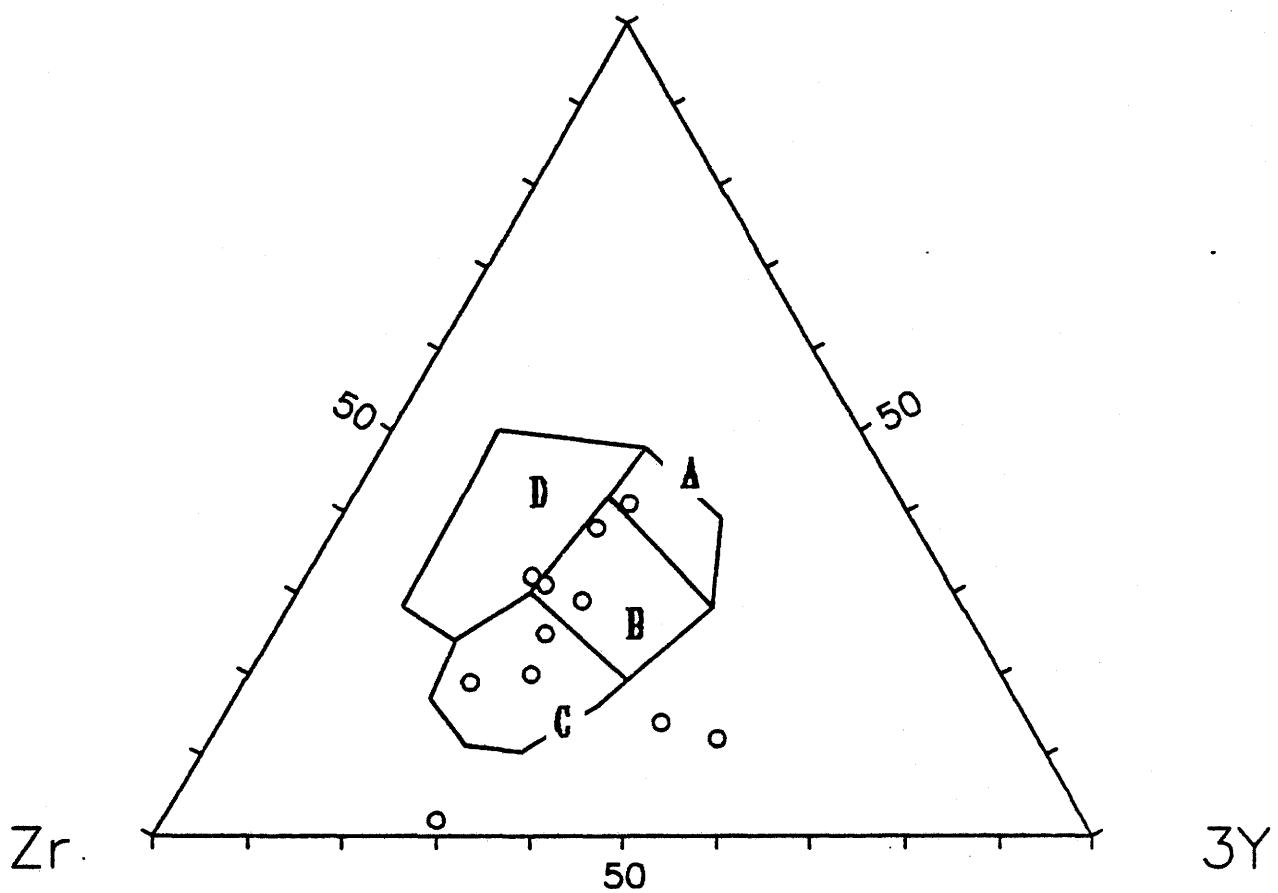

FIGURE 5.2 A

Titanium-zirconium-yttrium discrimination diagram (Pearce and Cann, 1973) for the WBAC gabbronorites

Low-potassium tholeiites - Fields A and B
Calc-alkaline tholeiites - Fields B and C
"Within-plate" basalts - Field D
Ocean-floor basalts - Field B

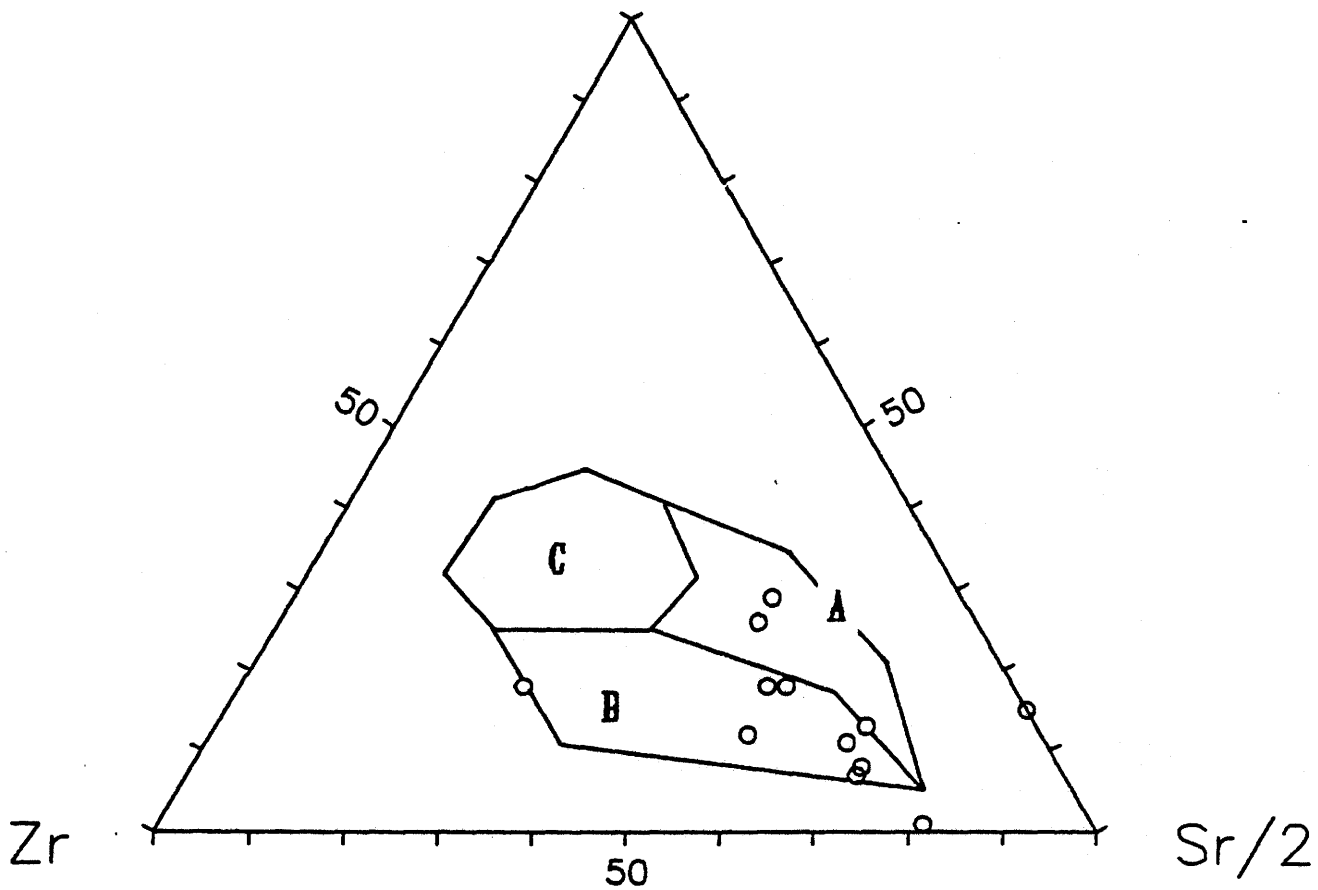

FIGURE 5.2 B

Titanium-zirconium-strontium discrimination diagram (Pearce and Cann, 1973) for the WBAC gabbronorites

Field A = low-potassium tholeiites
B = calc-alkali basalts
C = ocean-floor basalts

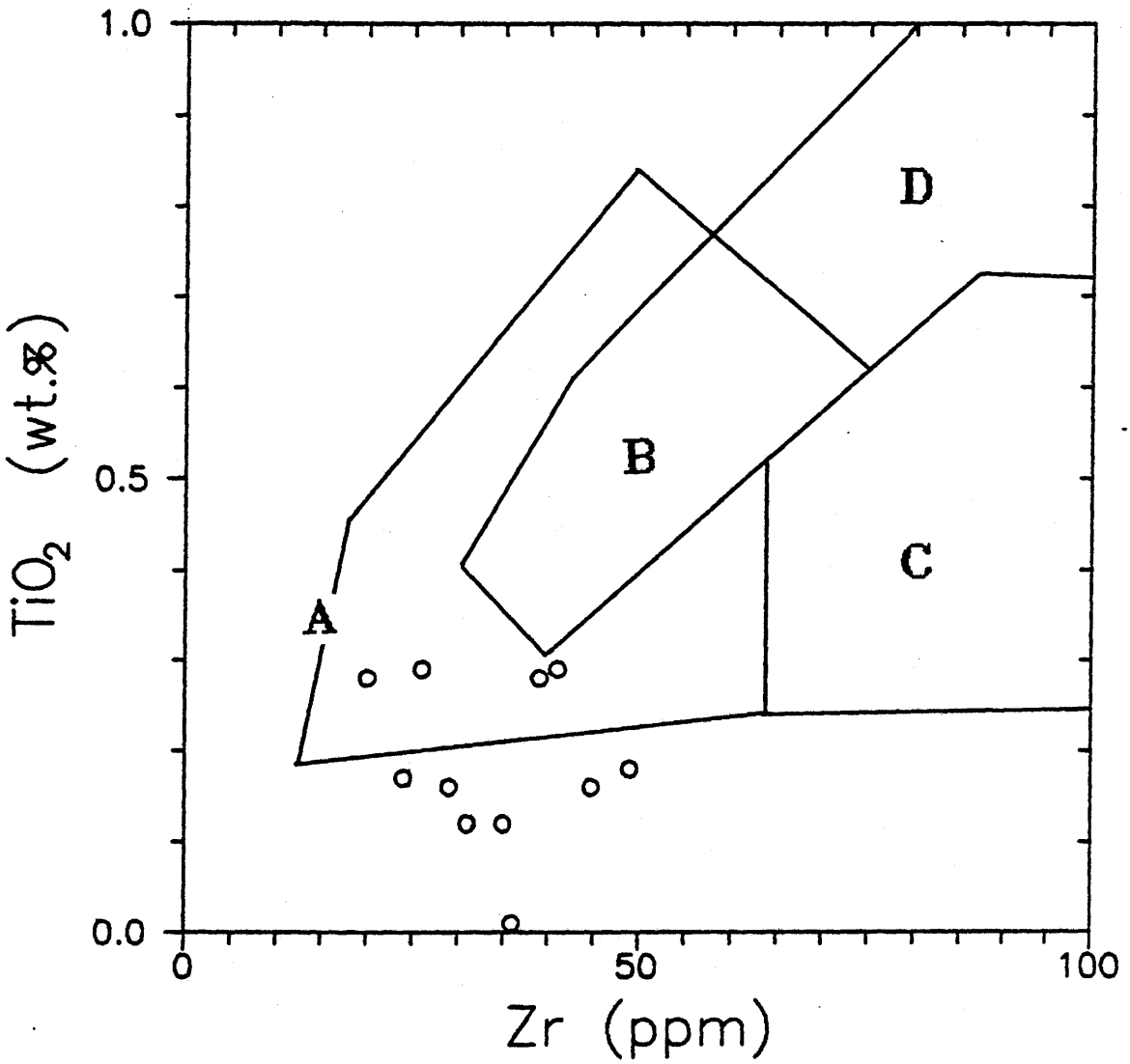

FIGURE 5.3

Titanium-zirconium discrimination diagram
(Pearce and Cann, 1973) for the WBAC gabbronorites

Low-potassium tholeiites - Fields A and B
Calc-alkali basalts - Fields B and C
Ocean-floor basalts - Fields B and D

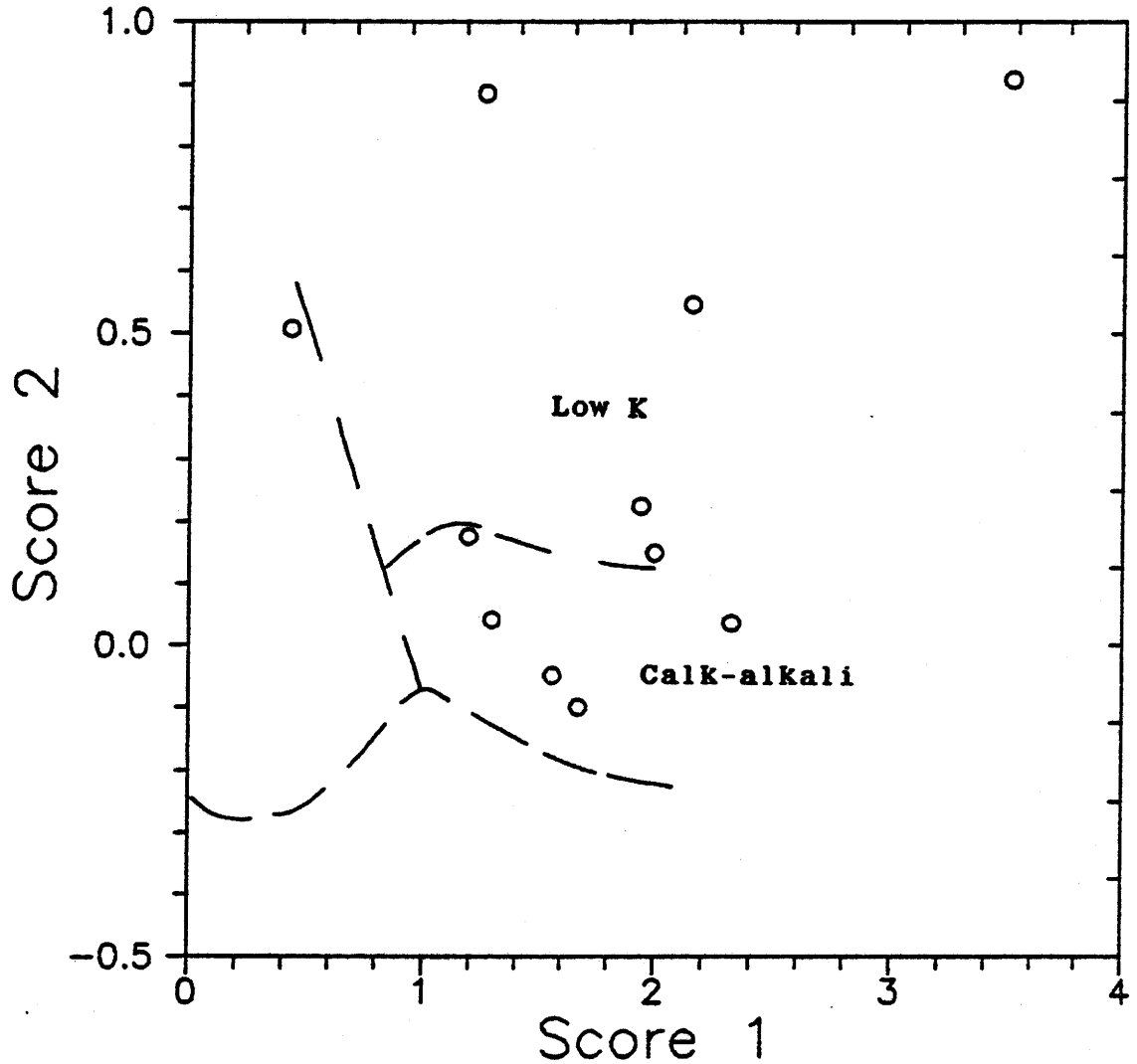

FIGURE 5.4

Basalt discrimination diagram based on the trace elements Ti, Zr, Y and Sr (Butler and Woronow, 1986) (See text for definition of variables)

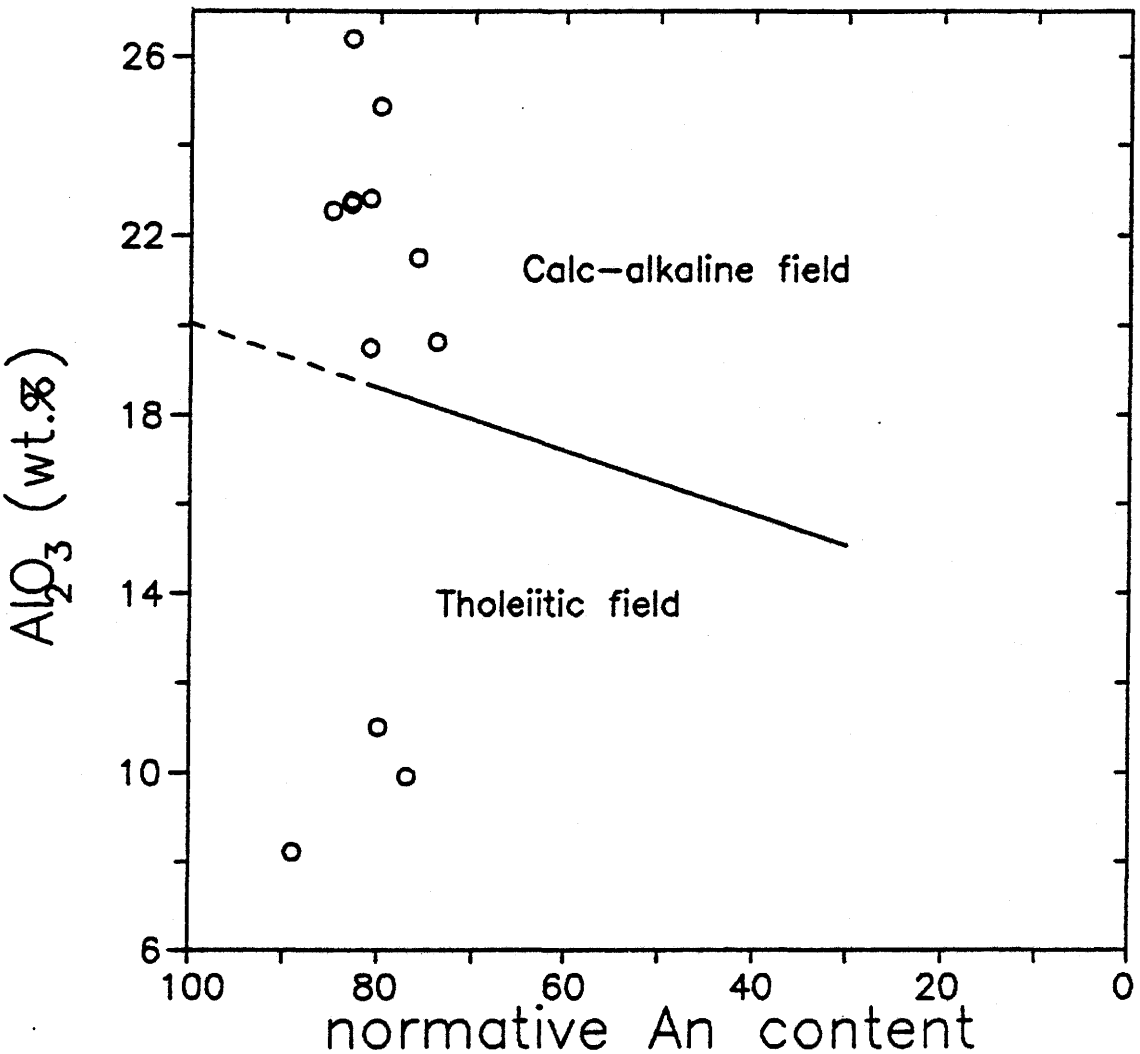

FIGURE 5.5

Basalt discrimination diagram using alumina and the normative An content of plagioclase (Irvine and Baragar, 1973) for the WBAC gabbronorites

and binary trace element variation diagrams. The WBAC gabbronorites lie within both the low-K and calc-alkaline basaltic fields for Score 2 against Score 1 (Fig. 5.4) and for alumina against the normative anorthite content of plagioclase (Fig. 5.5), although the majority of the samples are calc-alkaline in the latter diagram.

Hence, incompatible trace elements suggest a calc-alkakine or low-K tholeiitic affinity for the WBAC gabbro-orites.

5.2 Classification of Felsic Units

The major and trace element geochemistry of the WBAC monzonite, the PAP, and the PMGB gneisses are presented in Appendix 3. The metasedimentary origin of the PMGB rocks is reflected by the high normative corundum content (from 5.5 to 16.8 %), relative to the other rocks in this study (see Appendix 4 for normative mineralogies). Another means of distinguishing orthogneiss from paragneiss has been applied using the Discriminant Function of Shaw (1972), defined as:

$$DF = 10.44 - 0.21\ SiO_2 - 0.32\ Fe_2O_3\ (\text{total Fe}) - 0.98\ MgO + 0.55\ CaO + 1.46\ Na_2O + 0.54\ K_2O$$

After using the screening criteria as defined by Shaw, the value of DF (see Appendix 4) for ten out of fifteen WBAC and PAP granodiorites give positive values of DF, corresponding to

an igneous origin. Alternatively, all PMGB rocks, screened or unscreened, give negative DF values, suggesting a sedimentary origin (Shaw, 1972). These calculations support the petrographic interpretations regarding the origin of these units.

5.3 Origin of the Gabbronorites

For layered mafic sequences with associated felsic rocks, differentiation trends can be seen in plots of silica against other major element oxides. The WBAC gabbronorites to monzogabbros to granodiorites show trends between these oxides, but these can also be interpreted as mixing lines between unrelated mafic and felsic rocks. Petrographic and major element geochemical evidence suggesting a cumulate origin for the WBAC gabbronorites indicates that these are unlikely to represent liquid lines of descent. Plotting silica against CaO for the igneous units (the WBAC gabbronorites, the WBAC 'monzonites', and the PAP; Figure 5.6) shows a distinct trend of decreasing CaO with increasing silica, reflecting a decreasing abundance of calcic plagioclase. A plot of $\Sigma Fe/(\Sigma Fe + MgO)$ against silica (where $\Sigma Fe = FeO + Fe_2O_3$), shown in Fig. 5.7, indicates a very primitive magma when compared to similar plots for mafic extrusives (Osborn, 1979). Three gabbronorite samples (8504, 8505 and 8603) which lie well below the trend defined by the other gabbronorites in

Fig. 5.6 and are distinct from the main cluster of gabbros in Fig. 5.7 are also enriched in normative olivine relative to the other WBAC gabbronorites. Emmett (1987) uses the differentiation index (D.I. = the sum of normative quartz, albite, orthoclase, nepheline, kalsilite and leucite) defined by Thornton and Tuttle (1960) to provide a quantitative chemical criterion to distinguish between cumulates and "congealed liquid", whereby samples with D.I. < 30 are cumulates and those with D.I. > 30 are representative of the liquid line of descent. However, the values of D.I. are between 6.9 and 20.1 for the gabbronorite samples in this study. Hence, either the suite collected are all cumulates, which is not inconsistent with the textural evidence, or the D.I. is not an adequate monitor in this case.

5.4 Origin of the Granodiorites

The WBAC monzonite and the PAP plot in the same or overlapping fields in terms of major elements (reflected by the similarity in normative mineralogies) and trace elements, where the wider variation in the monzonite relative to the PAP may reflect the larger database for the former unit. Therefore these units shared geochemically similar sources, and will be treated as cogenetic in this discussion. There are three possible geneses for the two granodioritic units; (i) Given the common association of anorthositic and gabbroic

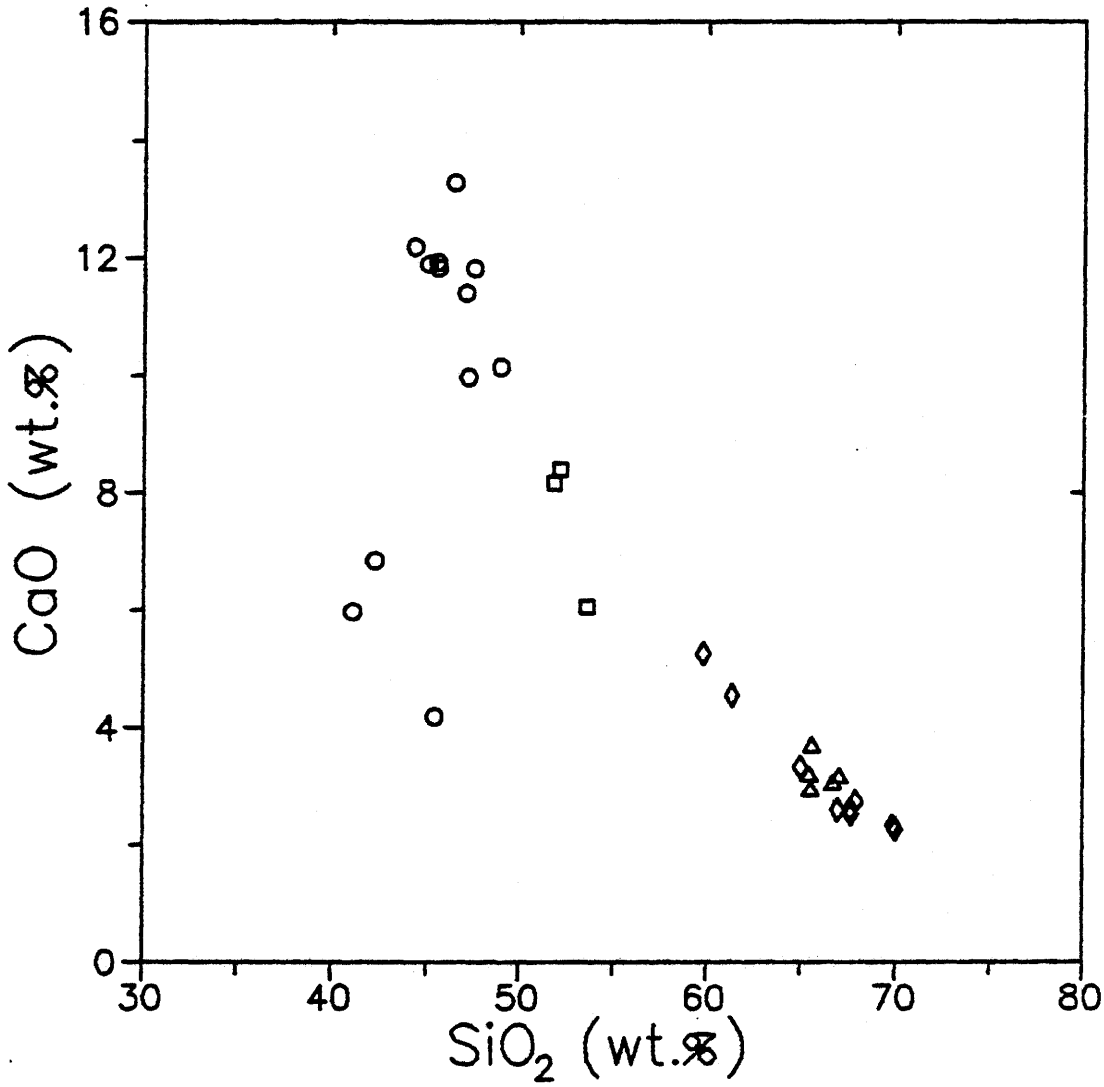

FIGURE 5.6

Variation in silica and CaO
for Hawke River Terrane plutonic rocks

Symbol: o = WBAC gabbronorites
□ = WBAC monzogabbros
◇ = WBAC monzonites
△ = Paradise Arm Pluton

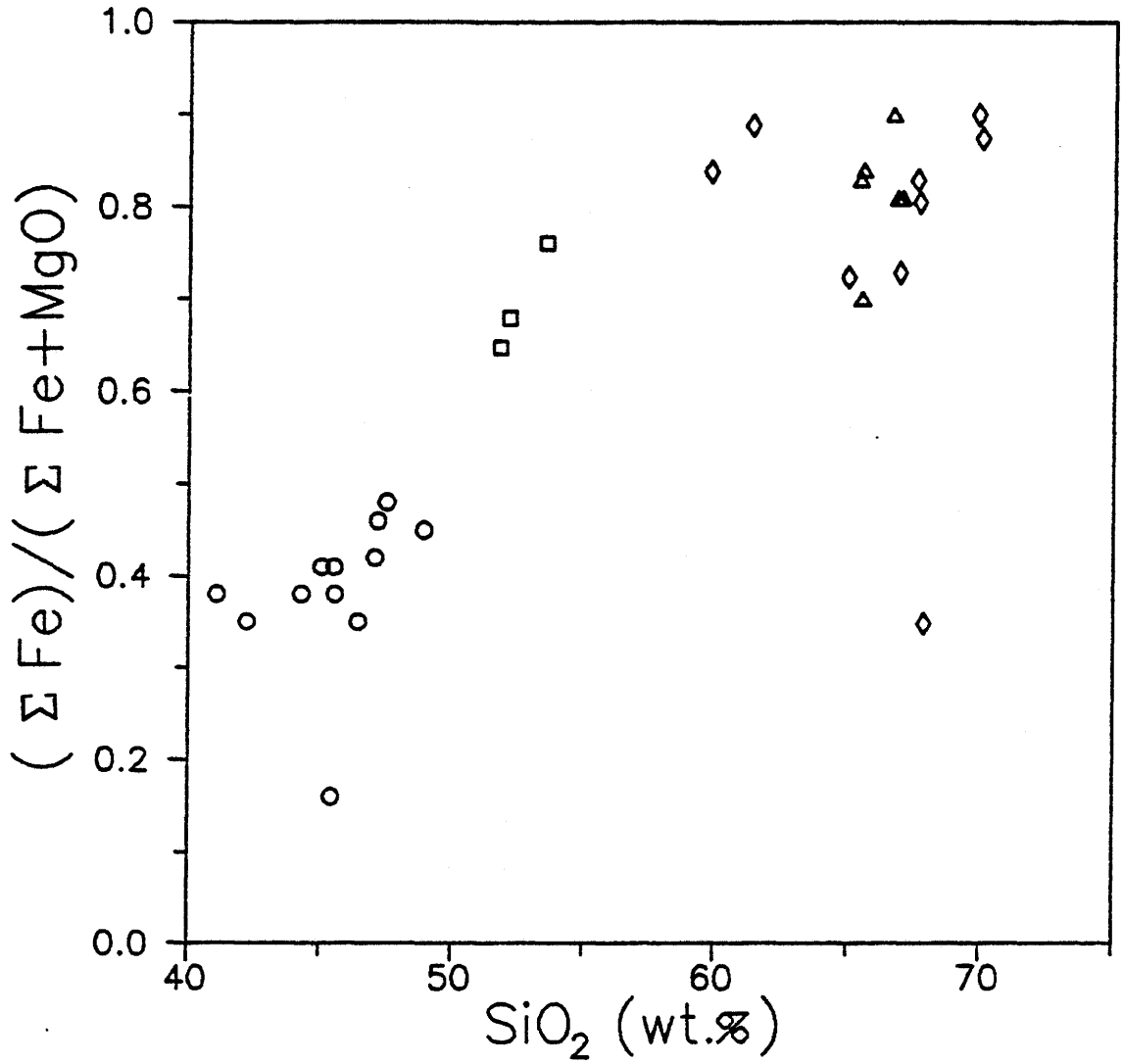

FIGURE 5.7

Variation in $(FeO+Fe_2O_3)/(FeO+Fe_2O_3+MgO)$ for Hawke River Terrane plutonic rocks

Symbol: o = WBAC gabbronorites
□ = WBAC monzogabbros
◇ = WBAC monzonites
Δ = Paradise Arm Pluton

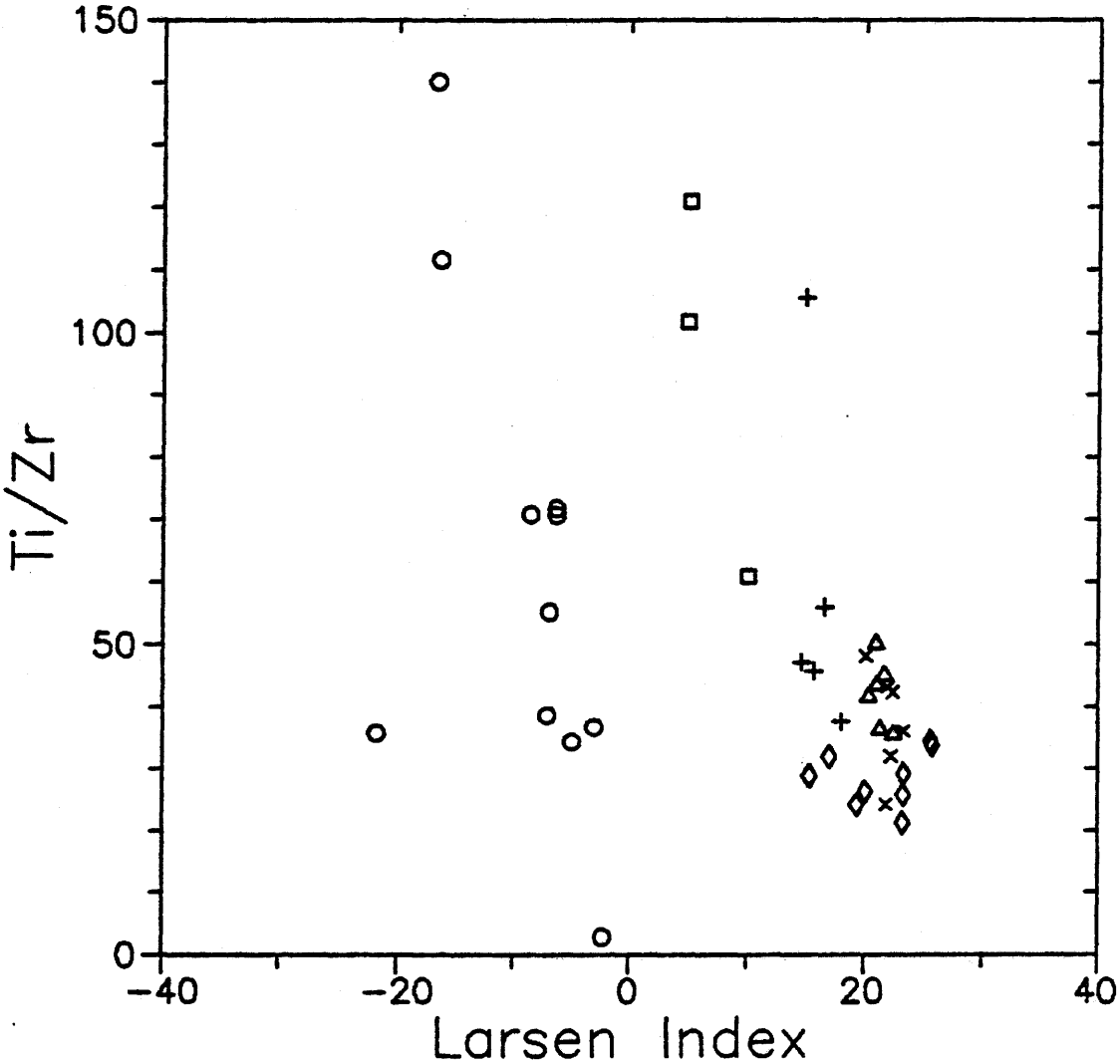

FIGURE 5.8

Variation in Ti/Zr ratio with modified Larsen Index (Shaw, 1972) for Hawke River Terrane rocks

Symbol: o = WBAC gabbronorites
□ = WBAC monzogabbros
◇ = WBAC monzonites
△ = Paradise Arm Pluton
\+ = Anhydrous PMGB rocks
x = PMGB gneisses

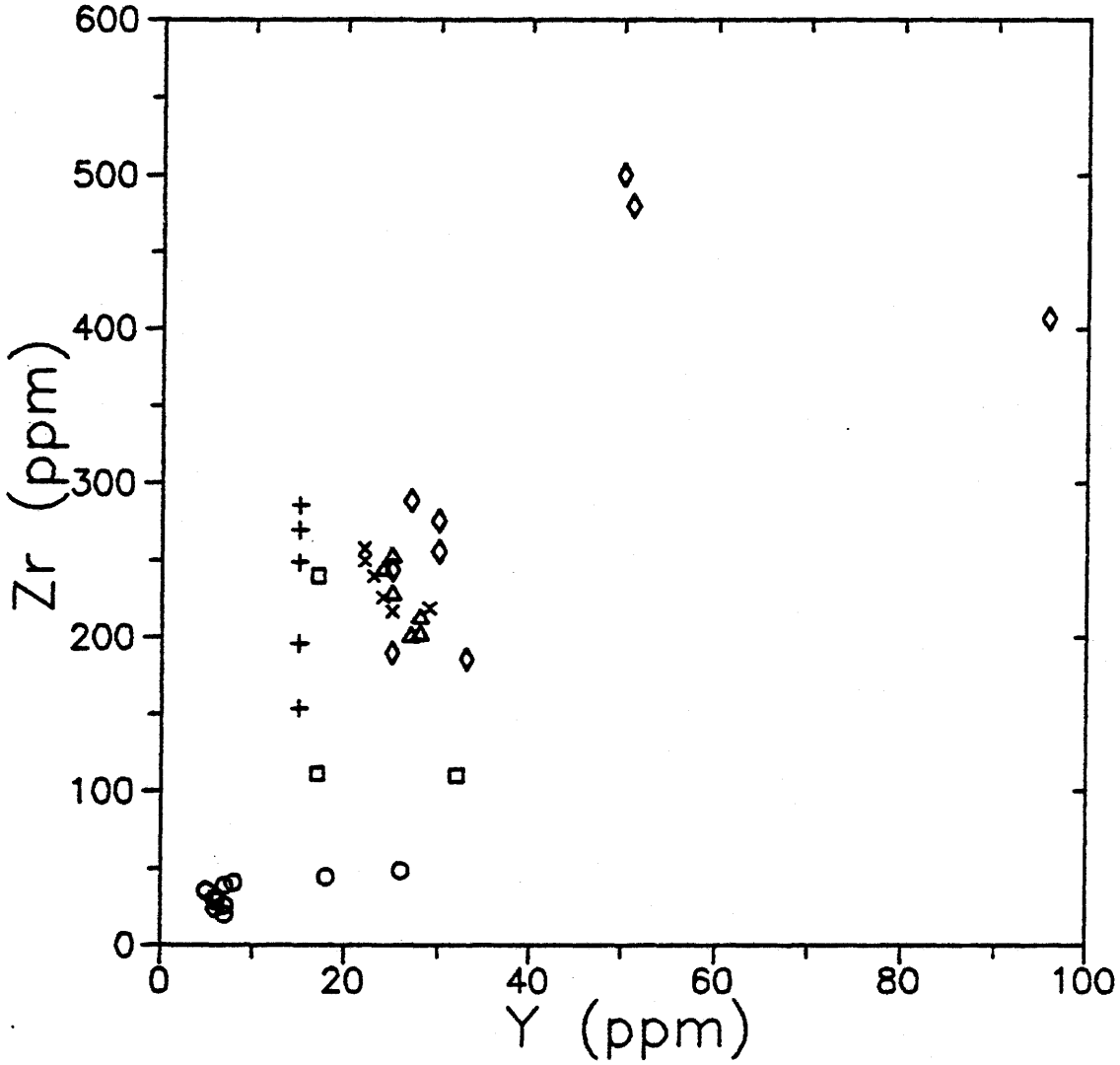

FIGURE 5.9

Variation of zirconium with yttrium concentration for Hawke River Terrane rocks

Symbol: o = WBAC gabbronorites
□ = WBAC monzogabbros
◇ = WBAC monzonites
Δ = Paradise Arm Pluton
\+ = Anhydrous PMGB rocks
x = PMGB gneisses

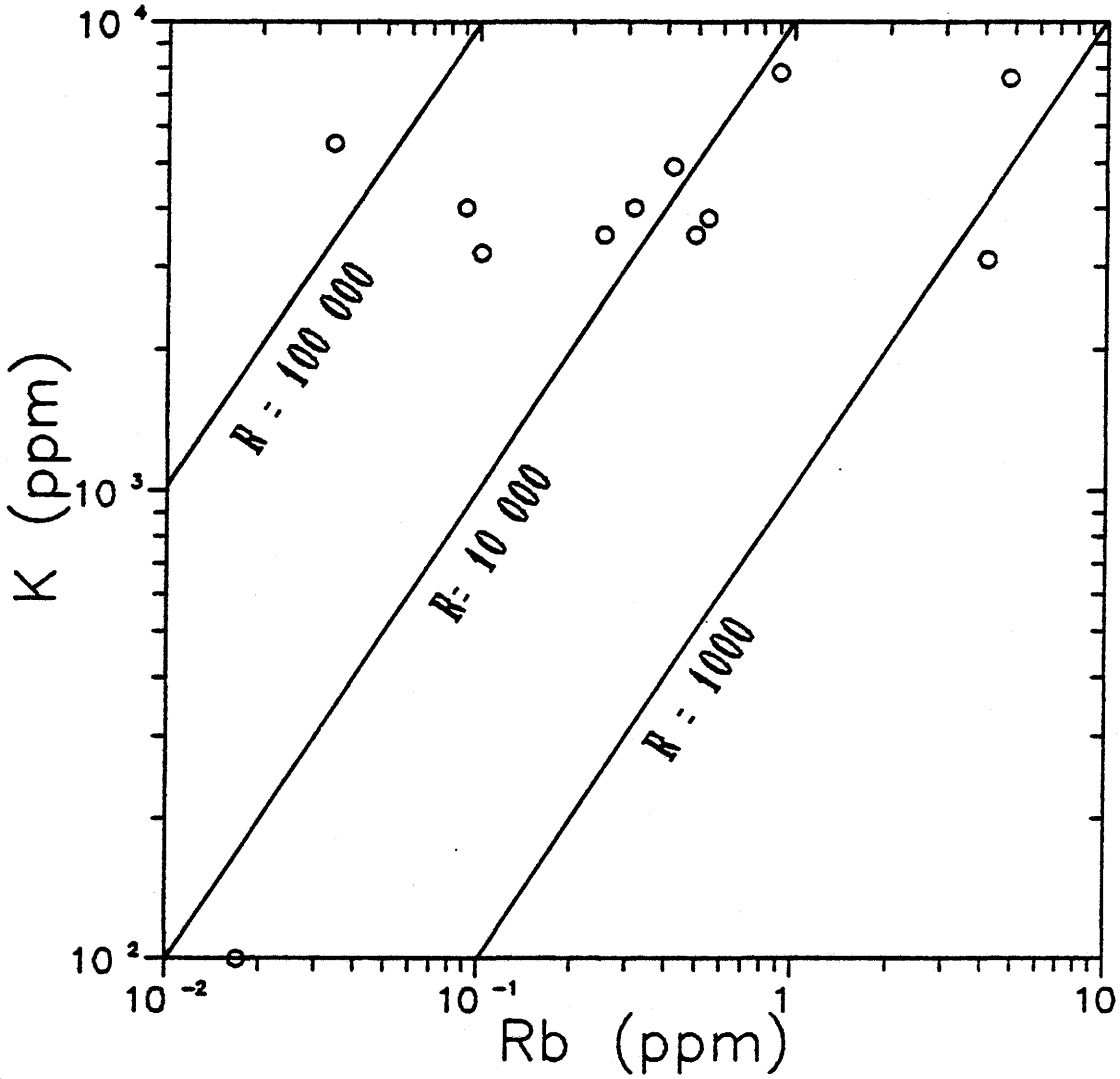

FIGURE 5.10 A

Variation of potassium with rubidium
for WBAC gabbronorites (log scales)

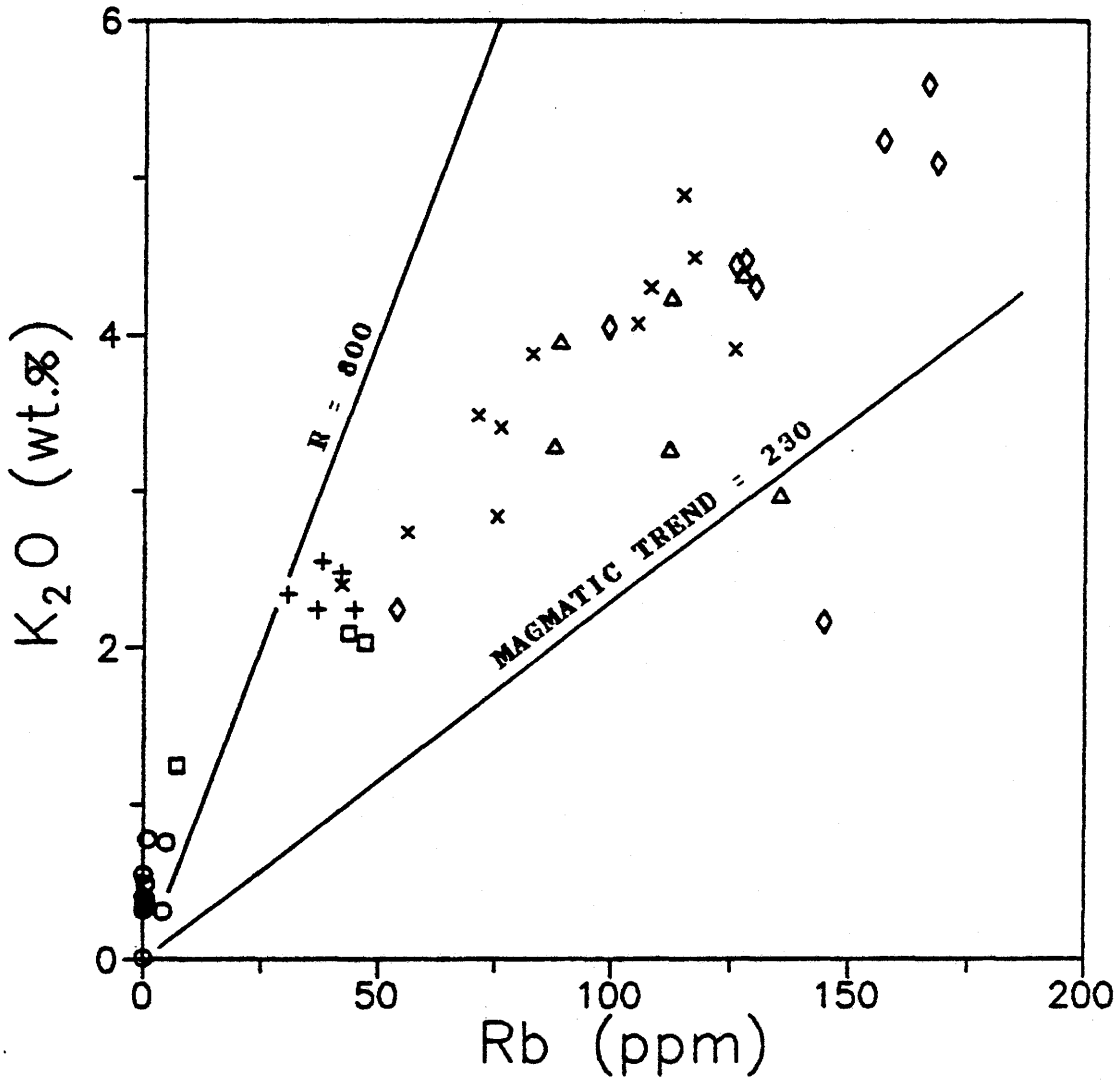

FIGURE 5.10 B

Variation of potassium with rubidium
for Hawke River Terrane rocks
"Magmatic Trend" (R=230) from Shaw (1968)

Symbol: o = WBAC gabbronorites
□ = WBAC monzogabbros
◇ = WBAC monzonites
Δ = Paradise Arm Pluton
\+ = Anhydrous PMGB rocks
x = PMGB gneisses

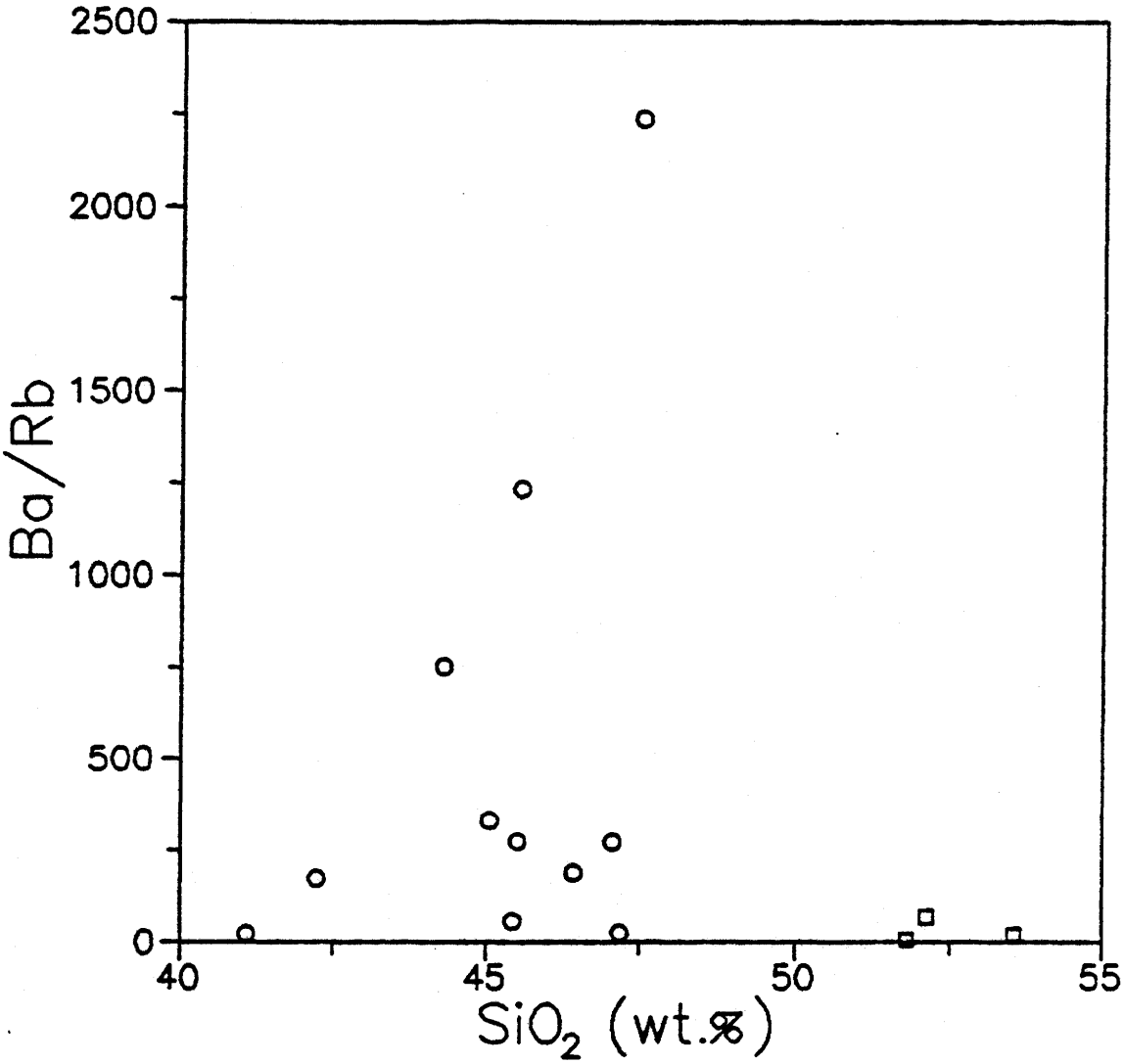

FIGURE 5.11 A

Variation of barium/rubidium ratio with silica for WBAC gabbronorites (log scales)

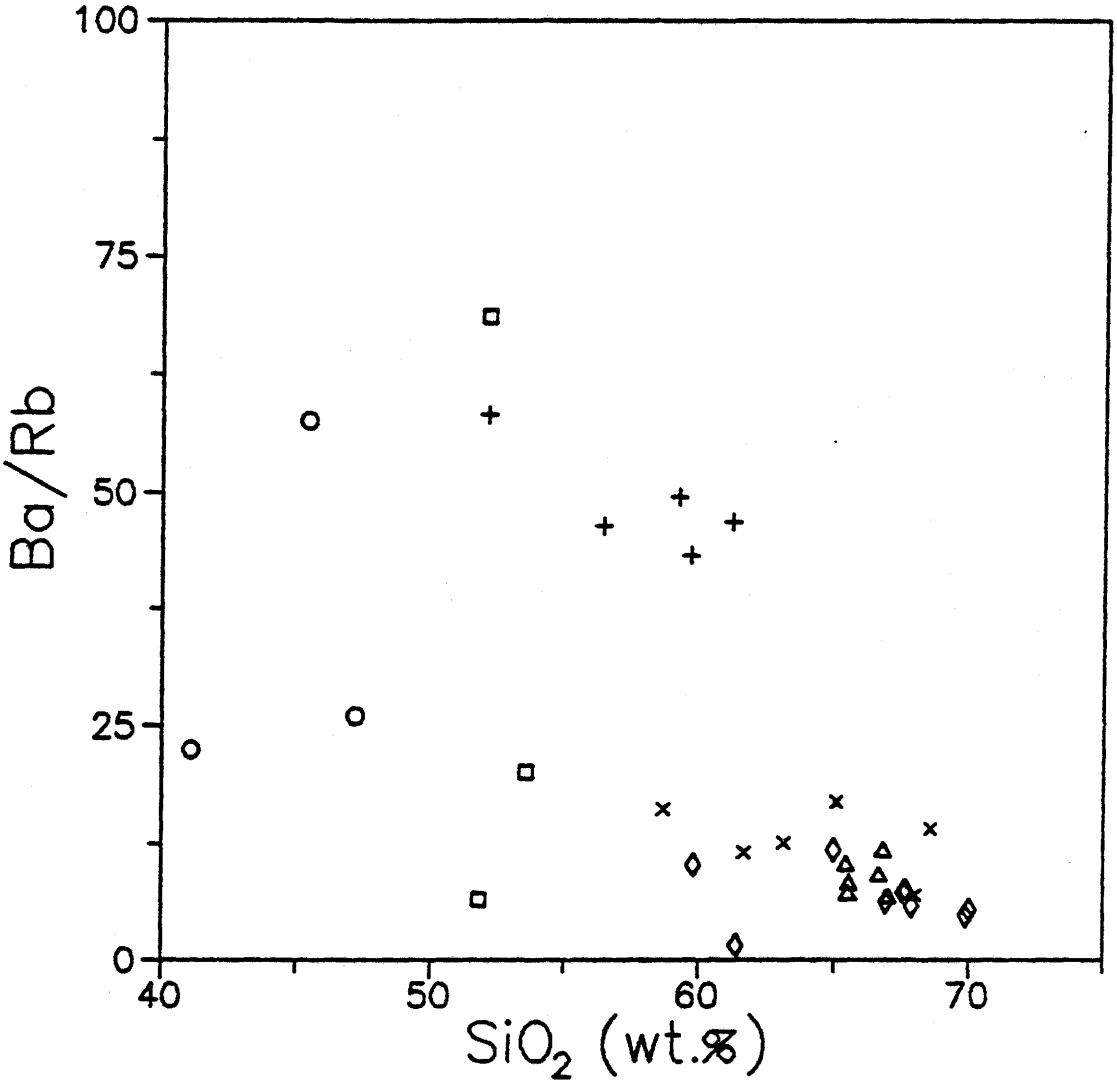

FIGURE 5.11 B

Variation of barium/rubidium ratio with silica for Hawke River Terrane rocks

Symbol: o = WBAC gabbronorites
□ = WBAC monzogabbros
◇ = WBAC monzonites
Δ = Paradise Arm Pluton
\+ = Anhydrous PMGB rocks
x = PMGB gneisses

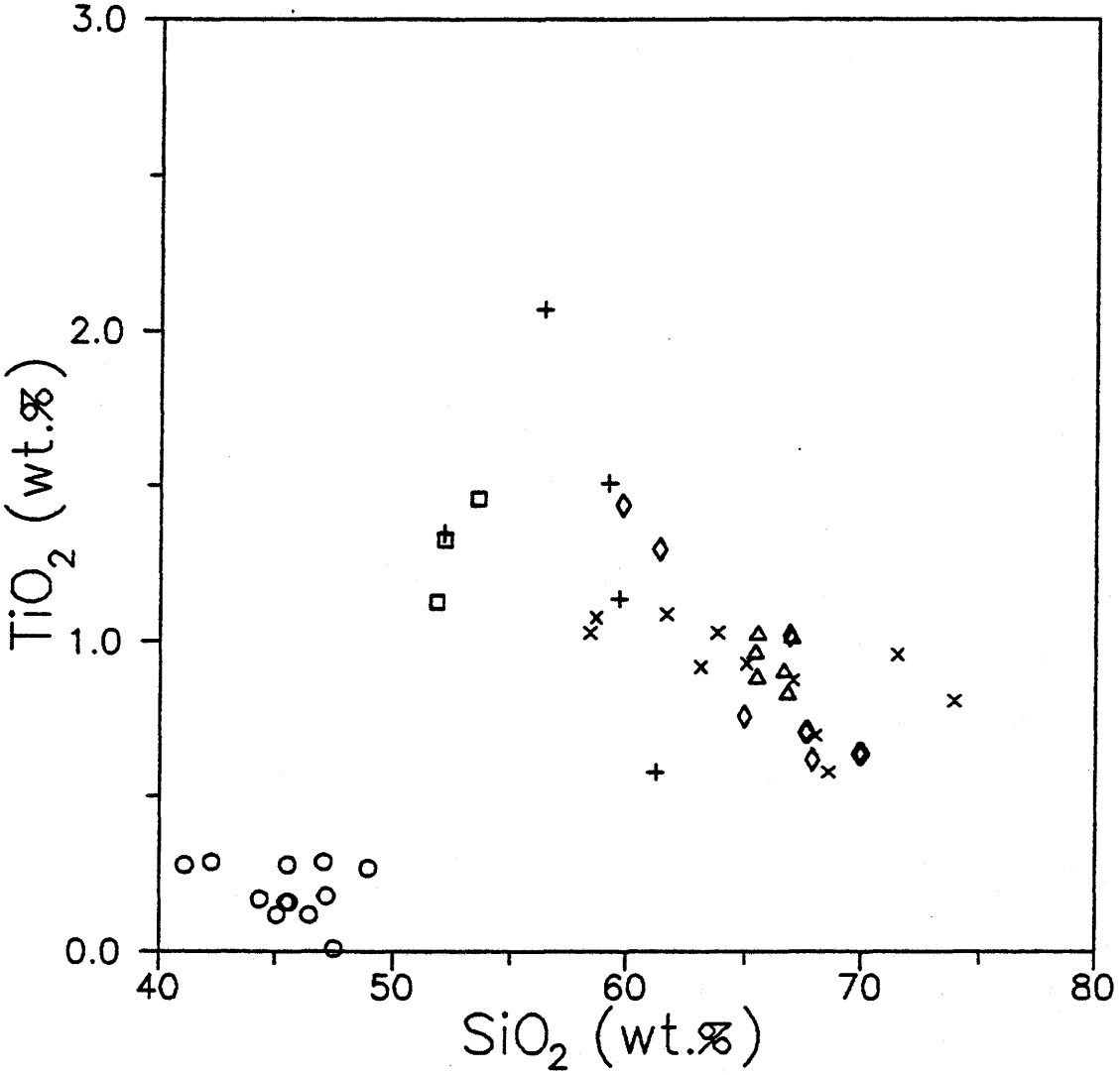

FIGURE 5.12

Variation in silica and TiO_2
for Hawke River Terrane rocks

Symbol: o = WBAC gabbronorites
□ = WBAC monzogabbros
◇ = WBAC monzonites
Δ = Paradise Arm Pluton
\+ = Anhydrous PMGB rocks
x = PMGB gneisses

rocks with quartz dioritic or monzonitic rocks related by differentiation (eg. O'Flaherty, 1986), the granodiorites may represent late, siliceous liquid from differentiation or partial melting of the gabbronorites, or (ii) the granodiorites may represent remelting or partial melting of the paragneissic rocks (ie. the PMGB gneisses) hosting the WBAC, or finally (iii) the source rock for the granodiorites could be a lower crustal or possibly upper mantle rock not exposed at the surface in the area.

There is no geochemical support for model (i) from incompatible elements such as titanium, yttrium and zirconium. Plotting Ti/Zr against a "modified" Larsen Index (Si/3 + K - Ca - Mg wt. % ;Shaw, 1972) shows two distinct trends; one for the gabbronorites and one for the granodioritic and metasedimentary rocks (Figure 5.8). Similarly, a plot of Zr against Y (Figure 5.9) shows two distinct clusters. In both cases the granodiorites and the paragneisses fall in overlapping fields, where the PAP rocks show a much stronger affiliation with the paragneissic rocks than do the WBAC granodiorites. Therefore incompatible elements favour formation of the granodiorites from remelting of or at least mixing with the PMGB paragneisses, as opposed to the gabbronorite.

Variation in the ratio of potassium to rubidium can be

used to investigate differentiation trends. The analytical error on Rb concentrations varies from 3 % (2σ) to 18 % (Appendix 10). Sample 8512, for which Rb = 0.017 ± 0.006 ppm, has been left out of this discussion as its K_2O concentration (0.01 wt. %) is too low for accurate analysis by XRF. K_2O concentrations have very low precision for all the gabbronorites, as shown by replicate analyses, in Appendix 9. Rb in the gabbronorites ranges from 4.80 ppm (in 8602-pyroxenite) to as low as .034 ppm, which is similar to Rb concentrations of achondritic meteorites (Shaw, 1968). The ratio $R = 10^4 \times K_2O/Rb$ for the gabbronorites varies from 759 up to 160,000 (Figure 5.10 A). Although very little published data exists for the trace elemental composition of coronites, the WBAC K/Rb ratios are significantly higher than the R = 400 to 609 presented for coronitic dolerites by Emmett (1982). Besides achondritic meteorites with R = 2250 to 3600 (Shaw, 1968), ratios of a similar order of magnitude to the WBAC coronites have also been noted in plagioclase in nephelinites (R = 780-2100: Heier, 1966) in primary hornblendes ($R \leq 5000$; Hart and Aldrich, 1966), and in abyssal tholeiites (R = 475 to 1830; Gast, 1965). In the first case the elevated ratios are accounted for by Rb depletion, although whether it is a primary or secondary process was not determined. The other two cases and the achondrites are instances of high primary ratios of potassium to rubidium. The implication of this is that the WBAC gabbronorites represent relatively primitive

mantle rocks, which may have had potassium metasomatism by Rb-poor material or depletion of Rb in order to generate the exceptionally high K/Rb ratios.

The K/Rb ratio of igneous rocks in the crust, whether of crustal or of upper mantle origin, show a relatively limited range between about 200 and 270 (Heier and Adams, 1964; Shaw, 1968), with the main trend at around R = 230 (Shaw, 1968). While none of the units studied display ratios as low as this except for one PAP sample, the ratios of the felsic units fall in a relatively narrow range (Figure 5.10 B). While it has been observed that the K_2O/Rb ratio decreases with increased differentiation (Heier and Adams, 1964; Shaw, 1968), the degree of variation generated by differentiation is not well quantified, although Heier and Adams (1964) present a gabbro to granodiorite transition reflected by a drop in the K/Rb ratio from 310 to 240. Thus, it seems more likely that the 'monzonites' and/or granodiorites were derived from some small degree of partial melting of the paragneisses than from extreme fractional crystallisation of the gabbronorite, although the latter cannot be ruled out.

Heier and Adams (1964) suggest that due to the relative insensitivity of the K_2O/Rb ratio to fractionation processes, the ratio Ba/Rb should be used as a fractionation monitor. A plot of Ba/Rb against silica for the gabbronorites shows two

trends (seen in Fig. 5.11 A); one is well defined by five points with a moderately steep positive slope, and the other less well defined by six points with a shallow negative slope. There is no apparent correlation between the $(Ba/Rb)/SiO_2$ value and modal or normative compositions distinguishing the two trends. However, Heier and Adams (1964) suggest that while both Ba^{+2} and Rb^{+1} substitute for K^{+1}, due to the similarity in sizes (atomic radii of 2.78 A, 2.98 A, and 2.77 A respectively), Ba is preferentially enriched in the early fractions because of its higher charge, and Rb may be enriched in the later fractions due to its large size. Hence, the Ba/Rb ratio should decrease with increasing differentiation. This predicted relationship between Ba/Rb and SiO_2 is not observed in the five samples with the positively sloping trend, but is observed in the six low Ba/Rb rocks, whose trend leads into the more siliceous rocks seen in Figure 5.11 B. Here also a trend of decreasing Ba/Rb with increasing silica is observed, progressing from the PMGB paragneisses to the two plutonic units; the PAP and the WBAC monzonite. The monzogabbros and the anhydrous PMGB rocks again display Ba and Rb concentrations as well as Ba/Rb ratios intermediate between the gabbronorite and the more siliceous units.

5.4 Mixing Origins - Monzogabbros and Anhydrous Metasediments

Mixing between the gabbronorite and the granodiorites and

the PMGB paragneisses for the WBAC monzogabbros and the anhydrous PMGB rocks from the contact zone , respectively, has been indicated by petrography of the latter two units. The latter two units also plot directly between the gabbronorites and the more felsic units for every major and trace element analysed for, with the partial exception of titanium.

The gabbros are relatively low in Ti content, compared to oceanic basalts for example (eg. Mullen, 1983), and have relatively constant Ti concentrations with a poorly defined trend of TiO_2 depletion with increasing silica (Fig. 5.12). The highest values of TiO_2 occur in the anhydrous PMGB rocks, also showing wide variation in Ti content, which correlates weakly with a similar trend in total iron, reflecting the relative abundances of spinel series phases. This supports a hypothesis of migration of oxidising fluids rich in iron and titanium from the gabbronorite into the adjacent units, indicated by the petrography of the contact zone rocks.

CHAPTER 6: ISOTOPE GEOCHEMISTRY

The radiogenic isotope systems ^{87}Rb-^{87}Sr and ^{147}Sm-^{143}Nd were studied for both geochronological and genetic information. As a result of the geochemical coherence of parent and daughter element, the ^{147}Sm-^{143}Nd system is relatively insensitive to secondary processes such as metamorphism (eg. McCulloch and Wasserburg, 1978) or deuteric alteration. Isotopic effects of pre-crystallisation processes such as mantle mixing and crustal contamination are potentially more visible in the Sm-Nd system than Rb-Sr since secondary metamorphic effects can complicate the latter system more easily. Isotopes of Rb, Sr, Sm, and Nd were analysed using the methods outlined in Appendix 2, and the isotopic data for Sr and Nd is listed in Appendix 5. All Rb-Sr and Sm-Nd "isochron" regressions are calculated using the method of York (1969), given with 2σ errors on the ages and initial ratios. All diagrams plotting $^{87}Sr/^{86}Sr$ versus $^{87}Rb/^{86}Sr$ and $^{143}Nd/^{144}Nd$ versus $^{147}Sm/^{144}Nd$ are referred to as "isochron diagrams" regardless of the degree of statistical validity of the plotted points. The criterion of Brooks *et al.* (1972) (ie. mean square of weighted deviates (MSWD) < 2.5) is not used to qualify the geologic validity of linear regression ages. However, slope and Y-intercept errors corresponding to expansion of the sample errors in Y proportional to the value of X until the MSWD = 1.0 are presented in Table 6.1, recog-

nising that the York II errors are not necessarily representative of meaningful uncertainty on the ages.

6.1 WBAC Gabbronorite

6.1.1 Sr isotopes

The Rb-Sr results for the gabbronorites show two distinct trends, shown in Figure 6.1, neither of which qualifies as an isochron. The slope of the steeper trend corresponds to an age of 17 Ga, which is more than three times the age of the earth and hence geochronologically meaningless. The initial $^{87}Sr/^{86}Sr$ ratio (I_{Sr}) is 0.7027 ± 1. A shallower trend defined by three samples is shown relative to a 1.65 Ga reference isochron.

Metamorphic events of insufficient "magnitude" (ie. temperature, water pressure or total pressure) to homogenise a given isotope system on the whole-rock scale may be reflected by the mineral systematics. Plagioclase, clinopyroxene and orthopyroxene were separated from samples 85-11 and 85-05, plus olivine and amphibole from the former sample. A three point plag-cpx-opx isochron from 85-11 gives an age of 1.7 ± 0.2 Ga, with an I_{Sr}=0.70243 ± 4 and a MSWD=12, shown in Figure 6.2 A. The amphibole and olivine separates from 8511 which are not colinear with the other three minerals are also the

only phases which have contain water; the amphibole has 1.5 to 2 wt.% structural water, as reflected by the oxide totals from microprobe analyses, and the olivine displays alteration to iddingsite and bowlingite. The whole-rock has been pulled off the line defined by the plag-cpx-opx towards the olivine and amphibole. There has also been a Rb depletion of the whole rock, as it is poorer in Rb than its component minerals. There are no low $^{87}Rb/^{86}Sr$ phases present in significant quantity and with enough Rb and Sr to account for the whole-rock composition, and analytical imprecision is also insufficient to account for the depletion. A four point w.r.-plag-cpx-opx isochron from 85-05 gives an age of 1650 ± 35 Ma, with an I_{Sr} = 0.70278 ± 6 and the MSWD = 75. Excluding the whole-rock, a three point mineral age of 1674 ± 15 Ma is produced, with an I_{Sr} = 0.70293 ± 4 and the MSWD = 0.4, shown in Figure 6.2 B.

There is a much greater spread in both $^{87}Rb/^{86}Sr$ and $^{87}Sr/^{86}Sr$ in the minerals of sample 85-05 than in those of 85-11, particularly from the opx. This reflects the alteration of opx and also amphibole to biotite, reflected in the modal mineralogies.

6.1.2 Nd Isotopes

The Sm-Nd results from the WBAC gabbronorites do not

provide precise constraints on the time of intrusion of the WBAC. Combining whole-rock plus minerals gives an age of 1555 ± 34 Ma, with I_{Nd} = 0.51077 ± 2 and a MSWD = 56, shown in Figure 6.3. A common problem with whole-rock Sm-Nd systematics in mafic rocks is the lack of isotopic variation sufficient to give precise isochron ages. Separating minerals with different Sm/Nd ratios can provide sufficient spread to improve the precision of the age. This was not the case for the two mineral-w.r. systems investigated from the WBAC gabbronorites (ie. although the variation in $^{147}Sm/^{144}Nd$ was increased, the scatter remained large). A four point w.r.-olivine-clinopyroxene-amphibole system from sample 8511 gives an age of 1390 ± 56, with I_{Nd} = 0.51104 ± 8 and the MSWD = 97. A three point w.r.-plagioclase-orthopyroxene line from 8505 gives an age of 1580 ± 70, with I_{Nd} = 0.51079 ± 6 and the MSWD = 210. The scatter on all of the Sm-Nd ages is well in excess of analytical error, as reflected by the very large MSWD values. This variation is interpreted in terms of crustal contamination, discussed in Section 7.2.2.

6.2 Felsic Units - Sr Isotopes

The WBAC 'monzonite', excluding the monzogabbros, gives a Rb-Sr age of 1621 ± 11 Ma with an I_{Sr} = 0.7035 ± 2 and a MSWD = 24, shown in Figure 6.4 A. Addition of the monzogabbros has no significant effect on the regression, giving an age of 1617

± 8 with an I_{Sr} = 0.70330 ± 3 and an MSWD = 67. The Paradise Arm Pluton gives a Rb-Sr age of 1573 ± 18 Ma, with an I_{Sr} = 0.7043 ± 2 and a MSWD = 9 (Fig. 6.4 B). The significance of these ages will be discussed in Section 7.3.

The PMGB gneisses, shown in Figure 6.5, give an age of 1629 ± 16 Ma with an I_{Sr} = 0.7043 ± 2 and a MSWD = 35. Combined with the anhydrous PMGB rocks, the PMGB gives an age of 1664 ± 9 Ma and I_{Sr} = 0.70395 ± 3 and a MSWD = 45. However, the improved precision may be meaningless since the anhydrous gneisses are products of metasomatism of the metasediments from the gabbronorites, based on petrographic and geochemical evidence.

Table 6.1 shows the ages, initial ratios and errors calculated using York (1969), and also with errors derived by expansion of the $^{87}Sr/^{86}Sr$ sample errors proportional to $^{87}Rb/^{86}Sr$, until the MSWD = 1.0. (Gabbronorite is abbreviated "G-N".) Note that the PAP is distinctly younger than the other units based on the York II ages, but is within 2σ error of the other ages using the expanded ages. Hence, any conclusions based on significant age differences (see Section 7.3) are potentially suspect, depending on the interpretation of "significant".

TABLE 6.1

Rb-Sr AND Sm-Nd ISOCHRON DATA

Rb-Sr:

Unit	Age ± 2σ (Ma)	I_{Sr} ± 2σ	MSWD
WBAC G-N: 8511 minerals (n=3)	1742 ± 180 (600)	0.70243 ± 4 (14)	12
8505 minerals (n=3)	1674 ± 15 (10)	0.70293 ± 4 (2)	0.4
WBAC Monzonite (n=8)	1621 ± 11 (48)	0.7035 ± 2 (8)	24
Monzonite + monzo-gabbros (n=11)	1617 ± 8 (58)	0.70330 ± 6 (40)	67
PAP Granodiorite (n=5)	1573 ± 18 (40)	0.7043 ± 2 (5)	9
PMGB Gneiss (n=9)	1629 ± 16 (90)	0.7043 ± 2 (10)	35
Total PMGB (gneiss plus contact rocks) (n=14)	1663 ± 9 (64)	0.70395 ± 4 (40)	90

Sm-Nd:	Age ± 2σ (Ga)	I_{Nd} ± 2σ	MSWD
WBAC gabbronorite w.r. plus minerals (n=12)	1.56 ± 0.03 (0.26)	0.51077 ± 2 (30)	56
85-11 w.r.-cpx-ol-amph (n=4)	1.39 ± 0.06 (0.56)	0.51104 ± 4 (80)	97
85-05 w.r.-plag-opx (n=3)	1.58 ± 0.07 (1.0)	0.51079 ± 6 (100)	211

Errors are calculated by York II method; errors in parentheses calculated by proportional expansion of errors until MSWD=1.0.

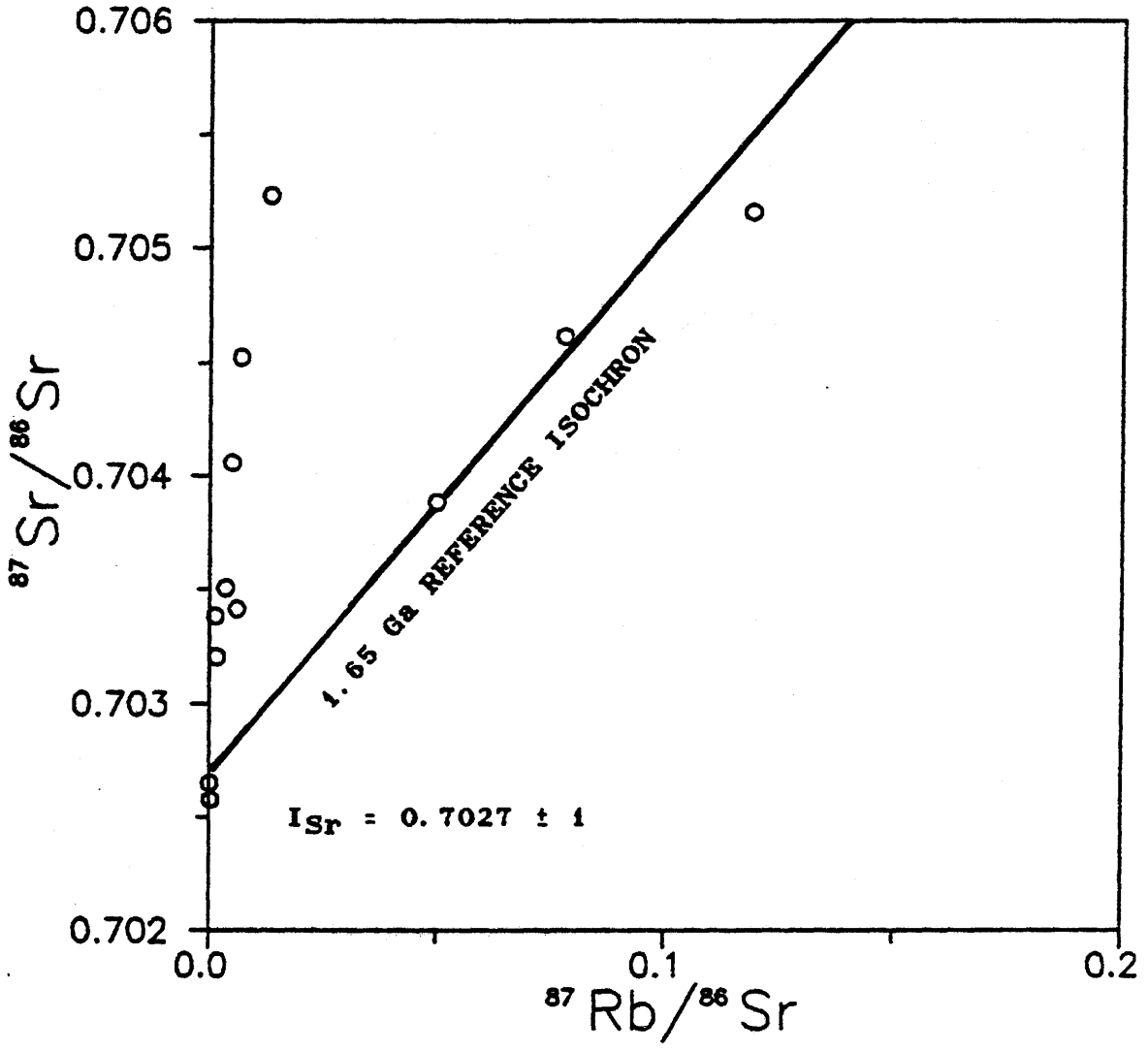

FIGURE 6.1

Rubidium-strontium whole-rock "isochron diagram" for the WBAC gabbronorite

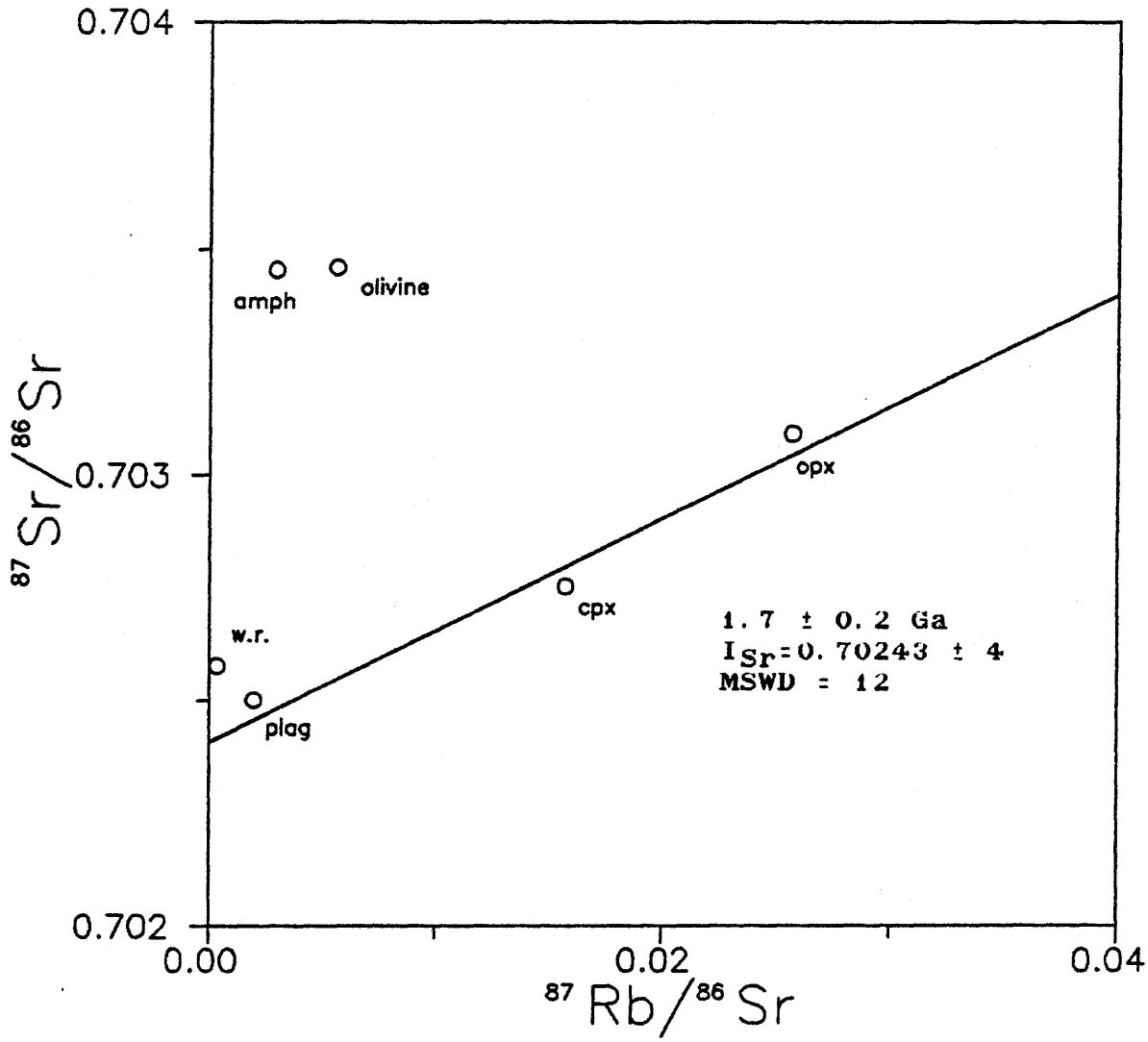

FIGURE 6.2 A

Rubidium-strontium mineral "isochron diagram"
for WBAC gabbronorite sample 8511
whole-rock plus five minerals

Regression is for plagioclase-
clinopyroxene-orthopyroxene

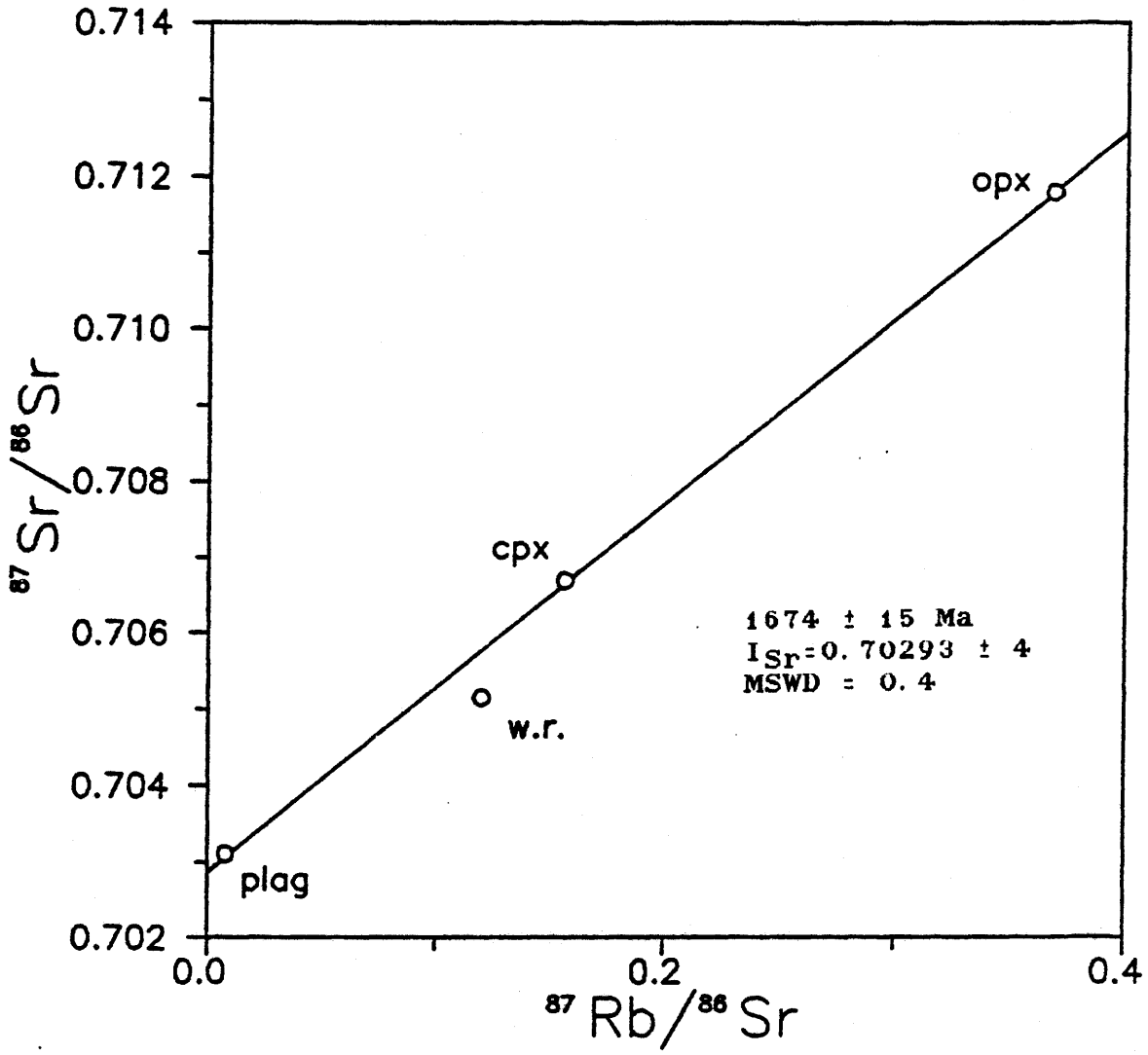

FIGURE 6.2 B

Rubidium-strontium mineral "isochron diagram"
for WBAC gabbronorite sample 8505
whole-rock plus three minerals

WR is excluded from the regression

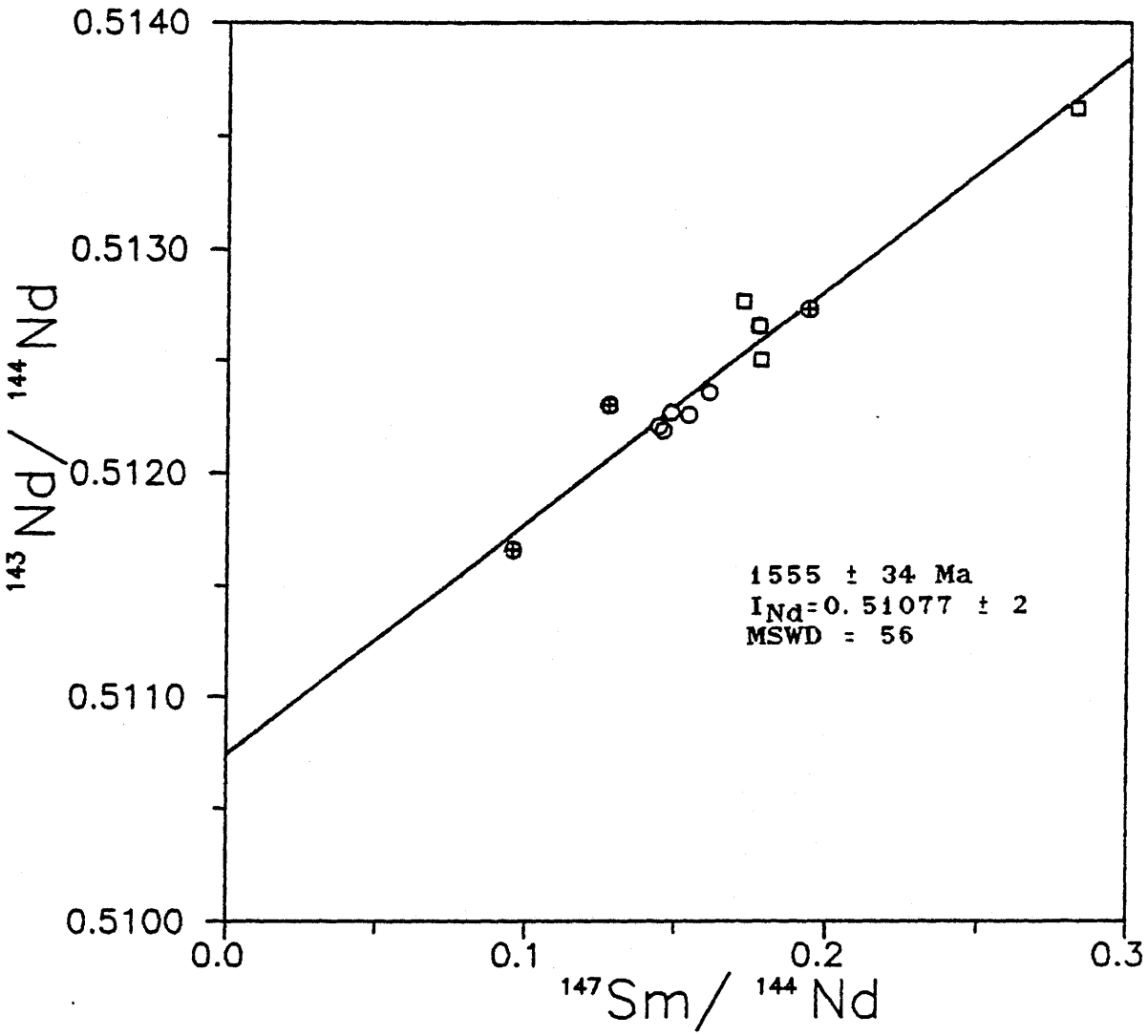

FIGURE 6.3

Samarium-neodymium "isochron diagram"
for WBAC gabbronorite whole-rocks plus minerals

Symbol: o = whole-rocks
□ = 8511 minerals
⊕ = 8505 minerals

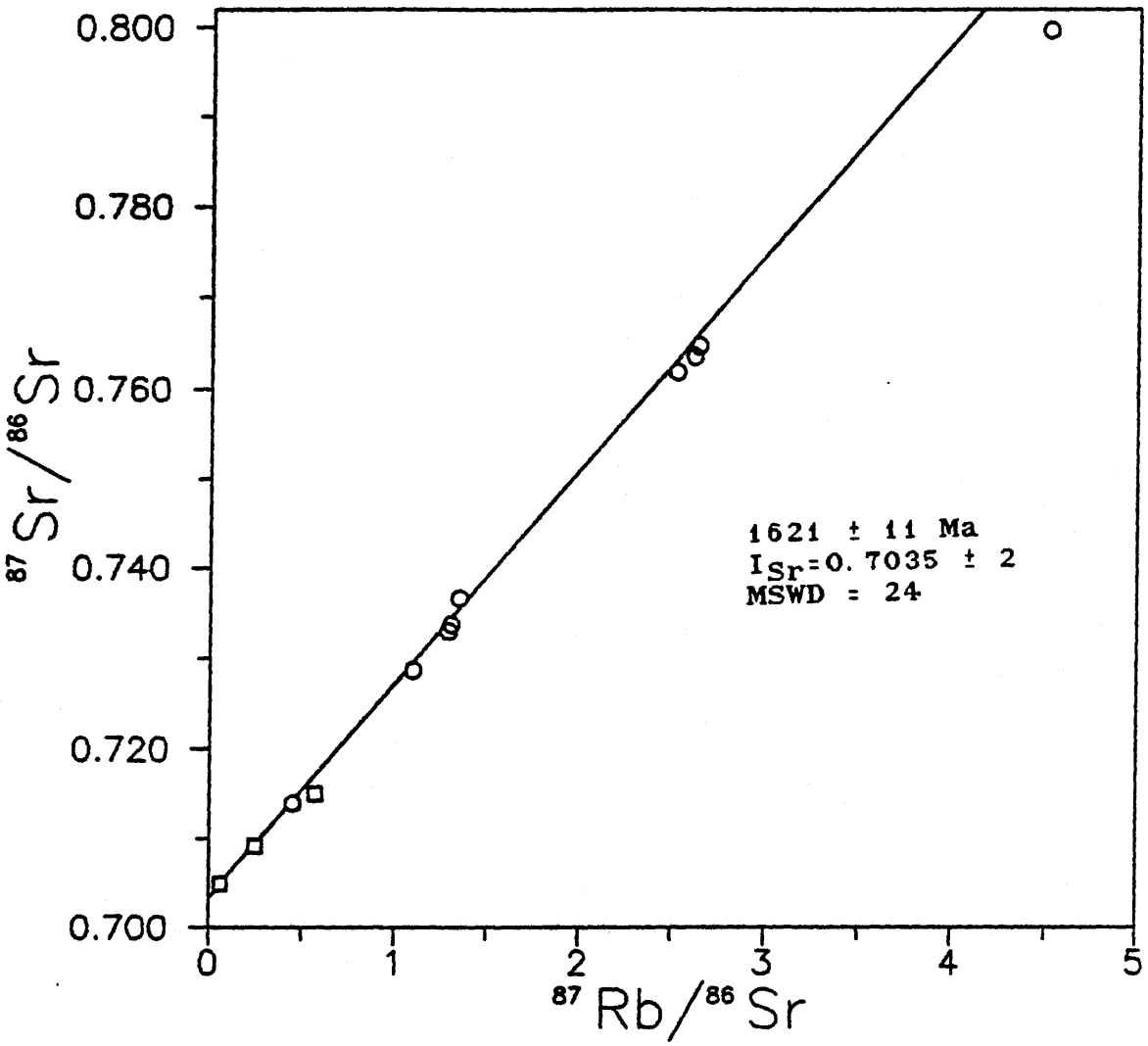

FIGURE 6.4 A

Rubidium-strontium whole-rock "isochron diagram" for WBAC monzonitic to monzogabbroic rocks

Symbol: o = WBAC monzonite
□ = WBAC monzogabbro

Regression excludes monzogabbros and Sample 85-10, in upper right corner, which is heavily weathered.

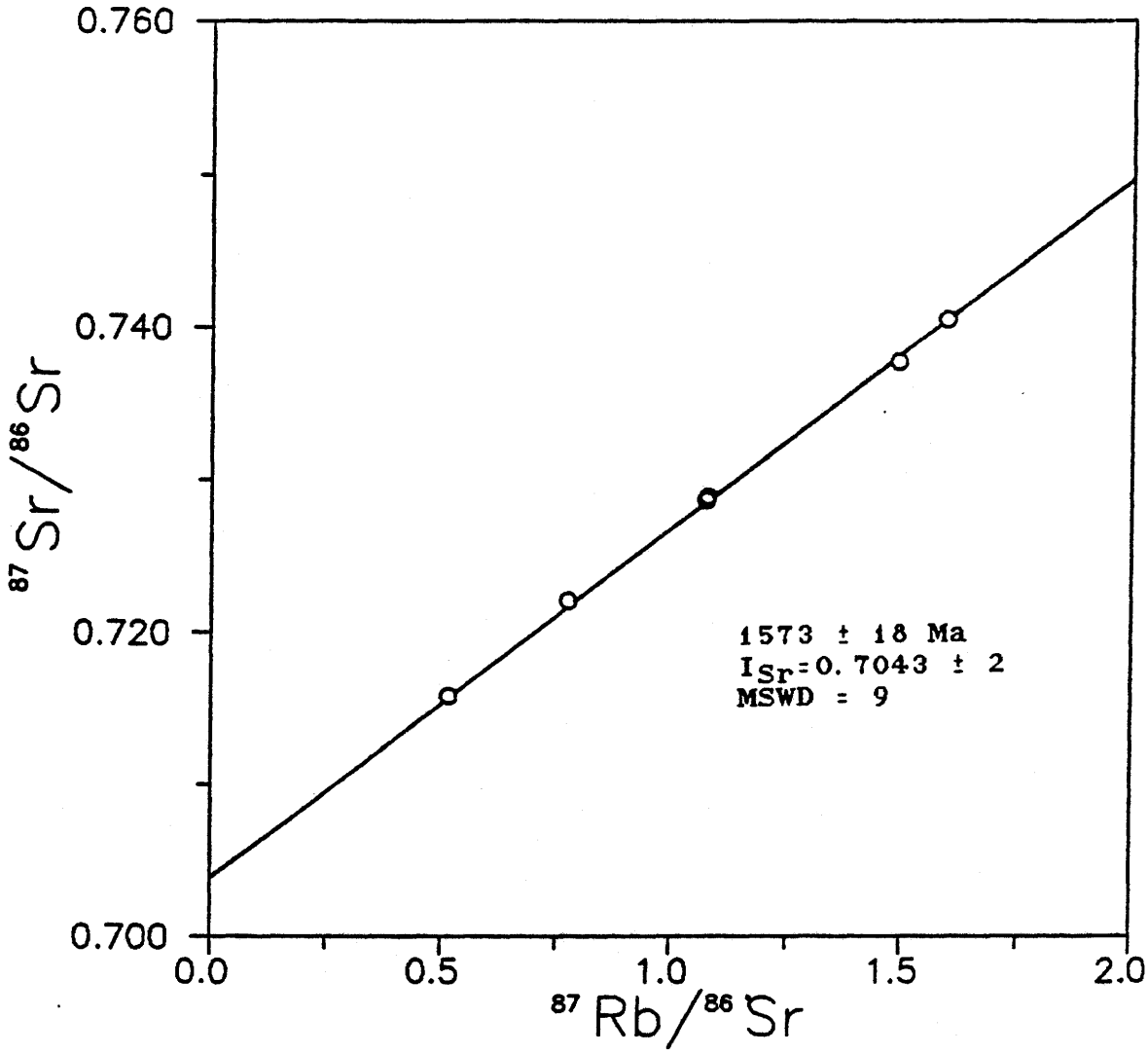

FIGURE 6.4 B

Rubidium-strontium whole-rock "isochron diagram"
for Paradise Arm Pluton rocks

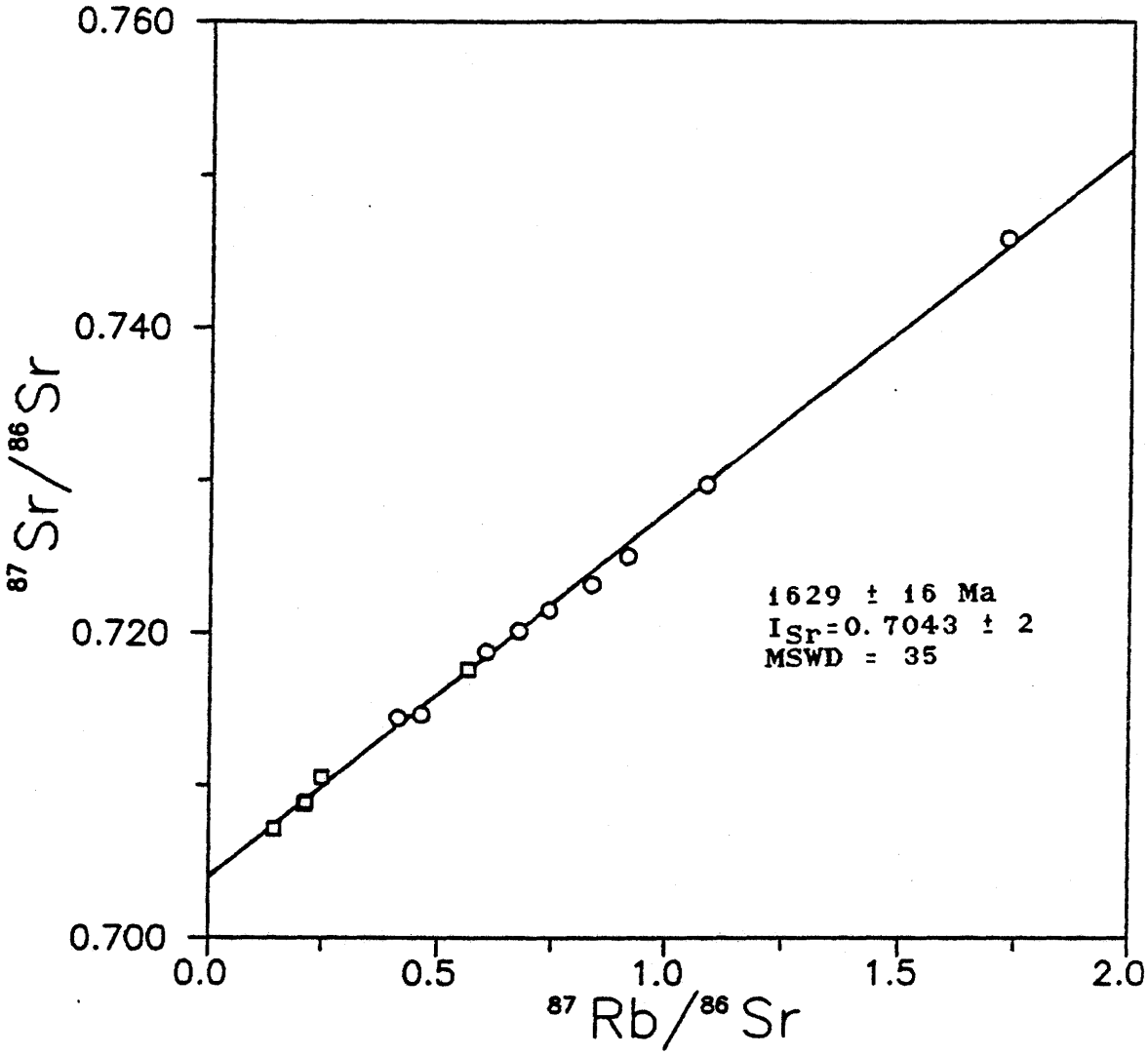

FIGURE 6.5

Rubidium-strontium whole-rock "isochron diagram" for Paradise Metasedimentary Gneiss Belt rocks

Symbol: o = PMGB gneisses
□ = PMGB anhydrous contact zone rocks

Regression excludes anhydrous contact rocks

CHAPTER 7: DISCUSSION

7.1 Coronite Geochemistry

The mineral stoichiometries of a WBAC coronite are given in Appendix 7, and the mineral major element analyses are listed in Appendix 6. The WBAC mineral compositions are from sample 8511, which is the coarsest-grained coronite sampled, possessing very well-defined corona structures. 8511 represents an early stage of corona development, and is therefore not necessarily representative of later stages of corona development. The microprobe mineral analyses, presented in Appendix 6, were screened by eliminating all data with atomic proportion totals more than ± 0.020 from the expected value for a given mineral, or if the oxide totals were not within 100 ± 2 %. All mineral compositions fit stoichiometric formulae except for plagioclase, which has insufficient alumina and silica to account for all the Ca and Na. Since the microprobe analyses on plagioclase were made principally on grain rims which show strong zoning, the non-stoichiometric plagioclase may be a function of diffusion-related disequilibrium, or may represent analysis of Na and Ca from underlying amphibole, the adjacent mineral in most cases. In order to reduce the likelihood of either of these complications, an average of five "undepleted" plagioclases, taken from furthest from the grain boundaries, was used in

diffusion calculations, although this plagioclase was still non-stoichiometric.

The bulk mineral compositions of labradorite, chrysolite, pargasite, and bronzite agree with those of other coronite occurences (eg. Reynolds and Frederickson, 1962; Mason, 1969; Gower, 1986). The clinopyroxene in coronites is generally augite, but in 8511 it is almost on the diopside-hedenbirgite join and is more aluminous than normal augite (6.0 wt.% Al_2O_3 as opposed to 3-4 wt.% (Deer *et al.*, 1966) or other clinopyroxene in coronites (eg. 2.93 wt.% in Gower, 1986). According to Deer et al (1966) augite is the only pyroxene with significant (ie. >2 wt.%) alumina, and equally calcic "augite" has been observed from the earliest stages of differentiation sequences, albeit in sills rather than larger layered mafic complexes.

Of the minerals studied, only plagioclase shows significant compositional variation, varying from An_{65} to An_{97}. Olivine shows very little compositional variation, such that the 2σ of the average MgO or Fe_2O_3 content from 11 analyses is only about 0.5 wt.%. Zoning in the augite was more difficult to monitor due to the interference of exsolved orthopyroxene bands, shown in Figure 7.1 A, but the composition of the augite is relatively consistent. The orthopyroxene exsolved from primary augite is more aluminous

than the bronzite in the coronas, but is otherwise similar. A symplectic intergrowth of opaque, bronzite and olivine shown in Figure 7.1 B is compositionally indistinct from other grains of the latter two minerals.

The plagioclase surrounding intercumulus augite or primary orthopyroxene shows inverse zoning from about An_{66} to An_{95} towards the contact, over 0.5 mm. Across the corona sequence plag-amph-opx-ol, plagioclase shows weak normal zoning from An_{77} to An_{66}, on the same order of magnitude as compositional oscillation away from the grain boundary, consistent with observations from other coronites (eg. Mason, 1969; van Lamoen, 1979).

Mineral densities were calculated based on their compositions, using Deer *et al.* (1966), except for pargasitic amphibole, for which the density of stoichiometric pargasite was used. The composition of the spinel in the amphibole-spinel symplectite was not obtained using the microprobe due to the small grain size, so a composition of $(Fe_{0.67}Mg_{0.33})(Al_2O_4)$ was used, based on compositions of spinels in other symplectites (van Lamoen, 1979; Joesten, 1986a). From the excess Al, Fe and Mg in the symplectite analyses, a spinel contribution of 1.82 volume %, or 13.04 molecular % of the symplectite was calculated. This lies between the values given by van Lamoen (1979) and Joesten (1986a) (0.125 vol.%

Figure 7.1

A: Grain of augitic clinopyroxene showing exsolved (lighter coloured) lamellae of bronzitic orthopyroxene, from 8511. Note the absence of any coronitisation at the plagioclase-clinopyroxene contact.

(xp: x25) width of field is 4 mm

B: Symplectic intergrowth of orthopyroxene (pale brown, with minor darker brown biotite), olivine (more birefringent material) and opaque in olivine adjacent to a clinopyroxene grain entirely surrounded by the olivine, also from 8511.

(xp: x25) width of field is 4 mm


A

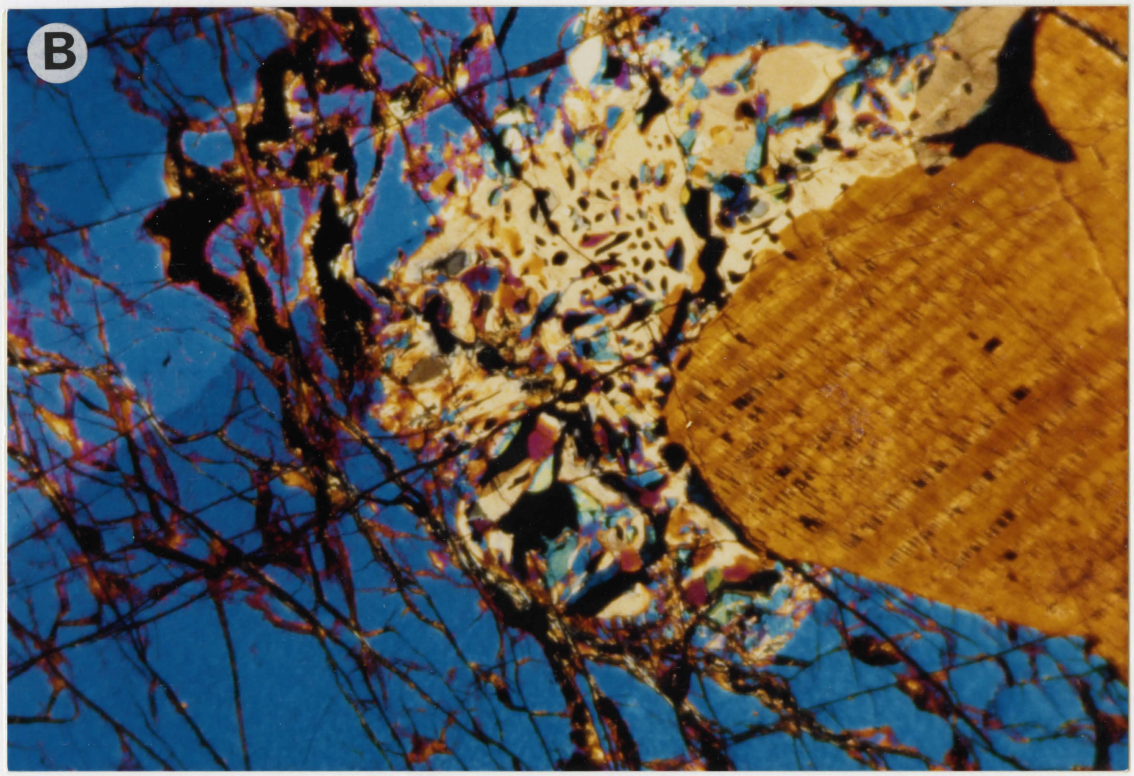
B

and 3.7 vol.%, respectively).

All previous workers have assumed that corona formation is a constant volume process, based on the lack of textural evidence to the contrary. The volume ratio of amphibole-spinel symplectite to bronzite is known from the modal analysis of sample 8511. Using these criteria, the following equation can be calculated, as shown in Appendix 7:

$$1.21\ \text{Chrysolite} + \text{Labradorite} + (0.14\ \text{Fe} + 0.47\ \text{Mg} + 0.03\ \text{K})_{\text{fluid}} \rightarrow$$
$$0.85\ \text{Bronzite} + 0.30\ \text{Pargasite} + 0.06\ \text{Spinel} + (0.13\ \text{Si} + 0.55\ \text{Al} + 0.16\ \text{Ca} + 0.16\ \text{Na} + 0.20\ \text{O})_{\text{fluid}}$$

If the labradorite is made stoichiometric with respect to Si and Al (requiring 0.12 Si and 0.12 Al), the above reaction becomes essentially closed for Si. Potassium could be supplied by fluids from the associated felsic units or from a mantle source. A source of Mg and Fe is less obvious, as all of the plutonic and paragneissic bodies associated with the WBAC are Mg poor. A possible explanation is that the amphibole analyses are enriched in Mg from overlap of the electron-beam onto the fine-grained spinel. Stoichiometric amphibole could be calculated with less Mg by replacing it with ferrous and/or ferric iron. There is no dissolution of primary spinel observed. However, the ratio of Mg to Fe in

the "fluid" phase is very similar to the 3:1 ratio in either the bronzite or the olivine. As replacement of the coronitic orthopyroxene is not observed, consumption of olivine is indicated. Internal replacement of olivine by bronzite-opaque symplectite observed in sample 85-11 (Fig. 7.1 B) must generate excess Mg, as the bronzite and olivine have almost identical Mg/Fe ratios, and the opaques are Mg-free. This Mg source is supported by van Lamoen (1979), who suggests open system behavior on the scale of single coronas, but closed system behavior on a whole-rock scale. He suggests that the excess Al, Na and Ca may go into amphibole coronas around primary spinel and pyroxene. A more detailed study is required in order to confirm this for the WBAC coronites, but available data supports van Lamoen's conclusion that a closed system for the conversion of olivine and plagioclase to ortho-pyroxene and amphibole-spinel is an unjustified oversimp-lification, and that on a whole rock scale potassium is the only ion not available in sufficient quantity from the original mineralogy.

The fact that the Mg/(Mg+Fe) ratio is identical for the olivine and the bronzite and that no excess iron or magnesium is produced by the plagioclase to symplectite transformation makes Starmer's (1969) suggestion that the corona reactions supply the ions for clouding of the plagioclase less likely. However, sample 8511 is relatively weakly clouded, and it is

possible that the olivines in more heavily clouded rocks produce bronzite with different Mg/(Mg+Fe) ratios (ie. as time passes and temperature decreases) generating excess ions and producing spinel in the adjacent plagioclase.

7.2 Age and Origin of the Coronites

7.2.1 Timing of Corona Formation

Petrographic and geochemical evidence cannot rule out (or confirm) a primary magmatic or post-crystallisation cooling origin for the coronas. Radiometric age data cannot separate these two mechanisms either, as the mineral and whole-rock ages are indistinguishable. A precise Rb-Sr mineral age from 8505 rules out a secondary metamorphic origin for the coronas, unless it occurred within 20 or 30 Ma of the intrusion of the gabbro-norite, in which case it would be indistinguishable based on available data.

Both the Sm-Nd and Rb-Sr isochron diagrams show variation in excess of analytical error. The disturbance of the isotope systems is also reflected by model ages.

7.2.2 Model Ages

Model ages can be calculated by calculating the time

elapsed since extraction from a known isotopic reservoir, most effectively for unaltered, unmetamorphosed mafic volcanics. Table 7.1 shows model ages for the WBAC gabbronorites. Strontium model ages are calculated assuming extraction from a 'uniform reservoir' (UR) of McCulloch and Wasserburg (1978). Neodymium model ages are calculated assuming from a chondritic reservoir, using modern chondritic $^{143}Nd/^{144}Nd$ from Wasserburg *et al.* (1981) and $^{147}Sm/^{144}Nd$ from Jacobsen and Wasserburg (1980), and from an increasingly depleted reservoir (DePaolo, 1981), designated T_{CHUR} and T_{DM} respectively. Whole-rock and mineral model ages for both Rb-Sr and Sm-Nd are inconsistent; strontium T_{UR} ages vary between an older age of 1.65 ± 0.15 Ga and a younger age of 1.0 ± 0.1 Ga, while T^{Nd}_{CHUR} ages vary between 1.8 ± 0.2 and 1.1 ± 0.2. Neodymium T_{DM} ages are slightly more consistent but are older than the intrusive age of the WBAC, constrained by zircon dates around 1710 Ma from adjacent crustal rocks (Shärer and Gower, in press).

Mechanisms of generating scatter include (partial) metamorphic resetting and mixing with one or more isotopically distinct reservoirs (ie. contamination).

7.2.3 Contamination of the Gabbronorite

Sr and Nd isotopes can be used to investigate the likelihood of crustal contamination of the gabbronorite.

Silica does not correlate with $^{87}Sr/^{86}Sr$ or with $\epsilon_{Sr}(1650)$, which would be expected from bulk rock contamination by a silica and radiogenic strontium enriched crustal rock. However, Sr and Nd isotopes are sensitive to small amounts of contamination which would not necessarily be reflected by major elements, so bulk contamination cannot be ruled out by lack of correlation between major elements and isotope ratios. A plot of $^{87}Sr/^{86}Sr$ against Sr concentration, shown in Figure 7.2, shows an inverse relationship with a high $^{87}Sr/^{86}Sr$ low Sr end member and a low $^{87}Sr/^{86}Sr$ higher Sr end member, consistent with contamination by crustal components (eg. Faure, 1987). However, all of the associated units as well as the Uivak I gneiss (Hurst, 1975), a potential sub-Grenville Province older crustal contaminant considered by Ashwal et al (1986), have Sr concentrations greater than or equal to those in the gabbronorite. Contamination by an unidentified (ie. either not exposed at the surface or exposed further south and not yet sampled) high $^{87}Sr/^{86}Sr$ low Sr component is possible, but variable contamination by available crustal material of an isotopically heterogeneous mafic magma cannot be ruled out.

Using depleting mantle (DePaolo, 1981) and uniform reservoir (McCulloch and Wasserburg, 1978) sources at 1650 Ma for neodymium and strontium, respectively, a plot of ϵ_{Nd} against ϵ_{Sr} is shown in Figure 7.3 A. ϵ_{Nd} for the whole rocks and minerals is depleted relative to bulk earth, and for one sample (8505) ϵ_{Nd} is depleted relative to the depleted mantle,

which has ϵ_{Nd}=+4.3 at 1650 Ma. ϵ_{Sr} is very slightly enriched relative to the uniform reservoir at 1650 Ma, placing the WBAC gabbronorites in the upper right-hand quadrant of the diagram. The effect of sea-water alteration draws altered rocks into this field, but there is no evidence for this in the WBAC. The gabbronorites could be enriched in radiogenic strontium but not in neodymium by K-metasomatism, which was indicated by the geochemical calculations in Section 7.1. Introduction of K^{+1}, hence also $^{87}Rb^{+1}$, could introduce radiogenic ^{87}Sr. The most likely contaminants are the host rocks to the WBAC, which are unlikely to be more than about 50 Ma older than the WBAC, so that not much radiogenic Sr would have been generated. If K was supplied by older crust beneath the Grenville province, such as Nain Province crust, then a much smaller amount of contaminant would be required. The extent of $^{87}Sr/^{86}Sr$ enrichment from K metasomatism is difficult to quantify, however. Contamination with LREE-enriched material is also indicated, so contamination cannot be by exclusively K-Rb bearing fluids.

Using the ϵ_{Nd}-ϵ_{Sr} variation diagram, mixing with potential crustal components can be investigated, as shown in Figure 7.3 B. Any mixing model involving assimilation of relatively cold crust by an intruding mafic magma requires sympathetic crystallisation of cumulate (Taylor, 1980) and produces a mixing line which is concave upwards on such a

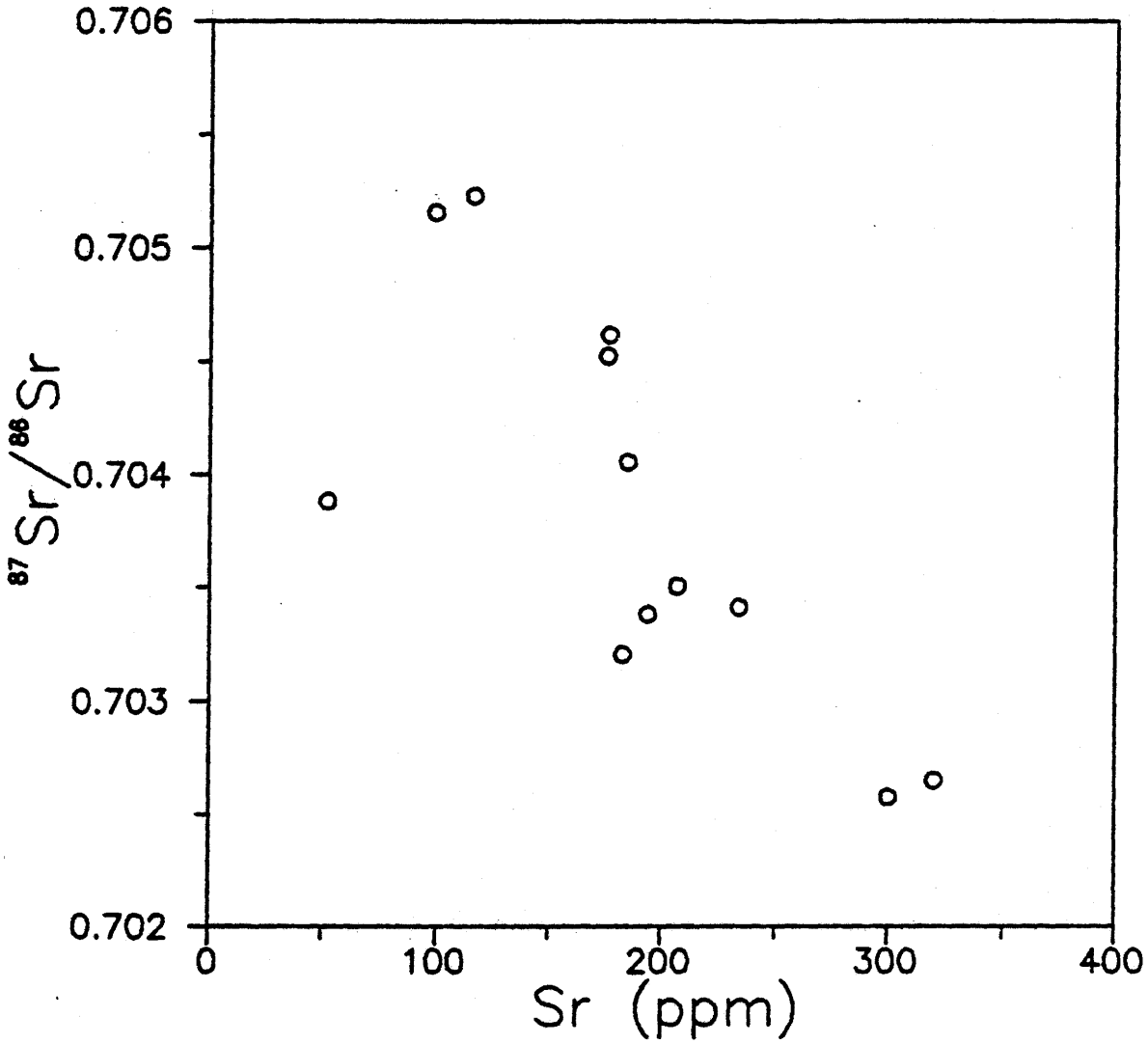

FIGURE 7.2

$^{87}Sr/^{86}Sr$ variation with Sr concentration for the WBAC gabbronorites (w.r.)

Table 7.1

Sr and Nd Model Ages and Epsilon Values

Name\Element	Tur	Tchur	Tdm	$\varepsilon_{Sr}(1.65)$	2σ	$\varepsilon_{Nd}(1.65)$	2σ	Fsr	Fnd
WBAC Gabbronorite									
SPM85-01	393	1361	2009	20.0	0.4	1.5	0.6	-0.9414	-0.2166
SPM85-03	945	1346	1916	11.6	0.4	1.9	0.3	-0.9839	-0.2593
SPM85-04	-732	1165	1801	33.8	0.4	3.0	0.3	-0.8400	-0.2466
SPM85-05	1274	750	1319	-2.7	0.2	7.9	0.3	0.4292	-0.3503
SPM85-07	1096	1192	1973	9.1	0.5	2.1	0.2	-0.9808	-0.1825
SPM85-08	-22	1250	1830	26.0	0.4	2.6	0.3	-0.9186	-0.2669
SPM85-11	1599	-119	1623	0.5	0.6	4.4	0.6	-0.9961	-0.0981
Mineral Separates									
11-ol	928	-788	1022	11.3	0.7	7.7	1.9	-0.9338	-0.1256
11-cpx	1774	1742	1291	-2.0	1.0	1.1	1.7	-0.8144	0.4357
11-amph	903	1108	2321	12.1	0.5	1.3	1.4	-0.9652	-0.0951
05-plag	1272	1471	1784	5.6	0.3	2.2	1.1	-0.9070	-0.5140
05-opx	1780	-4931	2426	8.7	0.6	2.4	1.2	3.3894	-0.0147

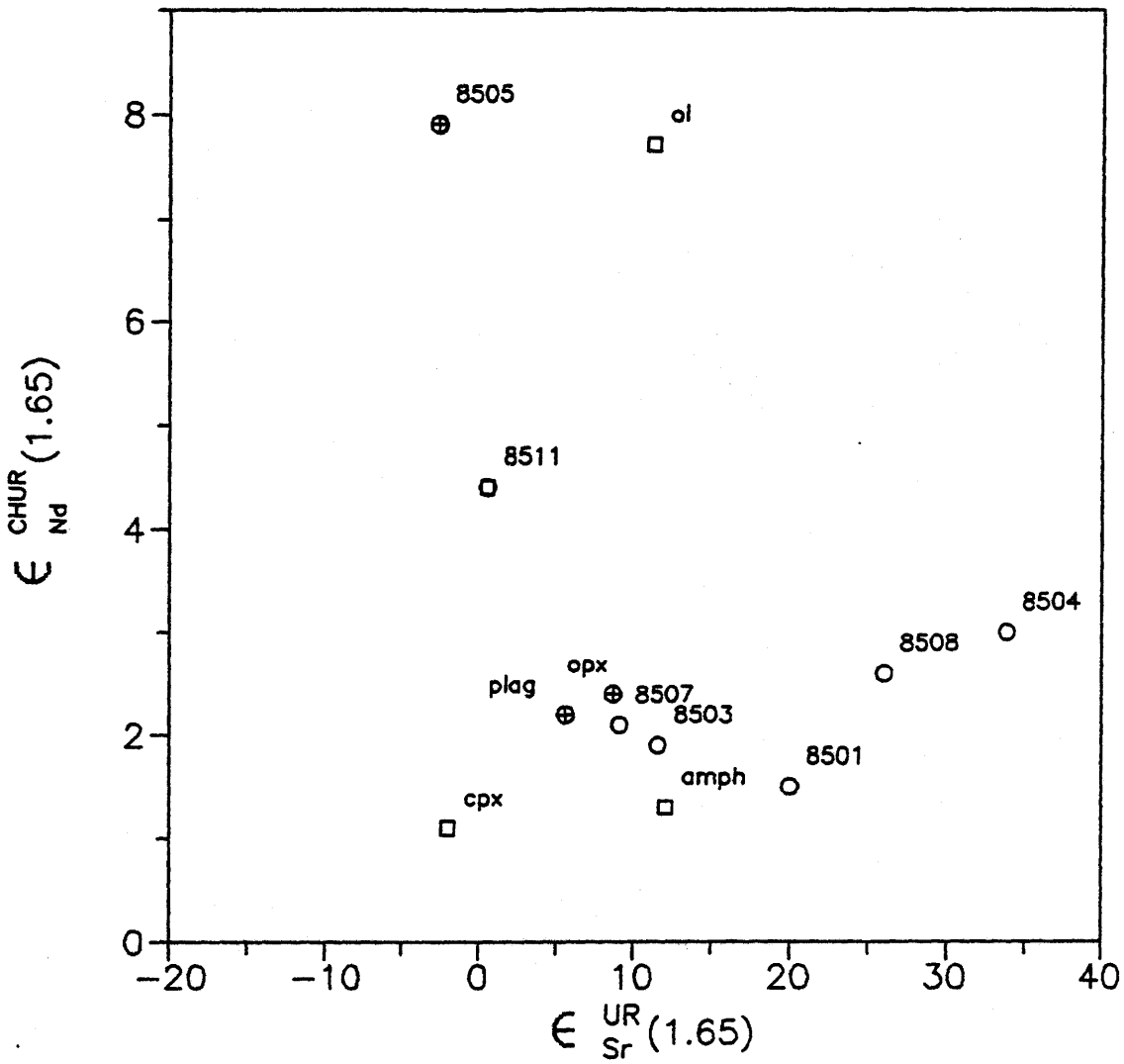

FIGURE 7.3 A

Neodymium and strontium isotopic compositions for WBAC gabbronorite whole-rocks and minerals expressed as ε_{Nd} and ε_{Sr} at time = 1.65 Ga, modelled from isotopic reservoirs with chondritic and "uniform reservoir" signatures for neodymium and strontium, respectively.

Symbol: o = whole-rocks
□ = 85-11 minerals plus w.r.
⊕ = 85-05 minerals plus w.r.

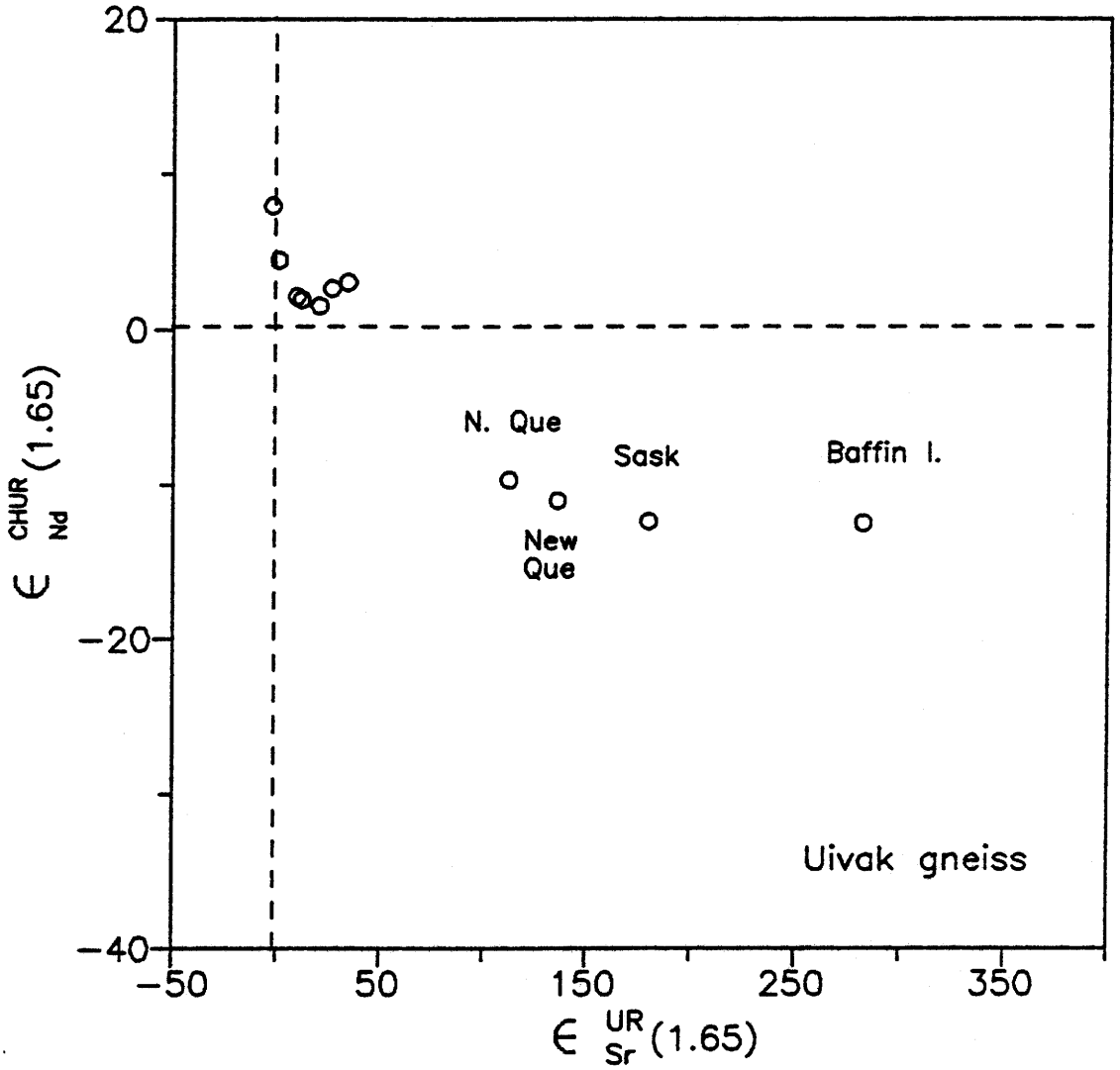

FIGURE 7.3 B

Contamination of an extremely LREE depleted mantle source by LREE and ^{87}Sr enriched older crustal material in $\varepsilon_{Nd} - \varepsilon_{Sr}$ space

Unlabelled circles are WBAC gabbronorite whole-rocks, Nd and Sr isotopic data for North Quebec, New Quebec, Saskatchewan and Baffin Island composites is from McCulloch and Wasserburg (1978), and the field for the Uivak 1 gneisses is based on Collerson and McCulloch (1982).

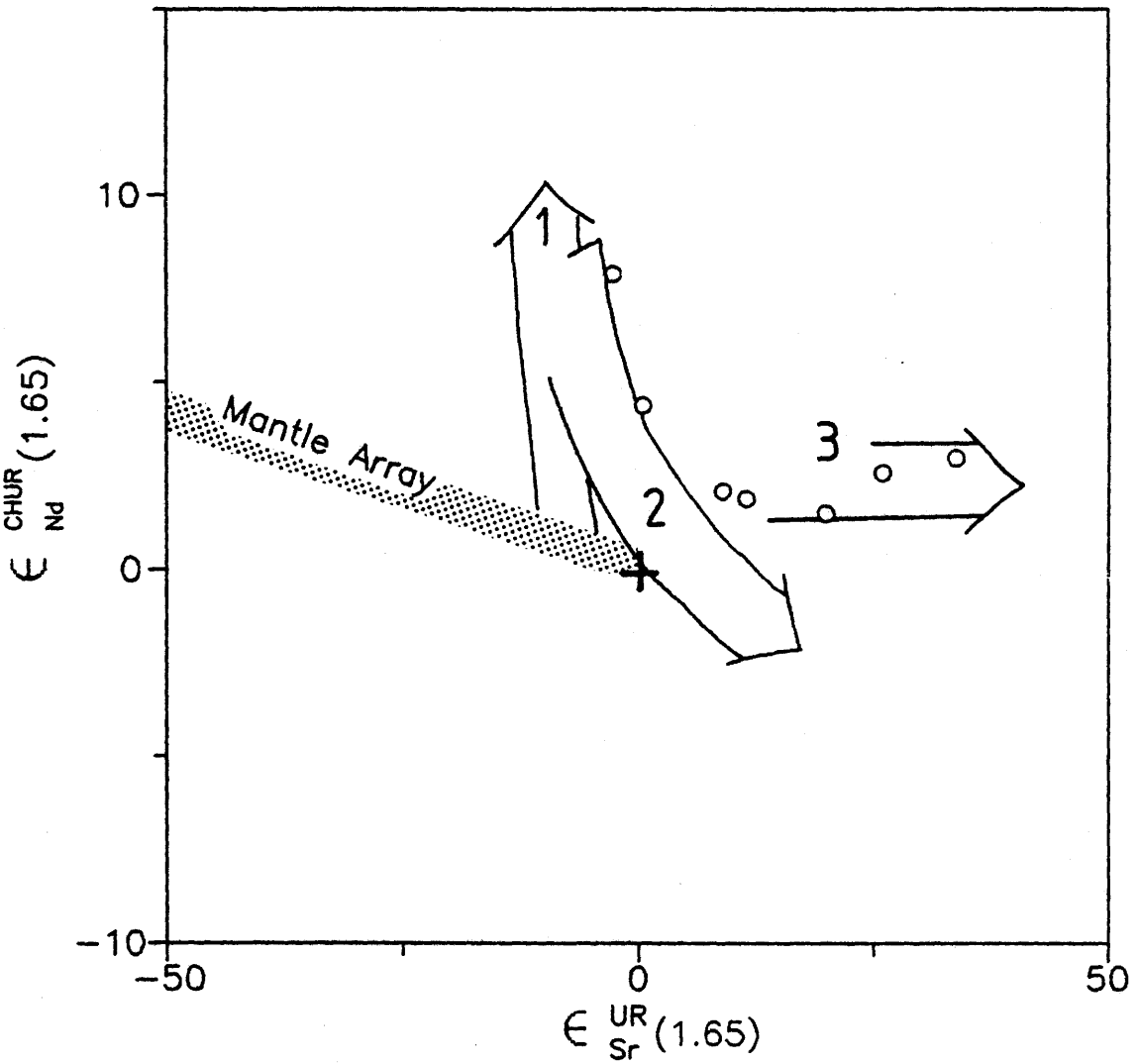

Figure 7.3 C

Three-stage evolution of the gabbronorite:

Stage 1: Upper mantle LREE and $^{87}Sr/^{86}Sr$ depletion, from a depleted mantle

Stage 2: Crustal contamination, pre or syn-crystallisation

Stage 3: Metasomatism by K-enriched, ^{87}Rb and ^{87}Sr-bearing fluids, syn or post-crystallisation

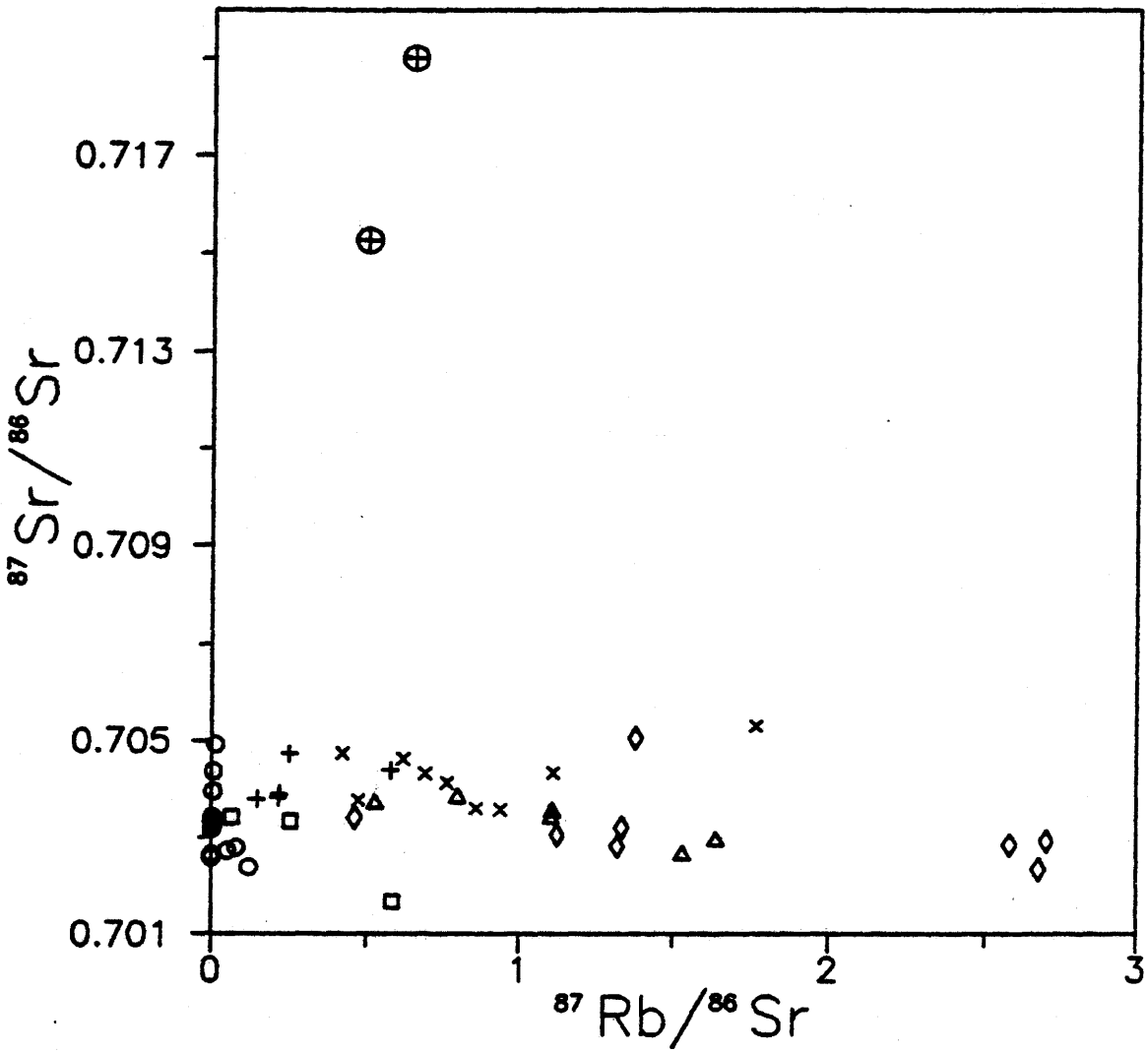

FIGURE 7.4 A

Plot of $^{87}Sr/^{86}Sr$ against $^{87}Rb/^{86}Sr$ for the Hawke River Terrane units plus an older lower-crustal unit (Uivak I gneiss), age-corrected to 1.65 Ga

Symbol: o = WBAC gabbronorites
□ = WBAC monzogabbros
◇ = WBAC monzonites
△ = Paradise Arm Pluton
\+ = Anhydrous PMGB rocks
x = PMGB gneisses
⊕ = Uivak I gneisses

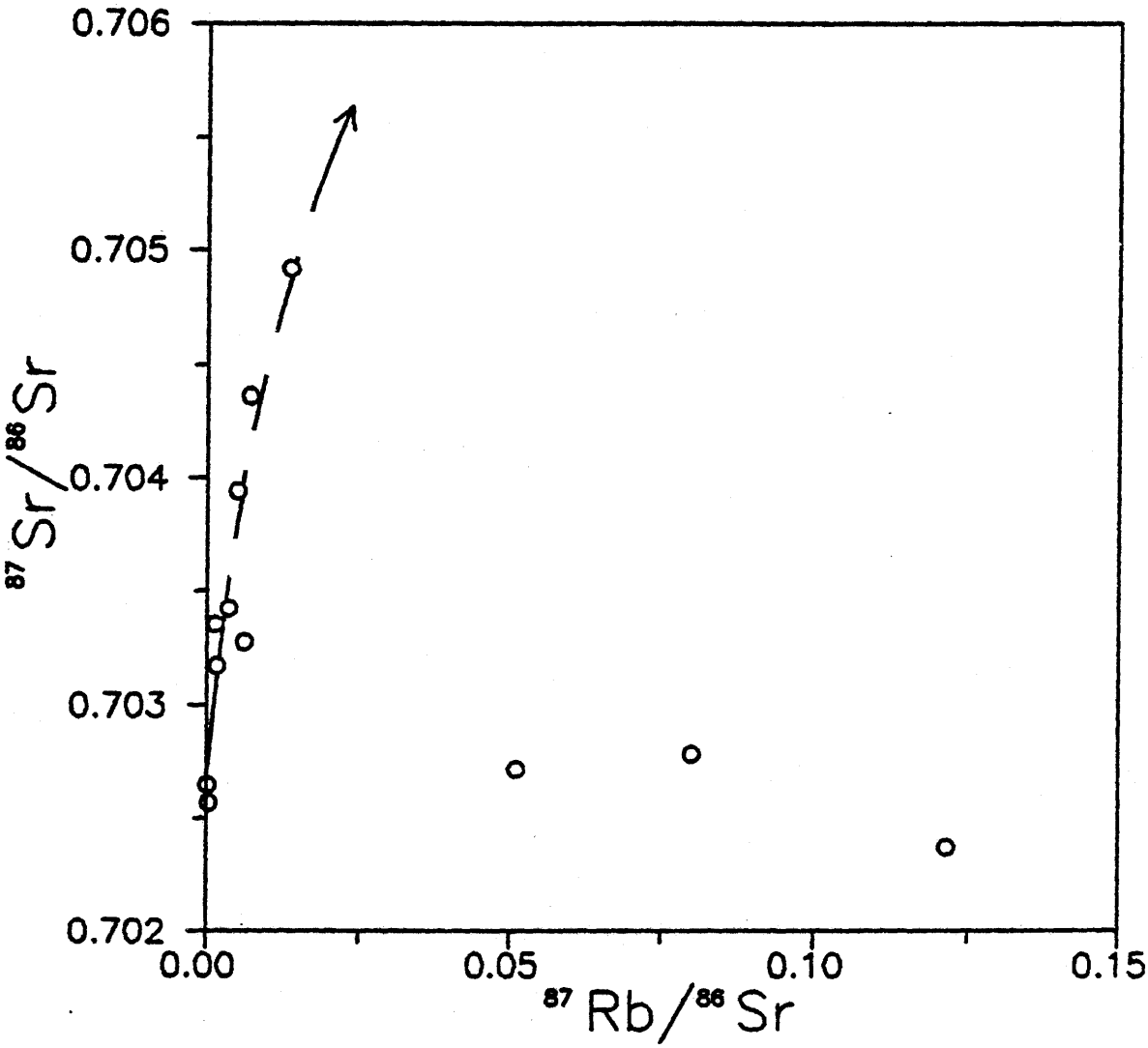

FIGURE 7.4 B

Plot of $^{87}Sr/^{86}Sr$ against $^{87}Rb/^{86}Sr$ for the WBAC gabbronorites, age-corrected to 1.65 Ga

diagram. Given the isotopic composition of available crustal contaminants, all of which have strongly enriched ϵ_{Nd} values relative to bulk earth (eg. McCulloch and Wasserburg, 1978; Ashwal *et al.*, 1986), it is not possible to generate sufficiently enriched ϵ_{Sr} values from mixing of crust and an end-member in the "mantle-array". The gabbronorites define a hyperbolic mixing curve towards a relatively LREE depleted crustal component. The large amount of Sr contamination indicated by the Rb-Sr isochron diagram suggests that the entire curve in ϵ_{Nd}-ϵ_{Sr} space may be displaced to the right, variably, so that the isotopic characteristics of a crustal end-member are difficult to constrain. A mixing model could be constructed using a mantle end member with very depleted ϵ_{Nd} (ie. +7.5 to +8) and ϵ_{Sr} slightly depleted relative to bulk earth. There is evidence for the presence of LREE-depleted mantle (relative to DePaolo's depleting mantle) to the west and south, in the Proterozoic. There is evidence for a mantle reservoir at least as depleted as $\epsilon_{Nd} = +6.7 \pm 1.2$ at about 1.5 Ga (Pettingill *et al.*, 1984) under the Appalachians, and ϵ_{Nd} values around +6 at 1.45 Ga from the Mealy Mountains about 200 km to the west (Ashwal *et al.*, 1986). Partial melting of mantle rocks could produce a LREE-depleted partial melt (eg. O'Nions *et al.*, 1977). The high $\epsilon_{Nd}(1.65)$ of sample 8505 WR ($\epsilon_{Nd} = +7.9 \pm 0.3$) is also observed in 8511-olivine, and 8505 is extremely olivine rich. The LREE depletion of olivine may reflect intrinsic original depletion, or selective

LREE depletion through hydrous alteration and replacement, which is less likely.

A mixing model using age-corrected $^{87}Sr/^{86}Sr$ and $^{87}Rb/^{86}Sr$ is shown in Figure 7.4 A and B. A possible older crustal contaminant is represented by the Uivak I gneisses (Hurst, 1975), also corrected back to 1.65 Ga. The two trends observed in the gabbronorite Rb-Sr distribution correspond to two distinct trends. Three samples define an approximately linear trend between a gabbronorite with $^{87}Sr/^{86}Sr$ of 0.7030 ± 5 and the associated crustal units, particularly the WBAC monzonite. Eight samples define a hyperbolic curve which is too radiogenic to be a result of mixing with Rb and Sr from the Hawke River Terrane crust, but could represent mixing with more radiogenic older crust such as the Uivak gneiss. Alternatively, selective contamination with ^{87}Rb (ie. via potassium metasomatism) from the HRT crust could produce the observed $^{87}Sr/^{86}Sr$ enrichment of the gabbronorite, conceivably.

The Rb-Sr isochron diagram for the gabbronorites is nearly identical to that of the low $^{87}Rb/^{86}Sr$ members of the Harp Lake Dikes, which have suffered crustal contamination (Ashwal et al, 1986). Similarly large and apparently random variation in anorthositic rocks can be attributed to later metamorphism (eg. Ashwal and Wooden, 1983). The scatter observed in the Sm-Nd isochron diagram is typical of such

diagrams for rocks with small spreads in $^{147}Sm/^{144}Nd$ values, such as anorthosites (eg. Ashwal and Wooden, 1983; Ashwal *et al.*, 1986), which are therefore sensitive to metamorphic events or crustal contamination.

In summary, variable amounts of unspecified crustal Nd and Sr have been introduced to a mafic magma at least as LREE-depleted as ϵ_{Nd} = +7.6 at 1.65 Ga and slightly depleted in ^{87}Sr relative to the bulk earth. The composition of the crustal component(s) is very poorly constrained isotopically, especially lacking Nd isotope data from the Hawke River Terrane crustal material. The lack of correlation between silica and $^{87}Sr/^{86}Sr$ does not rule out bulk-rock contamination, but suggests a relatively small amount of contamination. The amount of contamination indicated by the ϵ_{Nd}-ϵ_{Sr} diagram could easily be generated by less than 10 wt.% of crust added (eg. Ashwal *et al.*, 1986), which would not necessarily be reflected clearly by the major elements. Trace elements, discussed in Chapter 5, are ambiguous.

A possible genetic sequence excluding input from a hypothetical crustal component with low Sr concentrations (ie. ≤10 ppm) could involve intrusion and crystallisation of an isotopically homogeneous magma, contemporaneous with or followed shortly afterwards by fluid metasomatism and crustal contamination. The effect of fluids, originating from the

country rock or the mantle, conceivably, is to initiate or facilitate corona development and to add, variably, radiogenic strontium. Secondary LREE depletion seems unlikely. Since the crustal contamination probably occurred before or during crystallisation of the gabbronorite, the contamination must either predate or be synchronous with the fluid metasomatism. A combination of these two effects could generate both the $^{87}Sr/^{86}Sr$-Sr and ϵ_{Nd}-ϵ_{Sr} trends observed without requiring invention of a new contaminant reservoir. A three step genetic sequence involving depletion, contamination and fluid metasomatism is shown in Figure 7.3 C.

7.3 Significance of Rb-Sr ages

The Rb-Sr ages of the felsic units are around 1620 ± 40 Ma, which is consistent with the age constraints provided by previous geochronological work in eastern Labrador, summarised in Figure 7.5. The total PMGB isochron age of 1663 ± 9 Ma is within error of zircon ages from the Earl Island Domain to the north (Schärer and Gower, in press). The Rb-Sr age for the plutonic WBAC granodiorites is not an unreasonable intrusive age, although it is slightly younger than available U-Pb zircon ages. Both the WBAC and PAP granodioritic units show evidence of some prehistory, such as damaged garnets with internal structure, evidence of retrograde metamorphism and upper greenschist facies metamorphism. The high MSWD values

reflect some disturbance of the Rb-Sr systems. Hence, the Rb-Sr age of the WBAC granodiorite must be considered a minimum age of intrusion. If the errors on the samples are expanded until the MSWD=1.0, the 2σ errors on the granodiorite ages overlap, although the Paradise Arm Pluton is still significantly younger than 1650 Ma. If the PAP age of 1575 Ma is taken as a (minimum) emplacement age, it must represent a younger (ie. *ca.* 1575 Ma) remelting of the same source rock that produced the WBAC granodiorites. This would require partial melting to the same degree for both granodioritic units. They both have undergone similar geologic histories, there is no evidence for a *circa* 1550-1600 Ma old event in eastern Labrador, and there is petrographic and trace element geochemical evidence for mixing with the paragneisses, so this younger "age" represents a mixing line "pseudoisochron" and does not reflect a later event.

The Rb-Sr age of the PMGB rocks, varying from amphibolite to granulite facies metamorphism, must be considered a metamorphic age, although zircon ages from adjacent units (Schärer *et al.*, 1986; Schärer and Gower, in press) indicate a relatively short prehistory (ie. $\simeq$ 50-60 Ma). Initial ratios are all equal within 2σ expanded errors, around 0.704, significantly higher than the gabbronorites.

There is no evidence for a Grenville-aged (*ca.* 1.0 Ga

old) event, indicated by zircon and sphene ages in adjacent terranes. This supports the contention that the Hawke River Terrane, particularly the central portions, suffered relatively little from the Grenville Orogeny compared to neighbouring, underlying terranes (Gower, 1987). The only indication of Grenville-aged effects are the presence of Grenville paleomagnetic pole positions from magnetite in the WBAC gabbronorite (Hale, pers. comm.).

7.4 Origin of the Granodiorites

Petrographic and trace element data indicate that the WBAC granodiorite and the PAP are cogenetic and comagmatic, where the PAP has suffered more extensive mixing with the adjacent paragneisses. There is some evidence of relict paragneissic xenoliths in the PAP, but the granodiorites and the PMGB paragneisses are compositionally distinct, in terms of major elements and compatible trace elements, so it is unlikely that the plutons were derived by bulk melting of the paragneiss, although partial melting is feasible, based on K/Rb and Ba/Rb ratios. There is no clear evidence that the granodiorites were derived by partial melting of the gabbro-norite.

In conclusion, the granodioritic plutons could have originated by partial melting of the PMGB paragneisses or

possibly melting of an unexposed lower crustal component, but derivation from the gabbronorite is unlikely.

FIGURE 7.5

Distribution of radiometric ages in the
Hawke River Terrane and vicinity

U-Pb dates are from Schärer et al (1986) and
Schärer and Gower (in press), Rb-Sr from this study

Symbol: z = zircon date
t = titanite date
m = monazite date
r = Rb-Sr age

(All ages in Ma)

LMT = Lake Melville Terrane
HRT = Hawke River Terrane

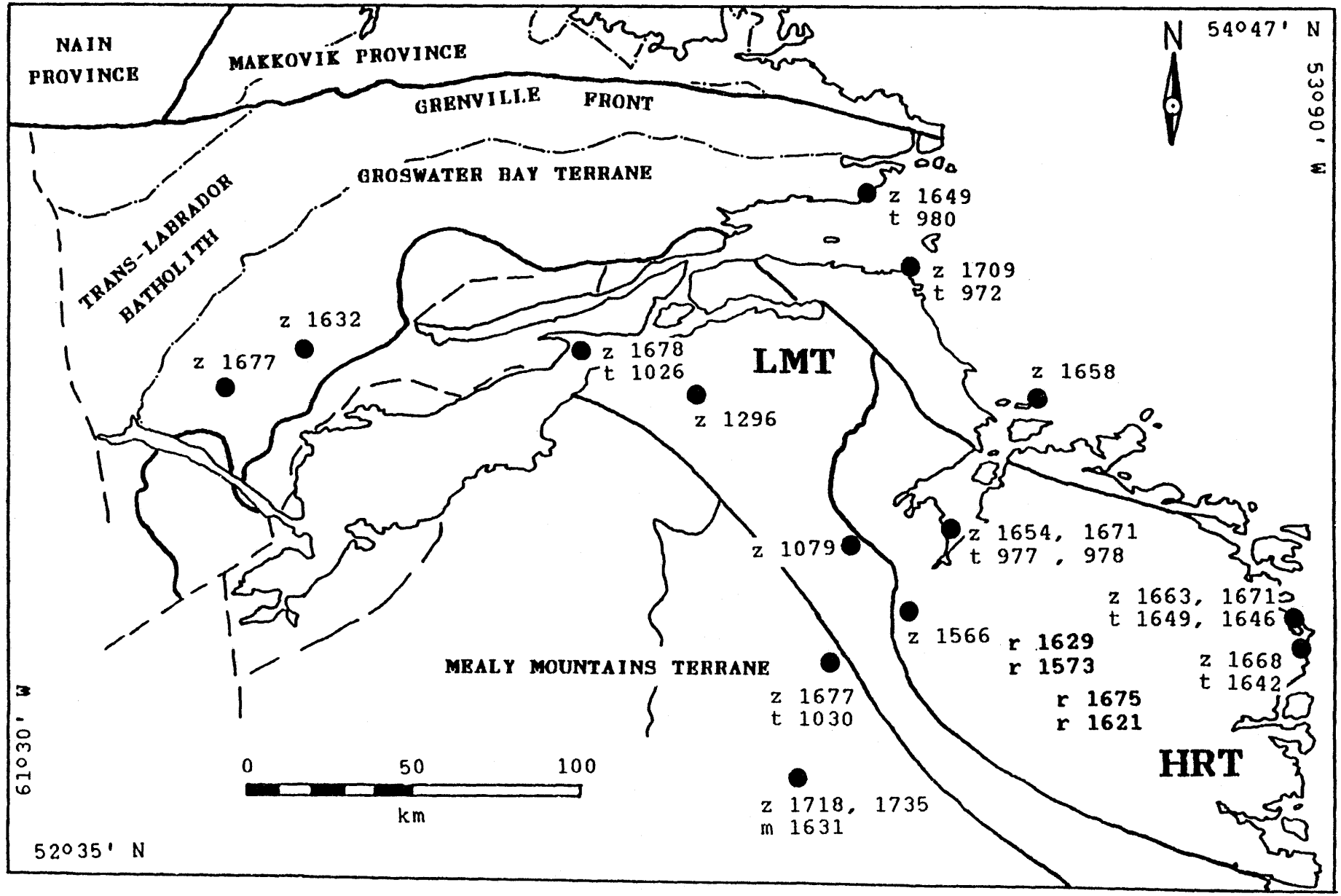
NAIN PROVINCE
MAKKOVIK PROVINCE
GRENVILLE FRONT
GROSWATER BAY TERRANE
TRANS-LABRADOR BATHOLITH
MEALY MOUNTAINS TERRANE
LMT
HRT
N
54°47' N
53°90' W
61°30' W
52°35' N
0
50
100
km
z 1649
t 980
z 1709
t 972
z 1632
z 1677
z 1678
t 1026
z 1296
z 1658
z 1654, 1671
t 977 , 978
z 1079
z 1566
z 1663, 1671
t 1649, 1646
r 1629
r 1573
z 1668
t 1642
r 1675
r 1621
z 1677
t 1030
z 1718, 1735
m 1631

CHAPTER 8: CONCLUSIONS

8.1 Geologic Evolution

The White Bear Arm Complex was intruded as a low-potassium, sub-alkakic gabbronorite body into slightly older (ie. < 60 Ma) high grade aluminous metasedimentary gneisses at around 1.65 Ga ago. During the emplacement and/or crystallisation of the gabbronorite, it was contaminated by crustal material (probably < 10 wt.%) and also caused (partial) melting of local crustal material, resulting in the emplacement of colinear granodioritic bodies. The two such bodies (the WBAC granodiorite and the PAP) show variable amounts of paragneissic influence, such that the unit nearer the PMGB gneisses (the PAP) shows more affinity towards the paragneiss. This is consistent with both mixing between a granodioritic magma and the paragneiss, or derivation of the former from the latter. During crystallisation or cooling of the gabbronorite, or during a metamorphism immediately thereafter, potassic fluids were introduced into the gabbronorite, probably from the adjacent country rocks, together with heat of emplacement or metamorphism facilitating the initiation of coronitic replacement of olivine and plagioclase by orthopyroxene and amphibole-spinel symplectite respectively.

A narrow zone of granulite-facies, coarse-grained recrystallised metasedimentary rocks was created by the heat of intrusion of the gabbronorite, displaying osumilite and sapphirine-bearing assemblages. As the complex cooled coronitisation continued to the amphibolitisation stage. The granodioritic units retrograded to upper greenshist facies assemblages.

There is no isotopic evidence for a later (younger) disturbance (specifically a Grenville-aged one).

8.2 Suggested Future Work

There are two major questions, the age of the WBAC and the age and origin of the granodioritic units, which could be made less ambiguous by further isotopic investigations. Sm-Nd isotopic work, particularly with regards to model extraction systems, should be able to clarify the relationship between the granodiorites and the paragneisses. This data would also constrain the characteristics of the probable contaminant of the gabbronorite, thus permitting quantification of the degree of contamination as well. More precise age data could be obtained by U-Pb isotopes in zircons from all units, although there is a danger of inherited older zircons, particularly in the granodioritic units.

The coronites and the granulite-facies zone surrounding the WBAC are both of petrographic interest. A more detailed study of the evolution of the coronites would contribute greatly to the relatively small database currently available. More precise constraints on the depth and temperatures of emplacement could be provided by studies of the compositions of osumilite and sapphirine from the contact zone.

The effects of Grenville-aged events on the central Hawke River Terrane reflected only by paleomagnetic data could be investigated through an isotopic system more sensitive than Rb-Sr, such as K-Ar, on the later, hydrous corona minerals such as biotite.

A detailed isotopic (radiogenic and stable) study, combined with the petrographic evidence indicating the area of country rock influenced by the WBAC intrusion would constrain the extent and source(s) of the fluid circulation system. This could clarify the source of the fluids involved in corona formation.

References

Abbey, S. (1981) The search for "best values" - A study of three Canadian rocks. Geostandards Newsletter, v. 5, no. 1, p. 13- 26.

Althaus, E. (1967) The triple point andalusite-sillimanite-kyanite. Contributions to Mineralogy and Petrology, 16, p. 29-44.

Arima, M. and Gower, C.F. (1987) Osumilite-bearing meta-sedimentary gneiss in the Grenville Province, eastern Labrador. Abstract In G.A.C.-M.A.C. Program with Abstracts, 12, May, Saskatoon.

Arima, M., Kerrich, R. and Thomas, A. (1986) Sapphirine-bearing paragneiss from the northern Grenville Province in Labrador, Canada: protolith composition and metamorphic P-T conditions. Geology, 14, p. 844-847.

Ashwal, L.D. and Wooden, J.L. (1983) Sr and Nd isotope geochronology, geologic history, and origin of the Adirondack Anorthosite. Geochimica et Cosmochimica Acta, 47, p. 1875-1885.

Ashwal, L.D., Wooden, J.L. and Emslie, R.F. (1986) Sr, Nd, and Pb isotopes in Proterozoic intrusives astride the Grenville Front in Labrador: Implications for crustal contamination and basement mapping. Geochimica et Cosmochimica Acta, 50, p. 2571-2585.

Ashworth, J.R. (1986 a) Myrmekite replacing albite in prograde metamorphism. American Mineralogist, 71, p. 895-899.

Ashworth, J.R. (1986 b) The role of magmatic reaction, diffusion and annealing in the evolution of coronitic microstructure in troctolitic gabbro from Risör, Norway: a discussion. Mineralogical Magazine, 50, p. 469-479.

Berg, J.H. (1976) Regional geobarometry in the contact aureoles of the anorthositic Nain Complex, Labrador. Journal of Petrology, 18, p. 399-430.

Berg, J.H. and Wheeler, E.P.II (1976) Osumilite of deep-seated origin in the contact aureole of the anorthositic Nain complex, Labrador. American Mineralogist, 61, p. 29-37.

Brooks, C. (1982) Supplement to the third report on the geochronology of Labrador: unpublished report to the Newfoundland Department of Mines and Energy. Newfoundland Department of Mines and Energy, Mineral Development Division Open File LAB (519), 23 pp.

Brooks, C. (1983) Fourth report on the geochronology of Labrador: unpublished report to the Newfoundland Department of Mines and Energy. Newfoundland Department of Mines and Energy, Mineral Development Division Open File LAB (519), 34 pp.

Brooks, C., Hart, S.R. and Wendt, I. (1972) Realistic use of two-error regression treatments as applied to rubidium-strontium data. Reviews of Geophysics and Space Physics, v. 10, no. 2, p. 551-577.

Brown, G.C. and Fyfe, W.S. (1971) Kyanite andalusite equilibrium. Contributions to Mineralogy and Petrology, 33, p. 227-231.

Butler, J.C. and Woronow, A. (1986) Discrimination among tectonic settings using trace element abundances of basalts. Journal of Geophysical Research, 91, no. B10, p. 10,289-10,300.

Collerson, K.D. and McCulloch M.T. (1982) The origin and evolution of Archean crust as inferred from Sr, Nd and Pb isotopic studies in Labrador. Abstracts, Fifth International Conference on Geochronology, Cosmochronology, and Isotope Geology, p. 61-62.

Davidson, A. (1986) Coronite survey. The Foghorn (newsletter of the Friends of the Grenville), v. 2, #1, 3 pp.

Deer, W.A., Howie, R.A. and Zussman, J (1966) An introduction to the rock forming minerals. Longman Group Limited, London, 528 pp.

DePaolo, D.J. (1981) Neodymium isotopes in the Colorado Front Range and crust-mantle evolution in the Proterozoic. Nature, 291, p. 193-196.

Eade, K.E. (1962) Geology, Battle Harbour - Cartwright, Labrador. Geological Survey of Canada, Map 22-1962.

Easton, R.M. (1986) Geochronology of the Grenville Province; Part I: Compilation of data; Part II:Synthesis and interpretation. In *The Grenville Province*, Special Paper 31, p. 127-174.

Ehlers, E.G. and Blatt, H. (1982) Petrology. W.H. Freeman and Company, 732 p.

Ellis, D.J. (1980) Osumilite-sapphirine-quartz granulites from Enderby Land, Antarctica: P-T conditions of metamorphism, implications for garnet-cordierite equilibria and the evolution of the deep crust. Contributions to Mineralogy and Petrology, 74, p. 201-210.

Ellis, D.J., Sheraton, J.W., England, R.N. and Dallwitz, W.B. (1980) Osumilite-sapphirine-quartz granulites from Enderby Land Antarctica - mineral assemblages and reactions. Contributions to Mineralogy and Petrology, 72, p. 123-143.

Emmett, T.F. (1982) The petrography and geochemistry of corona-bearing dolerites from the Jotun Nappe, central southern Norway. Mineralogical Magazine, 46, p. 43-48.

Emmett, T.F. (1987) A reconnaissance study of the distribution of Ba, Nb, Y, and Zr in some Jotun kindred gneisses from Central Jotunheimen, southern Norway. Journal of Metamorphic Geology, 5, p. 41-50.

Emslie, R.F. (1976) Mealy Mountains Complex, Grenville Province, southern Labrador. In Report of Activities, Part A: Geological Survey of Canada Paper 76-1A, p. 165-170.

Emslie, R.F. (1983) The coronitic Michael Gabbros, Labrador: assessment of Grenvillian metamorphism in northeastern Grenville Province. In Current Research, Part A, Geological Survey of Canada Paper 83-1A, p. 139-145.

Emslie, R.F., Loveridge, W.D. and Stevens, R.D. (1984) The Mealy dikes, Labrador: petrology, age, and tectonic significance. Canadian Journal of Earth Science, 21, p. 437-446.

England, R.N. (1974) Corona structures formed by near isochemical reaction between olivine and plagioclase in a metamorphosed dolerite. Mineralogical Magazine, 39, p. 816-818.

Fahrig, W.F. and Loveridge, W.D. (1981) Rb-Sr study of the Michael Gabbro, Labrador In Rb-Sr and U-Pb isotopic age studies, Report 4. In Current Research, Part C, Geological Survey of Canada, Paper 81-1C, p. 99-103.

Faure, G. (1986) Principles of isotope geology. Second Edition, John Wiley and Sons, Inc.

Frodesen, S. (1968) Coronas around olivine in a small gabbro intrusion, Bamble area, South Norway. Norsk Geologisk Tidsskrift, 48, p. 201-206.

Gast, P.W. (1965) Terrestrial ratio of K to Rb and the composition of the earth's mantle. Science, 147, p. 858-860.

Gittins, J. and Currie, K.L. (1979) Petrologic studies of sapphirine-bearing granulites around Wilson Lake, Labrador. In Current Research, Part A, Geological Survey of Canada Paper 79-1A, p. 77-82.

Gladney, E.S., Burns, C.E. and Roelandts, I. (1983) 1982 complilation of elemental concentrations in eleven United States Geological Survey rock standards. Geostandards Newsletter, v. 7, no. 1, p. 3-226.

Govindaraju, K. (1984) 1984 compilation of working values for 170 international reference samples of mainly silicate rocks and minerals: Appendix I - Working values for 170 Reference Samples. Geostandards Newsletter, v. 8, Special Issue, Appendix 1, 19 pp.

Govindaraju, K. (1987) 1987 compilation report on Ailsa Craig granite AC-E with the participation of 128 GIT-IWG laboratories. Geostandards Newsletter, v. 11, no. 2, p. 203-255.

Gower, C.F. (1986) Geology of the Double Mer White Hills and surrounding region, Grenville Province, eastern Labrador. Geological Survey of Canada, Paper 86-15, 50 pp.

Gower, C.F. (1987) The Hawke River Terrane - A newly defined lithotectonic entity in the Grenville Province of eastern Labrador. G.A.C./M.A.C. Program with abstracts, 12, Saskatoon.

Gower, C.F., Neuland, S., Newman, M. and Smyth, J. (1987) Geology of the Port Hope Simpson map region, Grenville Province, eastern Labrador. In Current Research, Newfoundland Department of Mines and Energy, Mineral Development Division, in preparation.

Gower, C.F., Noel, N. and Van Nostrand, T. (1985) Geology of the Paradise River region, Grenville Province, eastern Labrador. In Current Research, Part B, Geological Survey of Canada Paper 85-1B, p. 547-560.

Gower, C.F. and Owen, V. (1984) Pre-Grenvillian and Grenvillian lithotectonic regions in eastern Labrador - correlations with the Sveconorwegian Orogenic Belt in Sweden. Canadian Journal of Earth Science, 21, p. 678-693.

Gower, C.F. and Ryan A.B. (1986) Proterozoic evolution of the Grenville Province and adjacent Makkovik Province in eastern-central Labrador. In *The Grenville Province*, G.A.C. Special Paper 31, p. 281-296.

Gower, C.F., Ryan, A.B., Bailey, D.G. and Thomas, A. (1980) The position of the Grenville Front in eastern and central Labrador. Canadian Journal of Earth Science, 17, p. 784-788.

Gower, C.F., Van Nostrand, T., McRoberts, G., Crisby, L. and Prevec, S. (1986) Geology of the Sand Hill River - Batteau map region, Grenville Province, eastern Labrador. In Current Research, Newfoundland Department of Mines and Energy, Mineral Development Division, Report 86-1, p. 101-111.

Grew, E.S. (1982) Osumilite in the sapphirine-quartz terrane of Enderby Land, Antarctica: implications for osumilite petrogenesis in the granulite facies. American Mineralogist, 67, p. 762-787.

Griffin, W.L. and Heier, K.S. (1973) Petrological implications of some corona structures. Lithos, 6, p. 315-335.

Griffin, W.L., Mellini, M., Oberti, R. and Rossi, G. (1985) Evolution of coronas in Norwegian anorthosites: re-evaluation based on crystal-chemistry and microstructures. Contributions to Mineralogy and Petrology, 91, p. 330-339.

Harley, S.C. (1986) A sapphirine-cordierite-garnet-sillimanite granulite from Enderby Land, Antarctica: implications for FMAS petrogenetic grids in the granulite facies. Contributions to Mineralogy and Petrology, 94, p. 452-460.

Hart, S.R. and Aldrich, L.T. (1966) Fractionation of potassium/rubidium by amphiboles: implications regarding mantle composition. Science, 155, p. 325-327.

Heier, K.S. (1966) Some crystallo-chemical relations of nephelines and feldspars on Stjernoy, north Norway. Journal of Petrology, 7, p. 95-113.

Heier, K.S. and Adams, J.A.S. (1964) The geochemistry of the alkali metals. Physics and Chemistry of the Earth, 5, p. 253-382.

Hensen, B.J. (1977) The stability of osumilite in high grade metamorphic rocks. Contributions to Mineralogy and Petrology, 64, p. 197-204.

Holdaway, M.J. (1971) Stability of andalusite and the aluminum silicate phase diagram. American Journal of Science, 271, p. 97-131.

Hurst, R.W., Bridgwater, D., Collerson, K.D. and Wetherill, G.W. (1975) 3600-m.y. Rb-Sr ages from very early Archaean gneisses from Saglek Bay, Labrador. Earth and Planetary Science Letters, 27, p. 393-403.

Irvine, T.N. and Baragar, W.R.A. (1971) A guide to the chemical classification of the common volcanic rocks. Canadian Journal of Earth Sciences, 8, p. 523-548.

Jacobsen, S.B. and Wasserburg, G.J. (1980) Sm-Nd isotopic evolution of chondrites. Earth and Planetary Science Letters, 50, p. 139-155.

Joesten, R. (1986 a) The role of magmatic reaction, diffusion and annealing in the evolution of coronitic microstructure in troctolitic gabbro from Risör, Norway. Mineralogical Magazine, 50, p. 441-467.

Joesten, R. (1986 b) The role of magmatic reaction, diffusion and annealing in the evolution of coronitic microstructure in troctolitic gabbro from Risör, Norway: reply. Mineralogical Magazine, 50, p. 474-479.

Johansson, L. and Möller, C. (1986) Formation of sapphirine during retrogression of a basic high-pressure granulite, Roan, Western Gneiss Region, Norway. Contributions to Mineralogy and Petrology, 94, p. 29-41.

Keith, H.D. and Padden, Jr., F.J. (1963) A phenomenological theory of spherulitic crystallisation. Journal of Applied Physics, 34, No. 8, p. 2409-2421.

Loomis, T.P. (1986) Metamorphism of metapelites: calculations of equilibrium assemblages and numerical simulations of the crystallization of garnet. Journal of Metamorphic Geology, 4, p. 201-229.

Maijer, C., Andriessen, P.A.M., Hebeda, E.H., Jensen, J.B.H. and Verschure, R.H. (1981) Osumilite, an approximately 970 Ma old high-temperature index mineral of the granulite-facies metamorphism in Rogaland, SW Norway. Geologie en Mijnbouw, 60, 267-272.

Maijer, C., Jansen, J.B.H., Wevers, J. and Poorter, R.P.E. (1977) Osumilite, a mineral new to Norway. Contribution to the Mineralogy of Norway, No. 63, Norsk Geologisk Tidsskrift, 57, p. 187-188.

Mason, R. (1969) Electron-probe microanalysis of coronas in a troctolite from Sulitjelma, Norway. Mineralogical Magazine, 36, p. 505-514.

McCulloch, M.T. and Wasserburg, G.J. (1978) Sm-Nd and Rb-Sr chronology of continental crust formation. Science, 200, p. 1003-1011.

Moore, J.M. (1986) The 'Grenville problem' then and now . In *The Grenville Province*, G.A.C. Special Paper 31, p. 1-12.

Mørk, M.B.E. (1985) A gabbro to eclogite transition on Flemsøy, Sunnmøre, western Norway. Chemical Geology, 50, p. 283-310.

Mørk, M.B.E. (1986) Coronite and eclogite formation in olivine gabbro (Western Norway): reaction paths and garnet zoning. Mineralogical Magazine, 50, p. 417-426.

Murthy, M.V.N. (1958) Coronites from India and their bearing on the origin of coronas. Bulletin of the Geological Society of America, 68, p. 23-38.

Newton, R.C., Charlu, T.V. and Kleppa, O.J. (1974) A calorimetric investigation of the stability of anhydrous magnesium cordierite with application to granulite facies metamorphism. Contributions to Mineralogy and Petrology, 44, p. 295-311.

Nockolds, S.R., Knox, R.W. O'B. and Chinner, G.A. (1978) Petrology for students. Cambridge University Press, 435 p.

O'Flaherty, C.A. (1986) The geology of the layered mafic intrusion on Little Grady Island, south-eastern Labrador. Unpublished B.Sc. thesis, Memorial University of Newfoundland, St. John's, Nfld., 99 pp.

O'Nions, R.K., Hamilton, P.J. and Evensen, N.M. (1977) Variations in $^{143}Nd/^{144}Nd$ and $^{87}Sr/^{86}Sr$ ratios in oceanic basalts. Earth and Planetary Science Letters, 34, p. 13-22.

Osborn, E.F. (1979) The reaction principle In The evolution of the igneous rocks. H.S. Yoder, Ed., Princeton University Press, p. 133-171.

Pearce, J.A. and Cann, J.R. (1973) Tectonic setting of basic volcanic rocks determined using trace element analyses. Earth and Planetary Science Letters, 19, p. 290-300.

Pettingill, H.S., Sinha, A.K. and Tatsumoto, M. (1984) Age and origin of anorthosites, charnockites, and granulites in the Central Virginia Blue Ridge: Nd and Sr isotopic evidence. Contributions to Mineralogy and Petrology, 85, p. 279-291.

Reynolds, R.C., Jr. and Frederickson, A.F. (1962) Corona development in Norwegian hyperites and its bearing on the metamorphic facies concept. Geological Society of America Bulletin, 73, p. 59-72.

Richardson, S.W., Gilbert, M.C. and Bell, P.M. (1969) Experimental determination of kyanite-andalusite and andalusite-sillimanite equilibria; the aluminum silicate triple point. American Journal of Science, 267, p. 259-272.

Sanders, I.S., van Calsteren, P.W.C. and Hawkesworth, C.J. (1984) A Grenville Sm-Nd age for the Glenelg eclogite in north-west Scotland. Nature, 312, p. 439-440.

Schärer, U. and Gower, C.F. (in press) Crustal evolution in eastern Labrador: constraints from precise U-Pb ages.

Schärer, U., Krogh, T.E. and Gower, C.F. (1986) Age and evolution of the Grenville Province in eastern Labrador from U-Pb systematics in accessory minerals. Contributions to Mineralogy and Petrology, 94, p. 438-451.

Shaw, D.M. (1968) A review of K-Rb fractionation trends by covariance analysis. Geochimica et Cosmochimica Acta, 32, p. 573-601.

Shaw, D.M. (1972) The origin of the Apsley Gneiss, Ontario. Canadian Journal of Earth Science, 9, p. 18-35.

Starmer, I.C. (1969) Basic plutonic intrusions of the Risör-Söndeled area, South Norway: the original lithologies and their metamorphism. Norsk Geologisk Tidsskrift, 49, p. 403-431.

Stockwell, C.H. (1961) Structural provinces, orogenies, and time-classifications of rocks of the Canadian Precambrian Shield. In Age determinations by the Geological Survey of Canada; Report 2, Isotopic Ages: Geological Survey of Canada Paper 61-17, p. 108-118.

Streckeisen, A. (1976) To each plutonic rock its proper name. Earth Science Reviews, 12, p. 1-33.

Taylor, H.P., Jr. (1980) The effects of assimilation of country rocks by magmas on $^{18}O/^{16}O$ and $^{87}Sr/^{86}Sr$ systematics in igneous rocks. Earth and Planetary Science Letters, 47, p. 243-254.

Thomas, A., Nunn, G.A.G. and Krogh, T.E. (1986) The Labradorian Orogeny: evidence for a newly defined 1600 to 1700 Ma orogenic event in Grenville Province crystalline rocks from central Labrador. *In The Grenville Province*, G.A.C. Special Paper 31, p. 175-189.

Thornton, C.P. and Tuttle, O.F. (1960) Chemistry of igneous rocks I. Differentiation index. American Journal of Science, 258, p. 664-684.

Turner, F.J. (1980) Metamorphic petrology. Second Edition, McGraw-Hill Book Corporation, 524 p.

van Lamoen, H. (1979) Coronas in olivine gabbros and iron ores from Susimäki and Riuttamaa, Finland. Contributions to Mineralogy and Petrology, 68, p. 259-268.

Vernon, R.H. (1986) K-feldspar megacrysts in granites - phenocrysts, not porphyroblasts. Earth-Science Reviews, 23, p. 1-63.

Vernon, R.H. (1987) Growth and concentration of fibrous sillimanite related to heterogeneous deformation in K-feldspar-sillimanite metapelites. Journal of Metamorphic Geology, 5, p. 51-68.

Wager, L.R., Brown, G.M. and Wadsworth, W.J. (1960) Types of igneous cumulates. Journal of Petrology, 1, p. 73-85.

Wardle, R.J., Rivers, T., Gower, C.F., Nunn, G.A.G. and Thomas, A. (1986) The northeastern Grenville Province: new insights. In *The Grenville Province*, G.A.C. Special Paper 31, p. 13-30.

Wasserburg,G.J., Jacobsen, S.B., DePaolo, D.J., McCulloch, M.T. and Wen, T. (1981) Precise determination of Sm/Nd ratios, Sm and Nd isotopic abundances in standard solutions. Geochimica et Cosmochimica Acta, 45, p. 2311-2323.

Winkler, H.G.F. (1979) Petrogenesis of metamorphic rocks. Fifth Edition, Springer-Verlag New York Inc., 348 p.

York, D. (1969) Least squares fitting of a straight line with correlated errors. Earth and Planetary Science Letters, 5, p. 320-324.

Appendix 1: Modal Mineralogies

All igneous modes were determined by 800 to 1200 counts at intervals of 0.3 mm. The mode of sample 85-11 was determined by 1500 counts, due to its coarse grain size.

The modes of metasedimentary rocks were determined by 500 counts at intervals of 0.6 mm.

Mineralogical abbreviations are as follows:

plag	-	plagioclase	qz	-	quartz
ol	-	olivine	ksp	-	K-feldspar
cpx	-	clinopyroxene	hb	-	hornblende
opx	-	orthopyroxene	sill	-	sillimanite
amph	-	amphibole	ga	-	garnet
bi	-	biotite			

Sample	plag	ol	cpx	opx	amph	opaques	spinel	bi	other
8501	57.7	0.0	4.3	16.1	20.2	0.1	0.3	1.3	0.0
8502	91.9	0.0	3.6	2.0	1.1	0.4	0.3	0.8	0.0
8503	59.0	2.6	1.9	17.7	17.2	0.2	0.1	1.4	0.0
8504	30.1	22.7	7.8	16.8	20.2	0.0	0.2	2.3	0.0
8505	15.7	42.2	6.5	17.1	17.0	0.4	0.3	0.8	0.0
8506	64.3	6.3	3.0	10.1	15.4	0.0	0.3	0.6	0.0
8507	68.1	0.4	3.0	13.6	13.4	0.4	0.1	1.0	0.0
8508	66.9	1.0	7.0	15.4	3.7	0.1	0.0	5.1	0.3
8511	51.1	25.6	5.1	6.7	10.3	1.1	0.1	0.0	0.1
8512	48.5	28.0	0.5	7.9	14.7	0.2	0.1	0.0	0.1
8602	47.5	0.0	27.8	23.0	0.0	0.0	0.0	0.9	0.0
8603	0.0	49.9	0.6	18.0	26.5	0.6	4.3	0.3	0.0

Sample	qz	ksp	plag	bi	opx	hb	opaques	sill	ga	others
8604	12.4	0.2	43.6	2.4	23.6	0.0	5.4	3.0	0.0	9.4
8605	3.0	5.6	26.2	6.2	33.2	0.0	11.0	3.2	0.0	11.4
8606	6.8	13.2	43.4	2.2	16.0	0.0	7.4	2.4	0.0	8.6
8607	12.8	9.8	13.8	29.0	0.0	0.0	7.6	26.4	0.0	0.6
8608	17.8	16.0	1.4	1.4	50.2	0.0	5.8	1.4	0.0	6.2
310A	33.6	20.0	15.4	0.6	0.8	0.0	6.8	17.8	0.0	5.0
310B	48.2	22.2	15.4	1.8	0.0	0.0	3.8	7.2	0.0	1.4
310C	43.4	15.0	23.2	2.2	2.2	0.0	6.2	6.6	0.0	1.2
8609B	18.0	20.2	23.8	23.2	0.0	0.0	3.8	9.8	0.0	1.4
8610B	31.6	14.4	23.8	29.4	0.0	0.0	0.6	0.0	0.0	0.4
8611A	29.6	11.4	33.2	19.4	0.0	0.0	3.6	2.2	0.0	0.6
8612A	27.0	20.2	36.6	16.6	0.0	0.0	1.2	0.0	0.0	0.8
8613	26.0	11.0	26.8	30.8	0.0	0.0	4.5	0.0	0.0	1.0
8614	34.8	6.2	29.6	27.2	0.0	0.0	1.0	0.0	0.0	1.4
8509	29.4	13.8	37.6	12.3	0.0	5.4	1.3	0.0	0.6	0.0
8510	20.4	38.0	24.1	0.0	0.0	14.4	1.9	0.0	0.5	0.8
8513	25.8	18.6	41.3	12.5	0.0	0.0	1.3	0.0	0.4	0.3
8514	3.9	0.0	34.0	8.9	0.0	52.0	1.3	0.0	0.0	0.0
8515	24.9	17.3	32.9	19.8	0.0	0.0	3.9	0.0	1.0	0.6
8516	29.9	16.3	35.3	16.5	0.0	0.0	1.8	0.0	0.0	0.4
8616A	0.0	0.3	55.7	6.0	33.0	0.0	2.7	0.0	0.0	9.0
8616B	6.0	0.2	69.4	12.2	8.4	0.4	3.0	0.0	0.0	0.4
8617A	31.6	21.4	32.2	12.6	0.0	0.0	1.4	0.0	0.0	0.8
8618A	18.0	1.0	38.2	19.6	0.0	18.2	4.0	0.0	0.0	1.2
8618B	29.0	1.2	38.0	15.8	0.0	8.8	3.6	0.0	3.0	0.4

Appendix 2: Analytical Procedures

2. Analytical Procedures (Whole Rock)

2.1 Sampling Technique

Samples of approximately twenty to thirty kilograms each were obtained, in order to minimise the effects of secondary alteration due to weathering and to minimise the effects of possible sample heterogeneity. Samples that were heavily weathered or that contain veins or fractures were avoided, where possible. In sampling the metasediments and particularly in sampling the WBAC monzonites and the Paradise Arm Pluton rocks, sampling was restricted by the relatively limited number of suitably well exposed outcrops. Hence, essentially all of the samples from the latter two units are altered to some degree, usually in the form of sericitisation of the feldspars, despite efforts to minimise this. Most of the samples had their weathered surfaces removed at the sampling site by sledgehammer, or failing that, at the field base camp using a rock saw. Final purification of the samples was done at McMaster University by further hammering and hand picking of the fresh pieces. The final sample consisted of ten to fifteen kilograms of relatively fresh material.

The large sample volumes (averaging about 200 cm^3) were intended also to eliminate or minimise the effects of sample

variability, a potentially significant factor for exceptionally coarse-grained rocks such as some of the coronites or those with coarse-grained K-feldspar megacrysts, and for heterogeneous rocks such as the metasediments with alternatively restite-rich or leucosome-rich layers. In high grade metamorphic terranes, the scale of isotopic homogenisation is potentially large, particularly for Rb-Sr systematics, and possibly for REE as well. Ideally, sample volumes should be large enough to ensure that the isotopes have equilibrated at the "whole rock" scale, if not the mineral scale. Samples were taken at least five metres apart (ie. in the case of A and B samples from the same site) so as not to resample the sample spot, in effect.

The WBAC gabbronorites were sampled largely from one particularly large and variable outcrop. Areas with primary layering were sampled based on the premise that strong compositional variation would maximise isotopic variation while still remaining at the outcrop scale to minimise the possibility of sampling non-comagmatic rocks. Coarse grained coronites were sampled to facilitate ease of separation of the coronitic mineral phases for isotopic analyses. Rocks with very few mineral phases such as anorthosites, troctolites, or pyroxenites were sampled not only for bulk compositional variation but also to simplify the mineral isotope systematics, and in the case of olivine free rocks, to attempt

to limit the system to primary minerals only.

In order to discern the effects, if any, of the intrusion of the WBAC gabbronorites into the Paradise Metasedimentary Gneiss Belt rocks, samples were taken from within a few metres of the contact (probably; the contact is low lying at this point, under a lake arm and associated bog). Samples were also collected from two or three kilometres from the contact, and from ten to fifteen kilometres away, in rocks apparently unaffected by the gabbronorite intrusion.

Samples from the Paradise Arm Pluton and the WBAC monzonites were sampled wherever outcrop was reasonably well exposed and not excessively weathered. In almost all cases these were in river beds or banks.

2.2 Crushing

All samples were broken down by hand into approximately five to seven centimetre long chips, suitable for crushing in the jaw crusher, and following that, in a BICO ceramic disk pulveriser. Small aliquots (about 500 g) of sample were then isolated by repeated and prolonged mixing and quartering of the sample to ensure that the extract was representative of the bulk sample. This aliquot was ground to -300 Mesh using a tungsten- carbide ring and puck assembly in a SPEX tungsten-

carbide shatterbox. All sample were stored in new airtight plastic containers cleaned with compressed air before use.

Sample contamination from previous samples was minimised by cleaning each item of crushing equipment with both wire and soft bristled brushes, acetone, and compressed air. The shatterbox, ring, and puck were cleaned with hot water and thoroughly scrubbed between samples, and dried with compressed air. In order to further minimise contamination from either the shatterbox or the ceramic disk pulveriser, both of these instruments were precontaminated by grinding a small aliquot of sample for a short time (about two minutes) and then discarding it, after which the equipment was again cleaned. Sample contamination from the first stages of crushing was minimised by washing off potentially foreign rock flour before addition to the jaw crusher.

Contamination of the samples from the crushing equipment itself was less easily monitored. Due to the relatively poor condition of the ceramic plates in the pulveriser and the hot operating conditions, in at least one case (85-02) small flakes of ceramic were found in the final sample powder. New ceramic plates were later obtained which eliminated that risk for all of the 86-prefix samples. Hickson and Juras (1986) suggest that tungsten-carbide shatterboxes produce no contamination for any elements analysed for in this study.

2.3 X-Ray Fluorescence Spectrography - Major Element Analyses

0.5000 g of sample was mixed with 3.0000 g of flux consisting of a 1:1 mixture of lithium metaborate and lithium tetraborate in a glass vial, thoroughly mixed to facilitate rapid and homogeneous melting and subsequent fusion. Before heating, twenty microlitres of LiBr solution was added to the powder, as a disaggregating agent. The sample/flux mixture was heated to about 1200°C in a Pt/Au crucible until a homogeneous liquid formed, poured into a Pt/Au mold of 30 mm diameter, and cooled to produce a fused glass bead for XRF analysis. The crucible was cleaned between samples using hot dilute nitric acid.

2.4 X-Ray Fluorescence Spectrography - Trace Element Analyses

Approximately five grams of sample was mixed thoroughly with about one millilitre of Mowiol, an organic binding agent, in a clean four or five dram glass vial. The sample was then pressed into a 30 mm diameter Chemplex aluminum cup and compressed to about twenty five tons pressure in a SPEX thirty ton press. Three such powder pellets were made for each sample, to account for sample inhomogeneities.

Both major and trace element analyses were performed on a Philips Model PW1450 automatic sequential X-ray fluorescence

spectrometer. Precision levels based on replicate samples and replicate analyses of the same samples for the elements analysed for are listed in Appendices 9 and 10.

2.5 Mass Spectrometry Sample Preparation

For mass spectrometric analysis, between 500 and 900 mg of -300 mesh sample was weighed to within about ± 5 µg into a clean Savillex PFA teflon bomb of known weight. Approximately 10 ml of 42 % HF was added, the bombs were sealed, placed inside an outer jacket of FEP teflon, also sealed, and heated in an oven for about four days at 120°C. Following dissolution, the samples were evaporated to near-dryness, 3 to 5 ml of 16 N HNO_3 added to remove any insoluble fluorides, evaporated to complete dryness, and converted to chloride form by adding 5 ml of 6 N HCl, resealing, and heating at 120° for about two days. The solution was then evaporated to dryness and redissolved in about 8 ml of 2.5 N HCl and split and spiked appropriately. Rubidium was spiked using a 99.20 % enriched ^{87}Rb spike, calibrated against rock standards AGV-1 and W-1 giving a concentration of 1.668 ± 0.11 (2σ). The error on the standards includes variation from independent dissolutions and chemistry, weighing imprecision, and variability of the mass spectrometer on analyses of the same aliquot. Strontium was spiked using a ^{84}Sr spike calibrated against the same rock standards giving a spike concentration

of 5.57 ± 0.19 ppm. Blank levels for Sr analyses are approximately 0.3 - 0.4 ng. Samarium and neodymium were spiked using a total REE spike prepared from solid REE oxides and calibrated relative to rock standard BCR-1. Rock standards AGV-1 and W-1 gave concentrations as listed below, with 2σ errors on four and three analyses respectively:

	Measured		Gladney *et al.* (1983)	
Standard	Sm (ppm)	Nd (ppm)	Sm (ppm)	Nd (ppm)
AGV-1	5.8 ± 0.1	32.1 ± 0.5	5.9 ± 0.5	34 ± 4
W-1	3.35 ± 0.04	13.3 ± 0.2	3.5 ± 0.3	15 ± 3

The sample, spiked or natural, was then centrifuged in clean polystyrene centrifuge tubes to prevent any undissolved solids from being loaded onto the columns, transferred to quartz cation exchange columns (with Dowex Bio-Rad AG50W, 200 to 400 mesh, hydrogen form resin), and eluted with 2.5 N HCl, 3 N and 7 N HNO_3. The Sr, collected in the HCl, was evaporated to dryness and stored for mass spectrometry. Rb was collected in about 15 ml of HCl. The REE aliquot was also evaporated to dryness, redissolved in 0.155 N HCl and loaded on to quartz columns (with 200 mesh teflon beads coated with 2,2 diethyl-hexyl-orthophosphoric acid activator). The REE were eluted with 0.155 N and/or 0.5 N and 6 N HCl, evaporated to dryness, and redissoved in two drops of a 1.3:100 mixture of 0.3 M H_3PO_4 and 3.0 M HNO_3. This produces a solution of

approximately 0.004 M H_3PO_4 ensuring that all the REE were completely in solution.

Sr was dissolved in 0.3 or 0.4 M H_3PO_4 and loaded onto a single (centre) 0.030 mm wide tantalum filament, which had been preconditioned at approximately 2.5 Amps for 15 minutes at $5x10^{-6}$ torr. Neodymium and selected REE separates were brought into solution by gentle heating on a hotplate before loading, also serving to reduce the sample size to about a microlitre. This drop was then loaded onto the tantalum side filament (0.030 mm width) of a triple filament bead equipped with a tantalum side and a rhenium centre filament.

2.5 Mass Spectrometry

Rubidium was analysed by isotope dilution on the Sciex Elan 250 ICP/MS and corrected to the literature values for rock standards. Rb fractionation was monitored by regularly analysing the $^{85}Rb/^{87}Rb$ of an unspiked rock solution and comparing the result to the predicted normal value of 2.593. Sr, Nd and assorted LREE and HREE were all analysed on a VG 354 5-collector solid-source mass spectrometer, with 27 cm radius and 90° magnetic sector. Magnetic field switching and data analysis were controlled by a Hewlett-Packard 9121 computer. Precision levels are listed with the data in Appendix 5. All analyses were corrected to the mean standard

values obtained on this machine, as listed below, in cases where the standards were not within 2σ error of the acceptable value. NBS 987 and Eimer and Amend $SrCO_3$ standards gave the following values for $^{87}Sr/^{86}Sr$:

Standard	Mean value	Variation (2σ)	Dates Spanned
E+A Std.	0.707997	± 0.069/mil on 36	Jan '86-Aug '87
NBS 987	0.710224	± 0.080/mil on 23	Jan '86-May '86
NBS 987	0.710217	± 0.075/mil on 22	May '86-Dec '86
NBS 987	0.710226	± 0.055/mil on 34	Jan '87-May '87
NBS 987	0.710205	± 0.051/mil on 20	May '87-Aug '87

Replicate analyses from rerunning the same Sr separate and running multiple dissolutions also constrained analytical variation. Neodymium isotope analyses were compared to multiple analyses of the La Jolla Nd rock standard, which produced a mean value of $^{143}Nd/^{144}Nd=0.511852 \pm 0.057$/mil (2σ) on 16 analyses.

2.6 Mineral Separation

Mineral separation consisted of three stages; density separation using heavy liquids, done at the Geological Survey of Canada laboratory in Ottawa, magnetic separation and hand picking, done at McMaster.

The sample material used was the relatively coarse-grained pulverised rock, which was then further ground in a Bico ceramic disk pulveriser at the G.S.C. to -100 mesh. After crushing, the very fine material was floated off in water. The pulveriser was cleaned between samples with a soft-bristled brush and compressed air. There was a significant contribution to the sample by small chips of ceramic plate in one case, but this was eliminated by later processing. Samples were sieved through wire sieves, assisted by three ceramic spheres of about 1 cm diameter. The sieves were cleaned with water and compressed air between samples.

The heavy liquids used were dimethyl sulphoxide, (ρ=1.09 gcm^{-3}), Bromoform, (ρ=2.85 gcm^{-3}), and methylene iodide, (ρ=3.30 gcm^{-3}), or mixtures thereof. The degree of isotopic contamination introduced by the heavy liquids is unknown, and was minimised by washing the samples with acetone before drying.

Approximately 100 g of sample were settled in about 200 ml of heavy liquid of known density. After the collection of a given fraction, the samples were rinsed free of heavy liquid with acetone, and then dried.

The minerals separated by heavy liquids from three gabbronorite samples were plagioclase, in the fraction lighter

than 2.85 gcm^{-3}, amphibole (and plagioclase) in the fraction between 2.85 and 3.09 gcm^{-3}, and finally olivine and the two pyroxenes in the fraction heavier than 3.30 gcm^{-3}. Thin section observation indicated that biotite was present in trace amounts only, so it was not separated.

Following heavy liquid separation, the separation was further refined using a Franz Isodynamic Mineral Separator, in order to separate plagioclase from amphibole and any minor biotite present, and to isolate olivine, orthopyroxene, and clinopyroxene.

Before using the Franz, the separates were crushed further using a steel hand crushing mill to -120 mesh, where most of the sample was between 150 and 230 mesh, in order to maximise the number of monomineralic grains while still keeping them coarse enough to hand pick. The separates were then washed to remove the fines. In order to prevent the Franz from clogging up, the highly magnetic material such as magnetite was removed first at very low current and steep slope. Then plagioclase was separated from the more magnetic corona minerals using a moderately high current, and then olivine was separated from the two pyroxenes, which were in turn separated last. The current and tilt settings for the Franz are presented in Table II.1.

Finally, the separates were hand picked under a binocular microscope, to remove any polymineralic grains and any remaining pieces of ceramic, if necessary. The degree of purity of the separates was established by counting the number of "impurities" in 100 grains of homogeneous sample. All plagioclase separates were estimated to be 99+ % pure, olivine 99 % pure, amphibole 95 % pure (impurity mostly plag), clinopyroxene 80 % free of opx, and orthopyroxene was estimated to be only 70 % free of cpx and olivine in sample 8511 and 90 % pure in 8505. Given the small grain size of the separates, much purer extracts were impractical given, at the time, relatively poorly-established elemental blank levels and minimum yield levels for REE required for successful analysis.

Rather than crushing the mineral separates to -300 Mesh as was done with the whole rocks, in order to minimise the risk of contamination, potentially large due to the relatively small sample size and low Rb, Sr, Sm and Nd concentrations, the samples were dissolved in HF for a longer period of time than were the whole-rock powders. These separates were dissolved for one month at 120° C, but dissolution times of one to two weeks would probably suffice, depending on the grain size and composition of the phases. In this way complete dissolution was ensured, and the decrease in sample homogeneity due to the coarser grain size was compensated for by the fact that a much larger proportion of the total

original sample was dissolved for the mineral separates than for the whole rock samples.

2.7 Electron Microprobe Analysis

Electron microprobe analyses were conducted over one day at the Memorial University of Newfoundland, on a JEOL JXA-50A electron probe microanalyser. Data was standardised to a clinopyroxene and an olivine standard, as listed in Appendix 8. The detection limit and the precision are reportedly 0.1 % of the oxide total.

Polished thin sections were prepared from slabs by Vancouver Petrographic Inc., in Vancouver.

Table II.1

Magnetic Mineral Separation Settings

High-mag. fraction	Low-mag. fraction	Current	Slope	Tilt
Fraction: >3.30 g/cc				
magnetite	plag, ol, cpx, opx	0.1-0.2	30-40	15
ol, cpx, opx	plag	0.6	25	15
cpx, opx	ol	0.3	15	20
opx	cpx	2.7-2.8	17.5	25
Fraction: 2.85-3.30 g/cc				
magnetite	plag, amph	0.1	30	15
amph, plag	plag	0.5-0.6	25	15
amph	plag	0.25-0.3	15	10
Fraction: <2.85 g/cc				
magnetite	amph	0.2	25	15
impure plag	plag	1.80	25-30	10-15

Appendix 3: XRF analyses for major and trace elements

Major element concentrations are given in weight percent, and trace elements concentrations are given in ppm. Analytical techniques are given in Appendix 2, sections 2.3 and 2.4.

Name\Element	SiO2	Al2O3	Total Fe as Fe2O3	MgO	CaO	Na2O	K2O	TiO2	MnO	P2O5
WBAC Gabbronorite										
SPM85-01	45.51	22.82	7.4	9.95	11.93	1.5	0.4	0.28	0.09	0.11
SPM85-02	46.43	26.39	4.22	7.46	13.28	1.57	0.35	0.12	0.04	0.13
SPM85-03	45.56	22.77	7.14	10.65	11.83	1.31	0.4	0.16	0.08	0.09
SPM85-04	42.23	11.03	14.1	23.99	6.86	0.85	0.38	0.29	0.18	0.1
SPM85-05	41.08	9.91	16.65	24.7	5.98	0.8	0.31	0.28	0.22	0.08
SPM85-06	45.05	22.71	7.81	10.53	11.9	1.32	0.35	0.12	0.09	0.12
SPM85-07	44.29	22.56	7.72	11.43	12.19	1.13	0.32	0.17	0.09	0.1
SPM85-08	47.06	19.5	8.63	11.1	11.4	1.31	0.49	0.29	0.1	0.11
SPM85-11	48.93	19.63	8.73	9.69	10.14	1.84	0.55	0.27	0.07	0.08
SPM85-12	47.5	24.88	6.31	6.31	11.82	1.74	0.01	0.01	0.07	0.07
SPM86-02	47.18	21.52	8.79	9.56	9.97	1.84	0.76	0.18	0.09	0
SPM86-03	45.43	8.2	7.14	33.5	4.19	0.27	0.78	0.16	0.23	0.09
WBAC Transitional Phases (Amphibolite, Monzogabbro)										
SPM85-14	51.81	15.61	12.45	6.26	8.17	2.07	2.03	1.13	0.19	0.04
SPM86-16A	52.14	17.14	12.04	5.17	8.41	1.96	1.25	1.33	0.19	0.37
SPM86-16B	53.56	17.3	12.89	3.74	6.06	2.41	2.09	1.46	0.17	0.32
WBAC Monzonite										
SPM85-10	66.92	13.87	5.89	2.06	2.6	1.89	5.59	1.02	0.09	0.07
SPM85-09	64.97	15.72	6.44	2.3	3.33	2.2	4.05	0.76	0.14	0.09
SPM85-13	67.88	15.75	4.86	4.86	2.74	1.91	4.3	0.62	0.09	0.09
SPM85-15	67.66	16.13	5.16	1.18	2.53	2.03	4.47	0.71	0.1	0.03
SPM85-16	67.58	15.79	5.56	1.08	2.6	2.11	4.44	0.71	0.09	0.04
SPM86-17A	70	15.11	3.85	0.53	2.26	2.07	5.23	0.64	0.07	0.24
SPM86-17B	69.86	15.08	4.05	0.43	2.32	2.18	5.09	0.64	0.09	0.26
SPM86-18A	59.81	16.28	8.86	1.6	5.26	3.77	2.24	1.44	0.2	0.53
SPM86-18B	61.37	16.25	8.89	1.04	4.55	3.7	2.16	1.3	0.24	0.49
Paradise Arm Pluton										
SPM86-11A	66.82	15.94	6.15	1.4	2.83	2.38	3.29	0.84	0.08	0.27
SPM86-11B	66.65	16.03	6.2	0.67	3.08	2.16	3.96	0.91	0.1	0.25
SPM86-12A	67.01	16.32	5.25	1.16	3.19	2.71	2.98	1.02	0.09	0.26
SPM86-12B	65.5	15.96	5.55	2.21	2.96	2.18	4.38	0.89	0.11	0.27
SPM86-13	65.42	16.5	5.84	1.15	3.22	2.28	4.24	0.97	0.1	0.28
SPM86-14	65.54	16.66	6.01	1.05	3.72	2.32	3.27	1.03	0.12	0.28
Anhydrous PMGB										
SPM86-04	59.68	20.42	7.59	2.57	3.83	2.26	2.24	1.14	0.14	0.13
SPM86-05	59.24	20.66	8.31	2.29	3.34	1.94	2.48	1.51	0.12	0.11
SPM86-06	56.43	20.58	10.59	2.45	3.62	1.77	2.24	2.07	0.11	0.13
SPM86-07	52.13	22.78	15.22	3.58	1.46	0.92	2.34	1.35	0.13	0.09
SPM86-08	61.21	19.93	10.12	4.26	0.66	0.47	2.55	0.58	0.14	0.08
PMGB Gneisses										
CG85-310A	67.06	16.34	6.12	2.75	1.22	2.1	3.41	0.88	0.06	0.07
CG85-310B	73.91	13.4	5.12	1.03	1.62	1.57	2.4	0.81	0.06	0.07
CG85-310C	71.49	13.47	6.54	1.99	1.29	1.41	2.74	0.96	0.06	0.05
CG85-310D	58.43	23.54	9.21	2.03	0.7	0.6	4.3	1.03	0	0.07
CG85-310E	58.69	23.31	8.36	1.58	0.92	1.01	4.89	1.08	0.09	0.08
CG85-310F	65.06	19.17	6.75	1.17	1.08	1.8	3.88	0.93	0.08	0.07
CG85-310G	63.83	18.56	7.5	2.81	1.13	1.46	3.49	1.03	0.11	0.08
SPM86-09A	63.12	19.81	7.19	1.85	1.29	1.11	4.49	0.92	0.1	0.13
SPM86-09B	61.67	19.44	7.61	3.03	1.5	1.35	4.07	1.09	0.1	0.15
SPM86-10A	68	16.15	5.38	2.48	1.83	1.35	3.91	0.7	0	0.12
SPM86-10B	68.58	16.12	5.75	1.31	2.57	1.9	2.84	0.58	0.25	0.09

Name\Element	Y	Zr	Ba	Ni	Cr
WBAC Gabbronorite					
SPM85-01	7	39	86	285	86
SPM85-02	5	35	92	147	73
SPM85-03	6	29	111	215	90
SPM85-04	7	26	93	848	419
SPM85-05	7	20	92	1027	521
SPM85-06	6	31	83	309	181
SPM85-07	6	24	76	294	361
SPM85-08	8	41	114	196	313
SPM85-12	5	36	38	165	20
SPM86-02	26	49	125		
SPM86-03	18	45	52		
WBAC Transitional Phases (Amphibolite, Monzogabbro)					
SPM85-14	17	111	306	111	198
SPM86-16A	32	110	480		
SPM86-16B	17	240	880		
WBAC Monzonite					
SPM85-10	51	480	1044	5	16
SPM85-09	27	289	1169	14	41
SPM85-13	30	256	759	12	25
SPM85-15	25	244	948	14	32
SPM85-16	30	276	921	13	30
SPM86-17A	25	190	850		
SPM86-17B	33	186	800		
SPM86-18A	50	500	550		
SPM86-18B	96	407	230		
Paradise Arm Pluton					
SPM86-11A	25	229	1040		
SPM86-11B	25	254	820		
SPM86-12A	27	202	930		
SPM86-12B	28	203	930		
SPM86-13	28	214	1170		
SPM86-14	24	245	940		
Anhydrous PMGB					
SPM86-04	15	249	1590		
SPM86-05	15	270	2075		
SPM86-06	15	196	2070		
SPM86-07	15	286	1780		
SPM86-08	15	154	1770		
PMGB Gneisses					
CG85-310A					
CG85-310B					
CG85-310C					
CG85-310D					
CG85-310E	22	250	1870		
CG85-310F	22	258	1410		
CG85-310G					
SPM86-09A	25	217	1480		
SPM86-09B	24	226	1220		
SPM86-10A	29	219	880		
SPM86-10B	23	240	1060		

Blank spaces indicate elements not analysed.

Appendix 4: Normative mineralogies

CIPW normative minerals are based on oxidised to reduced iron ratios as discussed in Chapter 5.

Normative mineral abbreviations are given as follows:

Q'	- quartz	di'	- diopside
or'	- orthoclase	hy'	- hypersthene
ab'	- albite	ol'	- olivine
an'	- anorthite	mt'	- magnetite
ne'	- nepheline	il'	- ilmenite
C'	- corundum	ap'	- apatite

The Discriminant Function (Shaw, 1972) is given where appropriate based on the geochemical screening criteria. DF is defined in the text in Chapter 5.

Sample	Normative analyses Q'	or'	ab'	an'	An content	ne'	C'	di'	hy'	ol'
WBAC Gabbronorite										
SPM85-01		2.36	12.69	54.36	81			3.3	3.84	20.07
SPM85-02		2.07	13.29	63.93	83			0.87	5.8	11.16
SPM85-03		2.36	11.08	55.07	83			2.43	6.21	19.91
SPM85-04		2.25	6.42	25.16	80	0.42		6.6		55.8
SPM85-05		1.83	6.77	22.54	77			5.25	6.58	47.05
SPM85-06		2.07	11.17	55.01	83			2.61	3.92	22.37
SPM85-07		1.89	9.56	55.54	85			3.43	1.44	25.15
SPM85-08		2.9	11.08	45.88	81			8.01	13.58	15.14
SPM85-11		3.25	15.57	43.68	74			4.93	20.05	9.19
SPM85-12		0.06	14.72	58.18	80		0.68		20.88	1.82
SPM86-02		4.49	15.57	48.22	76			1.01	9.37	18.46
SPM86-03		4.61	2.28	18.86	89			1.05	18.18	52.09
WBAC Transitional Phases (Amphibolite, Monzogabbro)										
SPM85-14	1.54	12	17.52	27.31	61			10.7	24.65	
SPM86-16A	6.56	7.39	16.59	34.28	67			4.16	23.55	
SPM86-16B	7.65	12.35	20.39	27.97	58		0.82		23.01	
WBAC Monzonite										
SPM85-10	24.91	33.04	15.99	12.44	44		0.15		7.72	
SPM85-09	24.17	23.93	18.62	15.93	46		1.88		10.54	
SPM85-13	26.35	25.41	16.16	13.01	45		3.19		14.53	
SPM85-15	30.46	26.42	17.18	12.36	42		3.42		5.54	
SPM85-16	29.73	26.24	17.85	12.64	41		2.88		6.01	
SPM86-17A	32.78	30.91	17.52	9.64	36		2.51		1.77	
SPM86-17B	32.43	30.08	18.45	9.81	35		2.39		1.92	
SPM86-18A	14.59	13.24	31.9	20.89	40			1.47	9.68	
SPM86-18B	18.4	12.77	31.31	19.37	38		0.73		9.76	
Paradise Arm Pluton										
SPM86-11A	31.25	19.44	20.14	12.28	38		3.97		7.31	
SPM86-11B	30.37	23.4	18.28	13.65	43		3.19		5.32	
SPM86-12A	31.37	17.61	22.93	14.13	38		3.46		4.3	
SPM86-12B	26.01	25.88	18.45	12.92	41		2.9		8.07	
SPM86-13	26.86	25.06	19.29	14.15	42		2.98		5.6	
SPM86-14	29.5	19.32	19.63	16.63	46		3.21		5.44	
Anhydrous PMGB										
SPM86-04	23.88	13.24	19.12	18.15	49		7.63		11.69	
SPM86-05	25.94	14.66	16.42	15.85	49		8.98		10.68	
SPM86-06	23.45	13.24	14.98	17.11	53		8.97		12.83	
SPM86-07	21.24	13.83	7.78	6.66	46		16.29		27.29	
SPM86-08	35.56	15.07	3.98	2.75	41		15.39		22.96	
PMGB Gneisses										
CG85-310A	31.28	20.15	17.77	5.6	24		7.14		15.62	
CG85-310B	47.49	14.18	13.29	7.58	36		5.44		9.8	
CG85-310C	42.96	16.19	11.93	6.07	34		5.96		14.3	
CG85-310D	28	25.41	5.08	3.02	37		16.79		18.58	
CG85-310E	24.45	28.9	8.55	4.04	32		14.87		16.13	
CG85-310F	31.43	22.93	15.23	4.9	24		10.21		12.67	
CG85-310G	30.63	20.63	12.35	5.08	29		10.52		17.9	
SPM86-09A	29.52	26.53	9.39	5.55	37		11.09		15.15	
SPM86-09B	25.94	24.05	11.42	6.46	36		10.45		18.51	
SPM86-10A	34.38	23.11	11.42	8.29	42		6.66		13.91	
SPM86-10B	35.35	16.78	16.08	12.16	43		5.46		12.26	

Blank spaces represent 0.0 % normative mineral

Sample	norms (cont.) mt'	il'	ap'	Shaw 1971 DF
WBAC Gabbronorite				
SPM85-01	2.58	0.53	0.25	-
SPM85-02	2.35	0.23	0.3	-
SPM85-03	2.41	0.3	0.21	-
SPM85-04	2.6	0.55	0.23	-
SPM85-05	24.14	0.53	0.19	-
SPM85-06	2.35	0.23	0.28	-
SPM85-07	2.42	0.32	0.23	-
SPM85-08	2.6	0.55	0.25	-
SPM85-11	2.57	0.51	0.19	-
SPM85-12	2.19	0.02	0.16	-
SPM86-02	2.44	0.34		-
SPM86-03	2.41	0.3	0.21	-
WBAC Transitional Phases (Amphibolite,				
SPM85-14	3.81	2.15	0.09	-
SPM86-16A	4.1	2.53	0.86	-1.2667
SPM86-16B	4.29	2.77	0.74	-0.6174
WBAC Monzonite				
SPM85-10	3.65	1.94	0.16	-0.3088
SPM85-09	3.28	1.44	0.21	-0.288
SPM85-13	3.07	1.18	0.21	-3.5152
SPM85-15	3.2	1.35	0.07	0.1929
SPM85-16	3.2	1.35	0.09	0.3188
SPM86-17A	3.1	1.22	0.56	1.078
SPM86-17B	3.1	1.22	0.6	1.2594
SPM86-18A	4.26	2.73	1.23	3.0835
SPM86-18B	4.06	2.47	1.14	2.7592
Paradise Arm Pluton				
SPM86-11A	3.39	1.6	0.63	-0.1243
SPM86-11B	3.49	1.73	0.58	0.7889
SPM86-12A	3.65	1.94	0.6	0.8714
SPM86-12B	3.47	1.69	0.63	-0.0808
SPM86-13	3.58	1.84	0.65	1.0954
SPM86-14	3.67	1.96	0.65	0.9234
Anhydrous PMGB				
SPM86-04	3.83	2.17	0.3	-
SPM86-05	4.36	2.87	0.25	-
SPM86-06	5.18	3.93	0.3	-
SPM86-07	4.13	2.56	0.21	-
SPM86-08	3.02	1.1	0.19	-
PMGB Gneisses				
CG85-310A		1.67	0.16	-2.7176
CG85-310B		1.54	0.16	-3.2497
CG85-310C		1.82	0.12	-4.3682
CG85-310D		1.96	0.16	-
CG85-310E		2.05	0.19	-
CG85-310F		1.77	0.16	-
CG85-310G		1.96	0.19	-3.4804
SPM86-09A		1.75	0.3	-
SPM86-09B		2.07	0.35	-
SPM86-10A		1.33	0.28	-2.9031
SPM86-10B		1.1	0.21	-1.3645

Blank spaces represent 0.0 % normative mineral

Appendix 5: Isotopic Data

Concentrations and isotope ratios of Rb, Sr, Sm and Nd are determined as outlined in Appendix 2. Errors given on isotope ratios are ± 1σ per mil. Errors on Rb concentrations are ± 1 standard deviation on the raw counts (10 repeats of 1 second counting times).

Blanket errors for X and Y used in the York II linear regressions are based on reproducability of standards as given in Appendix 2, except where the error on individual analyses was worse, in which case the latter error was used. This applies only to some of the gabbronorites, where large errors in Rb concentrations produced relatively large errors in $^{87}Rb/^{86}Sr$.

Name\Element	Rb	2σ	Sr	Rb/Sr	87Rb/86Sr	1σ	87Sr/86Sr	1σ (%.)
WBAC Gabbronorite								
SPM85-01	0.313	0.009	183	0.00171	0.00492	0.00002	0.70406	0.009
SPM85-02	0.489	0.024	232	0.00211	0.00607	0.00009	0.70342	0.010
SPM85-03	0.090	0.008	192	0.00047	0.00135	0.00005	0.70338	0.010
SPM85-04	0.537	0.017	115	0.00467	0.01344	0.00005	0.70523	0.009
SPM85-05	4.087	0.179	98	0.04170	0.12005	0.00142	0.70516	0.012
SPM85-06	0.251	0.033	206	0.00122	0.00351	0.00020	0.70351	0.010
SPM85-07	0.101	0.012	181	0.00056	0.00161	0.00008	0.70321	0.013
SPM85-08	0.418	0.032	176	0.00238	0.00684	0.00022	0.70452	0.010
SPM85-11	0.034	0.006	300	0.00011	0.00033	0.00003	0.70258	0.015
SPM85-12	0.017	0.006	316	0.00005	0.00015	0.00002	0.70265	0.009
SPM86-02	4.8		177	0.02715	0.07806	0.00259	0.70462	0.009
SPM86-03	0.9		52	0.01731	0.04982	0.02166	0.70389	0.011
Mineral Separates								
11-plag	0.304	0.021	448	0.00068	0.00195	0.00004	0.70250	0.010
11-ol	0.112	0.008	58	0.00194	0.00556	0.00001	0.70346	0.018
11-cpx	0.065	0.015	12	0.00546	0.01559	0.00166	0.70276	0.013
11-opx	0.174	0.013	20	0.00892	0.02504	0.00063	0.70309	0.016
11-amph	0.070	0.020	69	0.00101	0.00292	0.00037	0.70345	0.012
05-plag	1.286	0.066	474	0.00271	0.00781	0.00007	0.70311	0.008
05-opx	0.402	0.019	2	0.20100	0.36871	0.00887	0.71179	0.015
05-cpx	0.256	0.020	7	0.03459	0.15641	0.00114	0.70670	0.012
WBAC Transitional Phases (Amphibolite, Monzogabbro)								
SPM85-14	47		238	0.19806	0.57058		0.71503	0.010
SPM86-16A	7		317	0.02202	0.06337		0.70491	0.009
SPM86-16B	43.6		503	0.08677	0.24972		0.70919	0.008
WBAC Monzonite								
SPM85-10	166		107	1.55332	4.51208		0.79966	0.009
SPM85-09	99		263	0.38054	1.09776		0.72877	0.009
SPM85-13	130		251	0.46667	1.34726		0.73661	0.010
SPM85-15	128		276	0.45154	1.3032		0.73374	0.009
SPM85-16	126		281	0.44840	1.28945		0.73302	0.010
SPM86-17A	156.7		180	0.87163	2.52261		0.76193	0.008
SPM86-17B	168		186	0.90384	2.61626		0.76362	0.008
SPM86-18A	53.8		342.9	0.15685	0.45182		0.71400	0.009
SPM86-18B	144.7		158.6	0.91209	2.64044		0.76478	0.008
Paradise Arm Pluton								
SPM86-11A	87.6		488.1	0.17929	0.51655		0.71585	0.010
SPM86-11B	88.8		329.6	0.26954	0.77704		0.72208	0.008
SPM86-12A	135.3		243.9	0.55463	1.60181		0.74050	0.009
SPM86-12B	127.6		246.4	0.51808	1.49584		0.73772	0.009
SPM86-13	112.4		299.7	0.37512	1.08214		0.72892	0.009
SPM86-14	112.1		300.0	0.37388	1.07854		0.72870	0.008

Name\Element	Rb	Sr	Rb/Sr	87Rb/86Sr	87Sr/86Sr	1σ (%.)
Anhydrous PMGB						
SPM86-04	36.8	741.1	0.04969	0.14304	0.70715	0.009
SPM86-05	41.9	571.9	0.07337	0.21124	0.70878	0.009
SPM86-06	44.7	601.1	0.07445	0.21435	0.70892	0.008
SPM86-07	30.6	355.4	0.08604	0.24776	0.71054	0.009
SPM86-08	37.8	192.5	0.19613	0.56517	0.71762	0.009
PMGB Gneisses						
CG85-310A	76	295.0	0.25763	0.74267	0.72152	0.008
CG85-310B	42	293.0	0.14334	0.41292	0.71440	0.008
CG85-310C	56	267.0	0.20974	0.60445	0.71878	0.011
CG85-310D	108	287.0	0.37631	1.08566	0.72976	0.009
CG85-310G	71	303.0	0.23432	0.67538	0.72015	0.009
SPM86-09A	117.1	369.0	0.31736	0.91517	0.72502	0.008
SPM86-09B	105.2	362.8	0.29001	0.83615	0.72319	0.008
SPM86-10A	125.8	210.3	0.59810	1.72825	0.74579	0.008
SPM86-10B	75.3	468.0	0.16094	0.46363	0.71463	0.010

Name\Element	Nd	Sm	147Sm/144Nd	143Nd/144Nd	1σ (%.)
WBAC Gabbronorite					
SPM85-01	2.807	0.716	0.1541	0.51226	0.04
SPM85-03	1.844	0.444	0.1457	0.51219	0.02
SPM85-04	2.735	0.671	0.1482	0.51227	0.02
SPM85-05	2.702	0.651	0.1278	0.51230	0.02
SPM85-07	1.096	0.292	0.1608	0.51236	0.01
SPM85-08	2.574	0.604	0.1442	0.51221	0.02
SPM85-11	0.701	0.206	0.1774	0.51265	0.03
Mineral Separates					
11-ol	0.952	0.271	0.1720	0.51277	0.10
11-cpx	3.917	1.830	0.2824	0.51362	0.07
11-amph	0.957	0.281	0.1780	0.51250	0.07
05-plag	2.258	0.357	0.0956	0.51166	0.06
05-opx	0.421	0.135	0.1938	0.51273	0.06

Appendix 6: Electron Microprobe Analyses

Traverses were made across grain contacts and within grains from coronitic gabbronorite sample 85-11, at intervals of about 10 µm. Data was screened as described in Section 7.1.

ANALYSIS #	OXIDES: Na2O	MgO	Al2O3	SiO2	K2O	CaO
A1-11(cpx)	0.30	13.08	5.70	48.24	0.00	23.50
A2-11(cpx)	0.54	13.55	5.67	49.39	0.00	24.39
A3-11(plag)	4.32	0.01	29.68	51.41	0.11	13.64
A4-11(plag)	4.30	0.03	29.91	52.06	0.06	13.43
A5-11(plag)	0.73	0.04	32.27	45.30	0.02	18.69
A6-11(plag)	3.35	0.00	29.88	50.90	0.12	13.71
C1-11(cpx)	0.55	13.80	5.43	49.11	0.00	22.21
C2-11(px)	0.48	16.19	5.43	46.42	0.02	16.70
C3-11(opx)	0.03	26.08	4.16	51.47	0.01	0.31
C4-11(opx)	0.06	25.46	4.02	52.62	0.02	0.38
C5-11(cpx)	0.39	13.07	6.18	48.73	0.00	22.99
C6-11(cpx)	0.43	13.14	5.56	47.36	0.01	23.88
C7-11(px)	0.31	15.46	5.77	49.50	0.00	19.60
C8-11(opx)	0.02	24.83	4.18	52.16	0.00	0.32
C9-11(plag)	2.05	0.35	32.45	48.23	0.04	16.11
C10-11(plag)	3.80	0.01	30.73	50.99	0.10	14.27
C11-11(plag)	3.79	0.00	30.89	50.72	0.10	14.14
C12-11(plag?)	1.28	2.07	31.90	44.95	0.03	14.87
D1-11(cpx)	0.45	12.60	5.74	48.77	0.00	23.90
D2-11(cpx)	0.42	13.12	5.41	48.58	0.03	22.75
D3-11(cpx)	0.48	12.59	5.77	47.89	0.00	24.43
E1-11(plag)	3.29	0.00	30.11	51.61	0.14	14.14
E2-11(plag)	4.30	0.00	29.54	51.89	0.11	13.51
E3-11(plag)	3.48	0.09	30.06	51.38	0.10	13.97
E4-11(plag)	3.61	0.00	31.12	50.30	0.11	15.18
E5-11(cpx)	0.51	12.94	6.27	48.49	0.00	22.90
E6-11(cpx)	0.51	14.52	5.53	49.18	0.00	20.33
E7-11(cpx)	0.55	13.48	5.85	49.15	0.00	23.39
E8-11(cpx)	0.40	13.53	6.09	47.86	0.01	24.21
E12-11(ol)		37.07	0.00	37.97		0.00
E13-11(ol)		37.12	0.00	37.74		0.04
F1-11(opx)	0.04	27.39	3.04	53.67	0.01	0.34
F2-11(opx)	0.05	27.16	3.44	52.28	0.02	0.54
F3-11(opx)	0.00	26.64	3.41	52.98	0.00	0.37
F4-11(ol)		37.75	0.00	38.12		0.02
F5-11(ol)		37.15	0.02	37.80		0.00

ANALYSIS #	OXIDES:	Na2O	MgO	Al2O3	SiO2	K2O	CaO
G1-11(cpx)		0.50	13.85	6.36	48.69	0.00	23.39
G2-11(cpx)		0.26	14.01	6.59	49.02	0.00	21.73
G3-11(cpx)		0.46	14.66	6.39	48.70	0.00	22.45
G4-11(opx?)		0.09	26.37	2.15	53.87	0.00	2.80
H1-11(plag)		4.27	0.00	30.18	51.10	0.11	13.68
H2-11(plag)		4.11	0.04	29.19	51.42	0.11	13.98
H3-11(plag)		3.63	0.00	30.23	50.33	0.11	13.92
H4-11(plag)		2.30	0.00	33.34	47.95	0.04	16.21
H5-11(plag)		1.05	0.04	34.10	44.72	0.01	19.45
H7-11(opx)		0.03	27.40	3.56	53.23	0.01	0.36
H8-11(opx)		0.01	26.58	3.64	52.88	0.01	0.37
H9-11(opx)		0.02	28.16	1.48	54.38	0.00	0.25
H10-11(ol)			37.84	0.02	37.82		0.01
H11-11(ol)			37.82	0.00	38.05		0.00
H12-11(ol)			37.62	0.00	38.31		0.01
H13-11(ol)			37.50	0.02	38.16		0.02
I1-11(plag)		2.50	0.89	30.24	50.27	0.04	15.79
I2-11(plag)		3.73	0.00	30.29	51.07	0.07	13.32
I3-11(plag)		3.81	0.01	30.53	51.10	0.05	13.70
I4-11(plag)		3.72	0.02	30.53	51.22	0.07	13.54
I5-11(amph)		0.80	14.60	18.25	42.03	0.31	7.31
I6-11(amph)		2.09	15.21	18.97	41.73	0.53	8.24
I7-11(amph)		3.37	15.20	15.71	42.43	0.80	12.30
I8-11(amph)		3.13	15.50	27.88	32.79	0.62	10.21
I9-11(amph)		2.59	15.50	31.27	32.79	0.60	9.09
I10-11(amph)		3.32	15.27	20.05	36.50	0.59	12.16
I11-11(amph)		3.02	15.34	18.00	40.31	0.78	11.04
I12-11(opx)		0.01	28.07	1.68	54.37	0.01	0.29
I13-11(opx)		0.00	28.39	1.22	54.18	0.00	0.25
I14-11(opx)		0.00	28.21	0.82	55.41	0.01	0.25
I15-11(opx)		0.00	29.30	0.17	55.22	0.00	0.21
I16-11(ol)			36.77	0.00	38.57		0.00
I17-11(ol)			37.52	0.00	38.19		0.01
I18-11(ol)			37.45	0.02	38.28		0.03
J1-11(amph)		3.16	15.15	18.64	39.76	0.80	10.95
J2-11(amph)		2.12	14.30	16.55	41.47	0.60	10.49
J3-11(amph)		2.78	15.04	16.93	41.59	0.91	11.63
K1-11(cpx)		0.52	13.77	5.95	49.34	0.00	23.25
K2-11(cpx)		0.48	13.33	5.73	49.45	0.01	23.66

ANALYSIS #	OXIDES: TiO2	Cr2O3	MnO	Fe2O3	NiO	TOTAL
A1-11(cpx)	1.05	0.03	0.18	6.49	0.00	98.57
A2-11(cpx)	1.14	0.05	0.17	6.30	0.04	101.24
A3-11(plag)	0.02	0.01	0.03	0.12	0.02	99.37
A4-11(plag)	0.00	0.00	0.00	0.12	0.00	99.91
A5-11(plag)	0.00	0.00	0.00	0.06	0.00	97.10
A6-11(plag)	0.01	0.00	0.00	0.06	0.04	98.08
C1-11(cpx)	1.33	0.09	0.16	6.61	0.01	99.31
C2-11(px)	1.55	0.10	0.30	15.05	0.04	102.27
C3-11(opx)	0.12	0.07	0.31	18.26	0.03	100.86
C4-11(opx)	0.08	0.07	0.43	18.45	0.05	101.64
C5-11(cpx)	1.39	0.12	0.18	6.16	0.05	99.26
C6-11(cpx)	1.20	0.08	0.16	6.68	0.03	98.53
C7-11(px)	1.22	0.05	0.12	8.55	0.05	100.64
C8-11(opx)	0.09	0.09	0.51	18.35	0.05	100.60
C9-11(plag)	0.03	0.03	0.01	0.55	0.03	99.87
C10-11(plag)	0.00	0.02	0.00	0.00	0.00	99.92
C11-11(plag)	0.00	0.02	0.00	0.07	0.03	99.77
C12-11(plag?)	0.00	0.01	0.09	2.36	0.03	97.60
D1-11(cpx)	1.11	0.00	0.12	7.77	0.07	100.53
D2-11(cpx)	1.09	0.02	0.14	7.18	0.02	98.76
D3-11(cpx)	1.08	0.00	0.14	7.31	0.03	99.72
E1-11(plag)	0.00	0.05	0.04	0.07	0.05	99.52
E2-11(plag)	0.02	0.04	0.00	0.04	0.01	99.45
E3-11(plag)	0.00	0.03	0.03	0.07	0.00	99.21
E4-11(plag)	0.02	0.00	0.01	0.13	0.00	100.48
E5-11(cpx)	1.17	0.07	0.22	6.51	0.03	99.11
E6-11(cpx)	1.14	0.08	0.21	7.49	0.05	99.04
E7-11(cpx)	1.27	0.05	0.14	6.09	0.06	100.04
E8-11(cpx)	1.17	0.03	0.17	5.98	0.06	99.50
E12-11(ol)	0.03	0.04	0.36	23.39	0.13	98.97
E13-11(ol)	0.00	0.03	0.38	24.12	0.14	99.57
F1-11(opx)	0.11	0.01	0.34	15.66	0.05	100.65
F2-11(opx)	0.18	0.01	0.34	15.43	0.05	99.47
F3-11(opx)	0.13	0.03	0.37	15.15	0.04	99.12
F4-11(ol)	0.00	0.03	0.32	24.07	0.14	100.46
F5-11(ol)	0.03	0.00	0.37	24.52	0.12	100.01

ANALYSIS #	OXIDES: TiO2	Cr2O3	MnO	Fe2O3	NiO	TOTAL
G1-11(cpx)	1.37	0.07	0.09	5.30	0.00	99.62
G2-11(cpx)	0.98	0.04	0.09	5.60	0.01	98.34
G3-11(cpx)	1.18	0.07	0.17	6.25	0.11	100.43
G4-11(opx?)	0.09	0.01	0.30	14.04	0.02	99.74
H1-11(plag)	0.00	0.00	0.01	0.04	0.05	99.44
H2-11(plag)	0.01	0.05	0.00	0.07	0.01	98.99
H3-11(plag)	0.03	0.02	0.01	0.06	0.04	98.35
H4-11(plag)	0.00	0.03	0.01	0.08	0.01	99.96
H5-11(plag)	0.00	0.01	0.01	0.15	0.00	99.55
H7-11(opx)	0.05	0.00	0.36	16.03	0.00	101.64
H8-11(opx)	0.11	0.00	0.34	16.04	0.05	100.02
H9-11(opx)	0.02	0.02	0.32	14.68	0.03	99.37
H10-11(ol)	0.00	0.00	0.35	23.55	0.17	99.74
H11-11(ol)	0.00	0.01	0.28	23.30	0.16	99.62
H12-11(ol)	0.00	0.05	0.32	23.41	0.19	99.91
H13-11(ol)	0.00	0.03	0.20	23.44	0.17	99.54
I1-11(plag)	0.05	0.00	0.03	0.37	0.00	100.18
I2-11(plag)	0.02	0.00	0.00	0.03	0.00	98.53
I3-11(plag)	0.00	0.00	0.00	0.04	0.00	99.24
I4-11(plag)	0.00	0.00	0.03	0.23	0.05	99.41
I5-11(amph)	0.02	0.00	0.11	14.71	0.05	98.20
I6-11(amph)	0.02	0.04	0.14	11.28	0.04	98.28
I7-11(amph)	0.03	0.00	0.07	7.95	0.05	97.91
I8-11(amph)	0.03	0.02	0.07	11.65	0.14	102.04
I9-11(amph)	0.05	0.00	0.07	11.75	0.12	103.82
I10-11(amph)	0.05	0.02	0.08	8.41	0.03	96.48
I11-11(amph)	0.08	0.02	0.06	8.42	0.08	97.13
I12-11(opx)	0.00	0.00	0.26	15.85	0.02	100.56
I13-11(opx)	0.01	0.00	0.30	15.16	0.00	99.51
I14-11(opx)	0.00	0.00	0.30	15.22	0.11	100.32
I15-11(opx)	0.00	0.00	0.32	15.30	0.02	100.54
I16-11(ol)	0.02	0.00	0.31	23.12	0.14	98.93
I17-11(ol)	0.04	0.02	0.25	23.97	0.16	100.17
I18-11(ol)	0.01	0.00	0.29	23.95	0.17	100.20
J1-11(amph)	0.35	0.01	0.09	8.69	0.05	97.64
J2-11(amph)	0.34	0.00	0.15	9.68	0.01	95.71
J3-11(amph)	0.27	0.00	0.09	8.91	0.03	98.18
K1-11(cpx)	1.41	0.03	0.07	5.32	0.01	99.67
K2-11(cpx)	1.38	0.05	0.14	5.52	0.00	99.74

Appendix 7: Corona Chemical-Balance Calculations

Stoichiometric mineral compositions are based on crystallo-graphic site occupancies suggested by Deer et al (1966).

Olivine: $(Mg_{1.47}Fe_{0.52}Mn_{0.006})(SiO_4)$

Plagioclase: $(K_{0.004}Na_{0.377}Ca_{0.699}Fe_{0.002})(Al_{1.60}Si_{2.36}O_8)$

Orthopyroxene: $(Mg_{1.47}Fe_{0.48}Al_{0.04}Ca_{0.012}Mn_{0.01})$
$(Si_{1.93}Al_{0.07}O_6)$

Amphibole: $(K_{0.121}Na_{0.365})(Na_{0.362}Ca_{1.64})(Al_{0.69}Mg_{3.20}Fe_{0.79}$
$Fe_{0.29}Ti_{0.01}Mn_{0.01})(Si_{5.92}Al_{2.08}O_{22})(OH)_2$

Spinel: $(Fe_{0.67}Mg_{0.33})Al_2O_4$

Mineral	ρ (g/cm^3)	Molec. wt. (g/mol)	Molec. vol. (cm^3/mol)
Chrysolite	3.51	157.37	44.83
Labradorite	2.72	273.96	100.72
Bronzite	3.39	216.66	63.91
Pargasite	3.05	861.06	282.32
Spinel	4.40	173.81	39.02

Excess Fe^{+2} from the pargasite structure can be combined with Al to form spinel of arbitrary composition, based on

spinel compositions from other coronitic symplectites (van Lamoen, 1979; Joesten 1986a). Aluminum removed from the pargasite to create spinel can be replaced by converting Fe^{+2} to Fe^{+3}. Based on these assumptions, the proportion of spinel in the amphibole-spinel symplectite is calculated as 1.82 vol. % or 13.04 molecular %. This lies between the values of van Lamoen (1979) and Joesten (1986a) of 3.7 vol. % (30.6 molecular %) and 0.125 vol. % (1.029 molecular %) respectively. The calculated value of 1.82 vol. % is considered to be a minimum, since efforts were made to avoid analysing spinel grains during microprobe analysis of the amphibole.

The assumption of constant volume requires the following equalities, based on the molecular volumes given above:

1 olivine = 0.701 orthopyroxene

1 plagioclase = 0.363 symplectite

The following two balanced equations can be generated, where excess ions are represented as fluid phases, after van Lamoen (1979).

chrysolite + $(0.36\ Si + 0.08\ Al + 0.01\ Ca + 0.21\ O)_{fluid}$ →

(0.701) bronzite + $(0.19\ Fe + 0.44\ Mg)_{fluid}$

and

plagioclase + (0.37 Fe + 1.01 Mg + 0.03 K)$_{fluid}$ →

(0.306) pargasite + (0.061) spinel +

(0.55 Si + 0.63 Al + 0.62 Ca + 0.16 Na + 0.41 O)$_{fluid}$

A final constraint is provided by the observed (modal) proportions of inner and outer corona in this thin section (8511), based on 1500 counts. The production of 6.7 vol. % orthopyroxene for 10.3 vol. % symplectite corresponds to 2.80 molecules of orthopyroxene for each molecule of symplectite.

The final reaction can be expressed for the whole system as follows:

1.21 chrysolite + labradorite + (0.14 Fe + 0.47 Mg + 0.03 K)$_{fluid}$ → 0.85 bronzite + 0.30 pargasite + 0.06 spinel + (0.13 Si + 0.55 Al + 0.16 Ca + 0.16 Na + 0.20 O)$_{fluid}$

Appendix 8: XRF and Electron-Microprobe Standards

Literature values for XRF standards are given in the Appendix, and electron-micrprobe standard values were obtained from listings at the Memorial University of Newfoundland, St. John's.

	XRF Standards					Microprobe Stds.	
Oxide/Standard	AC-E	AC-E	G-1	NIM-N	NIM-N	FCPX	MOL
SiO2	71.04	70.32	72.53	52.47	52.56	49.750	40.240
Al2O3	14.96	14.95	14.57	16.60	16.61	7.956	0.025
Fe2O3	2.76	2.64	1.97	8.89	8.84	6.223	11.138
MgO	0.21	0.22	0.42	7.53	7.43	15.364	47.008
CaO	0.36	0.35	1.34	11.34	11.35	17.887	0.018
Na2O	5.95	6.69	3.38	2.49	2.52	1.276	n.a.
K2O	4.51	4.60	5.35	0.29	0.29	0.006	n.a.
TiO2	0.13	0.13	0.29	0.19	0.20	0.743	0.005
MnO	0.06	0.07	0.04	0.16	0.16	0.113	0.255
P2O5	0.02	0.01	0.11	0.04	0.04		
						(n=7)	(n=4)

Element/Std.	NIM-N	JG-1	JB-1	NIM-S	MRG-1
Rb (ppm)	3.5	175.7	40.3	542	7
	(n=6)	(n=7)	(n=3)	(n=2)	(n=1)
Sr (ppm)	263.5	178.6	447.3	63.5	272

Literature Values

Oxide/Standard	AC-E (1)	G-1 (2)	NIM-N (3)	FCPX	MOL
SiO2	70.35	72.46	52.64	49.85	40.24
Al2O3	14.70	14.23	16.50	7.86	0.01
Fe2O3	2.53	1.96	8.91	6.86	12.81
MgO	0.03	0.39	7.50	15.47	45.08
CaO	0.34	1.38	11.50	17.75	n.a.
Na2O	6.54	3.33	2.46	1.27	n.a.
K2O	4.49	5.48	0.25	n.a.	n.a.
TiO2	0.11	0.25	0.20	0.83	n.a.
MnO	0.06	0.03	0.18	0.14	0.28
P2O5	0.02	0.09	0.03	n.a.	n.a.

Element/Std.	NIM-N(3)	NIM-S(3)	JG-1(3)	JB-1(3)	MRG-1(4)
Rb (ppm)	6	530	181	41.2	8
Sr (ppm)	260	62	184	435	260

References:

(1) Govindaraju (1987)
(2) Gladney et al. (1983)
(3) Govindaraju (1984)
(4) Abbey (1981)

Appendix 9: Replicate XRF Analyses

Replicate analyses represent analyses of separate aliquots of sample, whether pressed powder pellets or fused glass beads. Triplicate analyses are given for major element analyses from two samples, for trace element analyses of three "86"-prefixed samples, and for all of the "85"-prefixed samples. The "n.a." in the barium analyses of sample 85-10 indicates "not analysed", as the powder pellet did not survive the final analysis.

Element/Oxide	Sample 8514	2-sigma	% error	8511	2-sigma	% error
SiO2	51.81	0.05	0.1	47.09	0.15	0.3
Al2O3	15.61	0.11	0.7	21.49	0.1	0.5
Fe2O3	12.45	0.07	0.6	8.71	0.05	0.6
MgO	6.26	0.22	3.5	10.04	0.51	5.1
CaO	8.17	0.07	0.8	10.11	0.25	2.5
Na2O	2.07	0.1	4.8	1.81	0.19	10.5
K2O	2.03	0.03	1.4	0.55	0.79	143
TiO2	1.13	0.01	0.8	0.19	0	0
MnO	0.19	0.03	0.1	0.05	0.09	200
P2O5	0.04	0.01	25.7	0.06	0.11	200

	8603	2-sigma	% error	8618B	2-sigma	% error	8613	2-sigma	% error
Rb	2	0	0	145.3	3.4	2.3	114	1.6	1.4
Sr	52.3	2.5	4.8	155.7	3.4	2.2	307.7	2.5	0.8
Y	18	0	0	95.7	0.9	1	28	0	0
Zr	44.7	0.9	2.1	406.7	52.5	12.9	213.7	21	9.8
Ba	51.3	19.3	37.7	230	8.2	3.5	1170	32.7	2.8

Element/Sample	All quantities in ppm Ni	Cr	Ba	Y	Zr
8501	282	78	86	8	41
	284	86	96	7	40
	289	93	75	7	36
8502	149	75	80	5	35
	140	73	99	6	37
	153	71	97	5	33
8503	214	90	103	6	29
	219	105	102	6	30
	213	76	127	6	27
8504	848	410	102	8	26
	867	440	92	7	27
	829	408	85	7	25
8505	998	505	101	8	23
	1040	537	87	7	19
	1042	521	88	7	17
8506	307	176	89	5	30
	310	188	87	7	31
	310	180	72	6	31
8507	305	396	70	6	24
	286	346	78	6	25
	292	340	79	7	24
8508	198	330	109	8	40
	202	312	128	8	40
	188	298	106	8	42

Element/Sample	All quantities in ppm Ni	Cr	Ba	Y	Zr
8509	15	39	1185	26	316
	13	40	1169	27	262
	15	44	1152	27	290
8510	5	15	1041	53	490
	5	18	1047	52	476
	5	14	n.a.	48	475
8512	170	24	36	5	39
	160	16	20	5	35
	165	21	58	4	35
8513	12	27	756	30	258
	12	23	743	30	253
	13	26	779	29	257
8514	114	200	310	17	107
	110	199	311	18	109
	109	195	297	17	116
8515	14	51	966	25	237
	14	20	943	25	240
	15	25	935	25	256
8516	13	31	887	32	303
	13	37	955	29	268
	12	23	922	30	256

Appendix 10: XRF Analyses of Rb and Sr

Rb and Sr were analysed by XRF using the molybdenum tube Compton peak method (as opposed to tungsten K_α, as was used for Rb and Sr in Appendix 9). Triplicate powder pellets were analysed, and reanalysed at a later time for the "85"-prefixed samples. XRF-determined rubidium concentrations were not used for the gabbronorites due to the large errors.

Sample/Element	Rb (ppm)						Mean Rb (ppm)	Error 2-sigma	%
8501	3	3	4	4	4	4	3.67	0.94	25.71
8502	1	1	2	2	2	3	1.83	1.37	74.97
8503	2	2	3	3	3	2	2.50	1.00	40.00
8504	4	4	5	4	4	4	4.17	0.75	17.89
8505	3	3	2	3	3	3	2.83	0.75	26.31
8506	3	2	3	3	3	3	2.83	0.75	26.31
8507	2	1	2	2	2	2	1.83	0.75	40.66
8508	4	4	5	5	6	5	4.83	1.37	28.44
8509	99	99	99	102	101	99	99.83	2.43	2.43
8510	167	166	164	170	168	164	166.50	4.28	2.57
8511	1	0	0				0.33	0.94	282.84
8512	0	0	0	0	0	1	0.17	0.75	447.21
8513	128	130	130	127	130	124	128.17	4.38	3.42
8514	47	47	47	46	48	47	47.00	1.15	2.46
8515	128	128	129	126	130	130	128.50	2.77	2.15
8516	126	127	126	127	127	128	126.83	1.37	1.08
8602	4.5	5	4.8				4.77	0.41	8.62
8603	1.3	1.1	0.4				0.93	0.77	82.68
8604	36.3	37.1	37				36.80	0.71	1.93
8605	41.4	42.1	42.3				41.93	0.77	1.84
8606	45.1	43.6	45.5				44.73	1.64	3.66
8607	31.1	30.9	29.8				30.60	1.14	3.74
8608	37.4	36.7	39.2				37.77	2.11	5.58
8609A	116.6	117.8	116.9				117.10	1.02	0.87
8609B	106.2	105.1	104.4				105.23	1.48	1.41
8610A	126.2	123.4	127.7				125.77	3.56	2.83
8610B	77.5	74.5	74				75.33	3.09	4.10
8611A	86	88.3	88.4				87.57	2.22	2.53
8611B	88.3	89.7	88.5				88.83	1.24	1.39
8612A	134.9	133.5	137.4				135.27	3.23	2.39
8612B	128.9	127	127				127.63	1.79	1.40
8613	113.7	112	111.6				112.43	1.82	1.62
8614	110.9	112.5	113				112.13	1.79	1.60
8616A	7.5	6.3	7.1				6.97	1.00	14.32
8616B	43.5	42.8	44.6				43.63	1.48	3.40
8617A	157.8	154.5	157.8				156.70	3.11	1.99
8617B	168.3	169.9	165.8				168.00	3.37	2.01
8618A	52.7	54.3	54.3				53.77	1.51	2.81
8618B	144.4	142.6	147				144.67	3.61	2.50
310A	76	76	76				76.00	0.00	0.00
310B	42	43	41				42.00	1.63	3.89
310C	56	56	55				55.67	0.94	1.69
310D	109	109	107				108.33	1.89	1.74
310E	114.1	113.3	117.1				114.83	3.27	2.85
310F	82.9	82.8	82.6				82.77	0.25	0.30
310G	69	71	70	70	72	71	70.50	1.91	2.72

Sample/Element	Sr (ppm)						Mean Sr (ppm)	Error 2-sigma	%
8501	185	185	184	180	181	183	183.0	3.8	2.09
8502	235	232	234	231	228	230	231.7	4.7	2.03
8503	195	193	193	189	193	191	192.3	3.8	1.96
8504	115	116	117	113	114	113	114.7	3.0	2.60
8505	99	98	99	96	97	98	97.8	2.1	2.18
8506	205	208	208	203	203	209	206.0	4.9	2.38
8507	182	183	183	181	180	178	181.2	3.5	1.96
8508	176	177	175	177	175	174	175.7	2.2	1.26
8509	262	262	262	265	265	260	262.7	3.6	1.37
8510	107	107	106	109	108	106	107.2	2.1	1.99
8511	301	296	302				299.7	5.2	1.75
8512	317	322	321	313	312	309	315.7	9.5	3.01
8513	254	254	254	248	251	245	251.0	6.9	2.76
8514	240	241	240	231	236	239	237.8	6.9	2.89
8515	276	276	276	274	276	276	275.7	1.5	0.54
8516	282	280	282	279	278	283	280.7	3.6	1.28
8602	177	178	175				176.8	2.9	1.63
8603	51	52	53				52.0	0.9	1.73
8604	730	743	750				741.1	16.9	2.28
8605	568	568	580				571.9	10.8	1.89
8606	607	593	603				601.1	11.5	1.91
8607	361	358	347				355.4	11.8	3.31
8608	193	187	197				192.5	8.2	4.25
8609A	364	372	371				369.0	7.4	2.01
8609B	364	362	362				362.8	1.4	0.38
8610A	213	205	214				210.3	8.2	3.91
8610B	474	466	464				468.0	8.5	1.81
8611A	482	490	492				488.1	8.8	1.80
8611B	330	333	326				329.6	5.2	1.57
8612A	240	247	245				243.9	5.9	2.41
8612B	246	246	248				246.4	1.7	0.68
8613	304	303	293				299.7	10.1	3.38
8614	299	301	301				300.0	1.5	0.50
8616A	318	324	310				317.2	10.9	3.43
8616B	498	503	508				502.7	8.3	1.66
8617A	183	177	180				179.8	4.9	2.74
8617B	187	188	183				185.9	4.3	2.30
8618A	340	346	343				342.9	4.8	1.41
8618B	159	157	159				158.6	2.1	1.34
310A	294	294	298				295.3	3.8	1.28
310B	295	295	289				293.0	5.7	1.93
310C	269	268	264				267.0	4.3	1.62
310D	287	288	286				287.0	1.6	0.57
310E	341	344	348				344.2	5.6	1.64
310F	301	296	299				298.9	4.3	1.42
310G	302	303	303	297	305	302	302.0	4.9	1.62